SU-SEL-67-102

Determination of Rates of Production and Loss of Electrons in the F Region of the Ionosphere from Observations of Geostationary Satellite Transmissions

by

Fred L. Smith, III

March 1968

Technical Report No. 10

Prepared under
NASA Research Grant No. NsG 30-60

RADIOSCIENCE LABORATORY

STANFORD ELECTRONICS LABORATORIES

STANFORD UNIVERSITY • STANFORD, CALIFORNIA

SEL-67-102

DETERMINATION OF RATES OF PRODUCTION AND LOSS OF ELECTRONS IN THE F REGION OF THE IONOSPHERE FROM OBSERVATIONS OF GEOSTATIONARY SATELLITE TRANSMISSIONS

by

Fred L. Smith, III

March 1968

Technical Report No. 10

Prepared under

National Aeronautics and Space Administration
Research Grant No. NsG 30-60

Radioscience Laboratory
Stanford Electronics Laboratories
Stanford University Stanford, California

ABSTRACT

Accurate measurements of the amount of Faraday rotation imposed on VHF telemetry transmissions from a geostationary satellite have been analyzed to study rates of production and loss of electrons in the F region of the ionosphere. The rate of photoionization of atomic oxygen, integrated with respect to height through the ionosphere (that is, the total number of O^+ ions produced per second in a vertical column of unit cross-sectional area extending through the ionosphere), was determined at sunrise over Hawaii. The analysis also yielded the magnitude of the linear loss coefficient (defined as the fraction of the electron concentration lost through recombination per second) at an altitude of 300 km. The integrated rate of production of O^+ ions at sunrise was used to deduce the total flux of solar radiation in the 165 to 911 Å wavelength range (the extreme ultraviolet, or EUV, range) incident on the earth's atmosphere. Atomic oxygen photoionization rates and solar EUV flux values were obtained on a daily basis, and loss coefficients on a monthly average basis, over the 2-year period extending from September 1964 through August 1966.

The analysis takes advantage of a nonequilibrium situation that exists in the ionosphere near the time of sunrise in order to determine the integrated photoionization rate and loss coefficient. Both quantities are determined by matching experimental measurements of the Faraday rotation vs time during a period of approximately 1 hour, centered around sunrise, to a Faraday rotation function computed on the basis of a theoretical model for the ionosphere.

The results include the following:

1. The integrated rate of production of atomic oxygen ions at sunrise over Hawaii averaged 1.7×10^9 ions/cm^2/s. The average is believed to be accurate to within ±15 percent. Day to day values fluctuated about a 30 day running mean with a standard deviation of ±15 percent. No seasonal variation was observed.

2. The linear loss coefficient at sunrise over Hawaii was found to average 1.4×10^{-5} s^{-1} at an altitude of 300 km, with winter values tending to be about 50 percent above average and summer values about 50 percent below average. The average value should be accurate to within a factor of 2.

3. The total flux of solar radiation in the 165 to 911 Å wavelength range incident on the atmosphere was found to average 4.5×10^{10} photons/cm^2/s. The average should be accurate to within ±30 percent.

CONTENTS

CONTENTS (Cont)

TABLES

ILLUSTRATIONS

SYMBOLS

A complete listing of symbols is contained in Section A of Chapter IV preceding the main body of the analysis.

ACKNOWLEDGMENT

The advice and encouragement of Professor Owen K. Garriott throughout the course of this work is sincerely appreciated. Professor Paul C. Yuen's efforts in supervising the station operation and data collection at the University of Hawaii are also gratefully acknowledged.

Chapter I

INTRODUCTION

A. Purpose

This research makes use of radio transmissions from geostationary earth satellites to study some of the physical processes governing the concentration of electrons in the ionosphere. One objective of the study was to determine the photoionization rate, integrated with respect to height through the ionosphere, that is, the total number of ion-electron pairs produced per second in a vertical column of unit cross-sectional area extending all the way through the ionosphere. Using this information, in conjunction with recent data regarding the composition of the neutral atmosphere, it was then possible to deduce the total flux of solar radiation in the extreme ultraviolet (EUV) portion of the spectrum incident on the earth's atmosphere. (In this study, "extreme ultraviolet" refers to radiation in the 165 to 911 Å wavelength range.)

Another objective was to determine the magnitude of the linear loss coefficient that governs the rate of recombination of electrons in that region of the ionosphere (the region of maximum electron concentration, known as the F_2 region) where the recombination rate is a linear function of the electron concentration. The linear loss coefficient is defined as the fraction of the total electron concentration at a particular altitude that is lost through recombination per second.

The integrated photoionization rate and the linear loss coefficient were determined over Hawaii at sunrise, as a function of date, during a period of almost 2 years. The results are examined to determine whether or not seasonal variations can be detected in either quantity.

B. The Situation

The existence of the ionosphere is due primarily to the photoionization of neutral constituents of the atmosphere that results from solar extreme ultraviolet, and to some extent X-ray, radiation. Most of the ionization is contained within the F region of the ionosphere, which extends in altitude from about 150 to 600 km and which is often further

subdivided into the so-called F_1 and F_2 regions. The concentration of electrons in the F region reaches a maximum around midday when the effects of the solar ionizing radiation are strongest. It decays to a minimum, due to processes leading to the recombination of ions and electrons, in the late night and early morning hours before sunrise.

Figure 1 shows the geometry involved. The angle χ, which is the angle of incidence of the solar ionizing radiation as seen by an observer situated at point 0, is known as the solar zenith angle. Note that $\chi = 0$ implies that the sun is directly overhead. At ground sunrise, when the solar radiation is arriving tangentially to the earth's surface, the angle χ is $90°$.

As a very rough approximation, the columnar electron content E of the ionosphere (that is, the total number of free electrons in a vertical

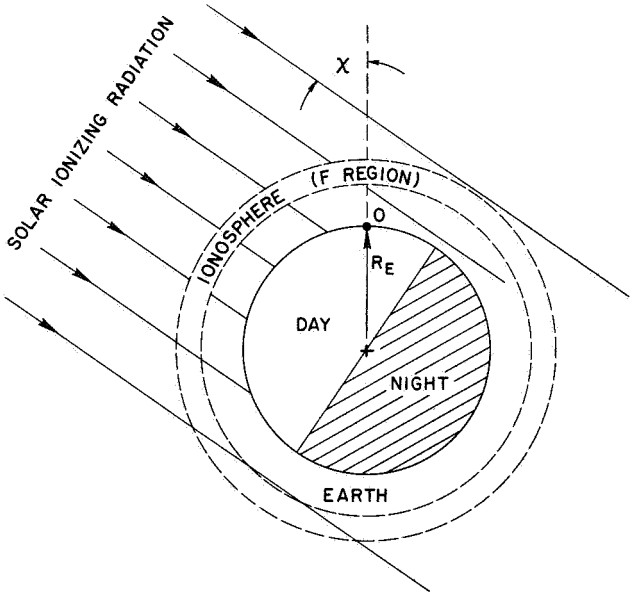

Fig. 1. A DIAGRAM SHOWING THE EARTH IN RELATION TO THE IONOSPHERE AND THE SOLAR IONIZING RADIATION. R_E is the radius of the earth, 0 is the location of an observer, and χ is the solar zenith angle at points above the observer. The diagram is not drawn to scale. The altitude of the lower edge of the F region is in reality only about 0.03 R_E. The thickness of the F region is about 0.08 R_E.

column of unit cross-sectional area extending all the way through the ionosphere) can be considered to be governed solely by an integrated loss rate L and an integrated photoionization rate Q, where Q is zero at night and is a nonzero constant, Q_m, between sunrise and sunset. For a simplified example, consider L to be only a function of E.

Consider the situation illustrated in Fig. 2 in which the dependence of Q on χ is neglected, so that the following continuity equation applies:

$$\frac{dE}{dt} = Q - L \tag{1-1}$$

where

$$Q = \begin{cases} Q_m & \text{for } t_r < t < t_s \\ 0 & \text{otherwise} \end{cases} \tag{1-2}$$

and where the letter t is used to represent time, with sunrise and sunset occurring at times t_r and t_s, respectively.

If the ion-electron recombination rates are large enough, virtually all of the ionization will disappear at night, leaving $E \approx 0$ when the sun rises at time t_r. At sunrise, in the example of Fig. 2, E begins

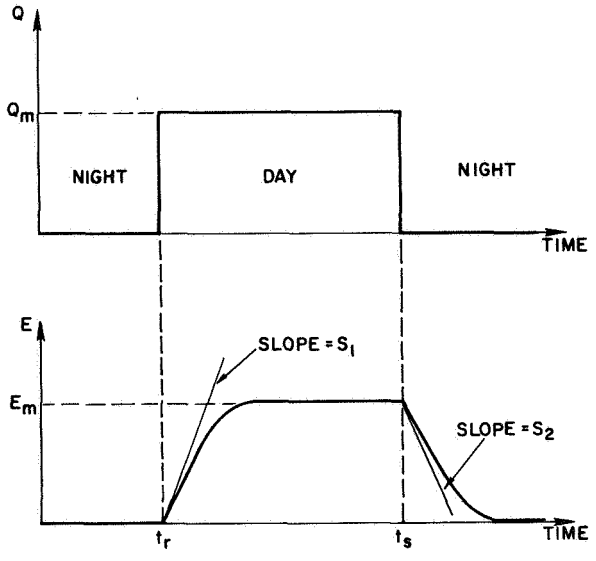

Fig. 2. THE DIURNAL VARIATION OF THE INTEGRATED PHOTOIONIZATION RATE Q AND THE ELECTRON CONTENT E OF THE IONOSPHERE FOR THE VERY SIMPLE MODEL CONSIDERED IN THE TEXT.

increasing at an initial rate S_1, where $S_1 = Q_m$. The initial rate of increase of E at sunrise must equal the daytime integrated photoionization rate, Q_m, since L must be zero when E is zero. The electron content eventually reaches an equilibrium level, E_m (assuming the time required to reach equilibrium is less than $t_s - t_r$), and begins decreasing at sunset. The rate of decrease of E immediately after sunset, S_2, must also equal Q_m in the simplified model, since $dE/dt = L$ an instant after t_s, and $Q_m = L$ an instant before t_s.

To the extent that the actual ionosphere is represented by the model in Fig. 2, the daytime integrated photoionization rate can be determined by measuring the rate of change of the electron content either immediately after sunrise or immediately after sunset. The functional relationship between L and E can be determined from the shape of the electron content vs time curve during either of the two periods of nonequilibrium (when $Q \neq L$). In actuality, the behavior of the ionosphere does resemble that illustrated in Fig. 2 in that a state of near equilibrium between production and loss of ion-electron pairs does exist during most of the daylight hours, but not during times near sunrise and sunset [Rishbeth and Barron, 1960]. Beyond this resemblance, however, the situation is more complicated than the simple picture indicates.

The electron content of the ionosphere, for example, does not decay to zero at night, though it does reach a minimum level that, over Hawaii, is typically lower by a factor of about 30 than the midday maximum [Garriott et al, 1965]. Often the electron content is observed to reach an apparent, nonzero, equilibrium level within an hour or two after sunset. That there must be some source of ionization other than the photoionization due to radiation coming directly from the sun is evidenced by observations that, on occasion, show the electron content increasing gradually during part of the night, after having first reached a post sunset minimum [Garriott et al, 1965; Yuen and Roelofs, 1967; da Rosa and Smith, 1967].

The integrated photoionization rate Q, shown as a constant in Fig. 2, is in reality not constant between sunrise and sunset; rather it is a function of χ, the solar zenith angle. Initially, before ground sunrise, only very high portions of the atmosphere are illuminated, and Q

is consequently small. As the sun rises and the ionizing radiation penetrates to lower altitudes, Q increases. Even at ground sunrise, though, when the atmosphere is illuminated at all altitudes, Q remains relatively small because of the severe attenuation of radiation arriving at a grazing incidence. Minimum attenuation, and hence maximum integrated photoionization rates, occurs when the radiation arrives at normal incidence; that is, when the sun is overhead. If the vertical distribution of the neutral constituents in the atmosphere is known, the amount of attenuation of the ionizing radiation can be computed as a function of χ. Hence if Q can be determined at any time during the daylight hours, its magnitude at any other time can be computed.

The situation is somewhat complicated by the fact that the solar EUV flux produces primarily two ions, O^+ and N_2^+, which apparently recombine at very different rates. The recombination time for N_2^+ is so short compared to that for O^+ that virtually all of the ions observed in the F region are O^+ ions. For practical purposes, as discussed in Section IV-D2, Q and L in Eq. (1-1) can be considered to refer to the production and loss of O^+ ions only.

The integrated loss rate L does not strictly correspond to the simplified model either. Reactions leading to the recombination of ions and electrons involve neutral constituents of the atmosphere as well as the ionization itself. Since the concentrations of neutral constituents vary with altitude, the integrated loss rate, as well as being a function of E, is also a function of the distribution of electrons with altitude. In the lower portion of the F region, loss rates tend to be proportional to the square of the electron concentration (Section II-E), whereas at higher altitudes loss rates are proportional to the first power of the electron concentration.

C. The Method of Analysis

At sunrise virtually all of the ionization exists at altitudes sufficiently high so that the rate of loss of electrons can be considered to be proportional to the electron concentration (see Section IV-E). Under this condition, even though the situation is not as simple as indicated

by Fig. 2, Eq. (1-1) is at least linear. Armed with (1) observations of E vs t during a period of nonequilibrium near sunrise, (2) a knowledge of the functional form of Q (the way Q varies as a function of χ, or equivalently, as a function of t), and (3) the information that the rate of loss of electrons is proportional to the electron concentration at all altitudes where significant amounts of ionization are present, it is possible to derive both the magnitude of Q at sunrise and the proportionality constant, or loss coefficient, that determines the loss rate. This is, in a condensed form, the approach used in this study. Equation (1-1) does not take into account effects of possible movements of the ionization during the period of observation, but these are considered later in the analysis.

By the time of sunset, a substantial quantity of ionization exists at lower altitudes, where the loss rate is proportional to the square of the electron concentration. Equation (1-1) is then nonlinear. Under these conditions, the problem of analysis would be considerably more complicated. The period of nonequilibrium near sunset was not considered in this study.

The integrated electron production rate and the magnitude of the linear loss coefficient are actually determined in this study from observations of the total amount of Faraday rotation imposed upon a linearly polarized radio wave transmitted from a geostationary satellite. The amount of Faraday rotation is, as discussed in Section III-A, a measure of the columnar electron content of the ionosphere. Theoretical values for the amount of Faraday rotation are computed as a function of time during an interval of approximately 1 hour near ground sunrise. The computations are based, among other considerations, upon assumptions regarding $Q_{90}[O^+]$, the rate of photoionization of atomic oxygen at sunrise ($\chi = 90°$) integrated with respect to height through the ionosphere, and β_{300}, the value of the linear loss coefficient at an altitude of 300 km. A curve-fitting process is then used to determine the values of $Q_{90}[O^+]$ and β_{300} which make the model agree most closely with experimental observations. It is found that the computations agree rather well with observations when $Q_{90}[O^+]$ and β_{300} are chosen properly. Furthermore, there is generally a well defined pair of values for these two quantities which provides the best agreement between the computations and the data. The values of Q_{90} and β_{300} which do provide the best agreement are taken to be the correct values. Using

values obtained for $Q_{90}[O^+]$, in conjunction with a model for the neutral atmosphere, the solar EUV photon flux is deduced.

D. The Presentation

Chapter II contains a review of ionospheric theory that pertains to the problem of determining rates of production and loss of electrons in the F region.

In Chapter III, the mechanism leading to Faraday rotation of the plane of polarization of a linearly polarized radio wave is briefly discussed. Also included in Chapter III are a description of the satellite whose transmissions are being monitored, a discussion of the technique for measuring the amount of Faraday rotation imposed upon these transmissions, and an estimate of the accuracy of the measurements.

Chapter IV contains a discussion of the scheme for determining $Q_{90}[O^+]$ and β_{300} from the Faraday rotation measurements. Section IV-B outlines the entire analysis, and subsequent sections supply the details.

Chapter V presents the results of an application of the analysis described in Chapter IV to data obtained at the University of Hawaii, and discusses implications of those results.

E. Contributions

The major contributions of this research may be summarized as follows:

1. A new method of analyzing measurements of the Faraday rotation imposed on transmissions from geostationary satellites to study both the rate of production of electrons and the loss coefficient in the F_2 region of the ionosphere is described.
2. Daily values of the integrated rate of production of O^+ ions at sunrise over Hawaii are computed for a 2-year period.
3. Monthly averages of the linear loss coefficient for electrons at an altitude of 300 km are determined for a 2-year period.
4. Estimates, based on the results in (2), of the total extreme ultraviolet photon flux from the sun incident on the earth's atmosphere are provided.

Chapter II

BACKGROUND

A discussion of the analysis used to derive the integrated rate of production of O^+ ions and the magnitude of the linear loss coefficient from Faraday rotation data appears in Chapter IV. The present chapter reviews the ionospheric theory upon which the analysis is based.

A. Continuity Equation

The physical processes determining the behavior of the ionosphere can be roughly divided into three classes: (1) those that result in the production of ionization, (2) those that result in the disappearance of ions and free electrons, and (3) those that lead to movements of the ionization. The time variation of the electron density, N, may be related to these processes through an equation of continuity. Using the symbols q and ℓ to represent, respectively, the rates of production and loss, and $\bar{v}$ to represent the net drift velocity of the ionization, the equation is

$$\frac{\partial N}{\partial t} = q - \ell - \mathrm{div}(N\bar{v}) \qquad (2\text{-}1)$$

The production of ionization is due primarily to the photoionization of N_2, O_2, and O by solar extreme ultraviolet (EUV) and X-ray radiation, although at times, particularly at high latitudes, ion-electron pairs can be created in substantial quantities by relatively energetic charged particles entering the atmosphere. Ions and electrons disappear principally through dissociative recombination, with many of the possible loss mechanisms involving more than one reaction. Movements of the ionization may be attributable to motions of the neutral portion of the atmosphere, such as those resulting from thermal expansion or winds, to a drift imposed by an electrostatic field, or to diffusion of the plasma through the neutral gas whenever there is an imbalance of forces acting on the plasma. These topics are covered in more detail in subsequent sections of this chapter.

B. Solar Radiation

Most of the photoionization in the F region is a result of solar radiation in the EUV portion of the spectrum, with wavelengths ranging from 165 to 911 Å. The low energy end of the range is set by the ionization potential of atomic oxygen at 911 Å. The ionization threshold for molecular nitrogen, 796 Å, falls within the range. Molecular oxygen with an ionization threshold of 1026 Å can also be ionized by radiation in the 911 to 1026 Å range, but O_2 is only a minor constituent of the atmosphere at F region altitudes. Still longer wavelength radiation can ionize even less abundant gases such as nitric oxide. Toward the soft X-ray end of the range, for wavelengths less than about 165 Å, the intensity of the solar radiation drops off rapidly. Too, the absorption cross sections of the atmospheric constituents decrease rapidly at the shorter wavelengths, allowing whatever radiation there is to penetrate well below the F region.

Most of the information available to date concerning the flux of solar X-ray and EUV radiation incident on the atmosphere has come from rocket experiments that enabled brief glimpses of the spectrum. More recently, spectrometers have been mounted in satellites to obtain more continuous observations of the solar flux. Neupert et al [1964] have reported observations of the spectrum from 50 to 400 Å over a 3-month interval during which the OSO-1 satellite was functioning. Data from other satellites in the OSO series should soon expand these observations.

For ionospheric problems, the main interest concerning solar radiation observations lies in the total flux incident on the atmosphere in various wavelength bands. The limits of the bands of interest are generally based upon natural features of the solar spectrum itself, on ionization potentials of the atmospheric constituents, and on wavelengths at which the absorption cross sections of various constituents change abruptly. Hinteregger et al [1965] have summarized the flux in 11 major groups and 91 subgroups of the solar spectrum from 1750 to 1 Å, based mainly on rocket observations during July 1963, a period of low sunspot activity.

Table 1 summarizes their data for three broad wavelength bands.

The portion of the solar radiation spectrum of interest here contains some detectable continuum but is mainly composed of the emission

Table 1

PHOTON AND ENERGY FLUX ABOVE THE ATMOSPHERE
DURING LOW SUNSPOT ACTIVITY

Wavelength Range (Å)	Photon Flux (photons/m^2/s)	Energy Flux (mW/m^2)
1027-911	13.4×10^{13}	0.27
911-165	50.5×10^{13}	2.55
165-1	3.0×10^{13}	0.70

From Hinteregger et al, 1965.

lines associated with the constituents of the solar corona and chromosphere. The most prominent feature of the spectrum in the 165 to 911 Å range is the He II Lyman α line at 304 Å, which contains about 7 or 8 percent of the total flux in this range.

C. Neutral Atmosphere

Not surprisingly, the properties of the ionosphere are strongly dependent upon the properties of the neutral atmosphere from which the ionization is produced. In relatively recent years, rockets and satellites have considerably expanded the amount of quantitative data available concerning the atmospheric density and pressure, its composition, and its temperature at ionospheric altitudes.

The density of the atmosphere, for example, has been derived directly from observations of the atmospheric drag on artificial satellites. Measurements of the change in period of satellites with known area-to-mass ratios yield the atmospheric density near the altitude of perigee. The technique has been used to determine systematically the densities between about 200 and 800 km (see Jacchia [1965a] and references contained therein). Below 200 km, most density measurements have come from rocket soundings [Champion, 1965].

The determination of the composition of the upper atmosphere is a more difficult problem. Consequently, the amount of data available in this area is limited. Data have been obtained with rocketborne mass spectrometers [Nier et al, 1964] and from measurement of the absorption of solar ultraviolet radiation as a function of altitude [Hall et al, 1965]. The second technique is in principle more accurate since it does not require correcting for vehicle contamination effects. However, the absorption measurements are limited at present by lack of accurate values for the absorption cross sections of the atmospheric constituents.

Data concerning the temperature of the neutral atmosphere in the F region have been derived primarily from the density vs altitude profiles obtained from satellite drag data and rocket soundings [Jacchia and Slowey, 1964].

A model for the neutral atmosphere, constructed to be as consistent as possible with the observations, is the COSPAR International Reference Atmosphere 1965, commonly referred to as CIRA 1965. Figures 3, 4, and 5

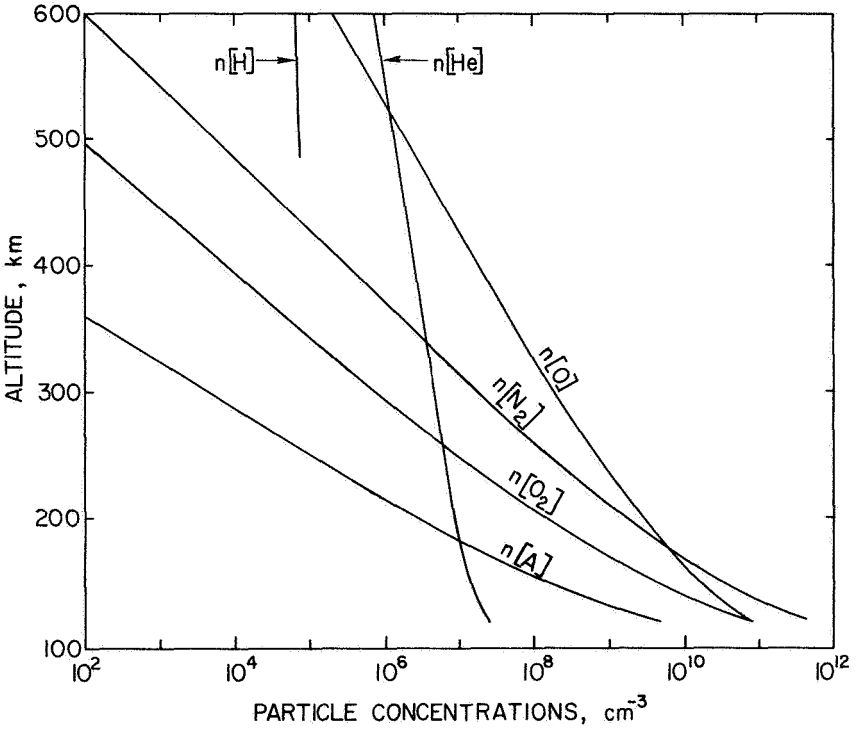

Fig. 3. CONCENTRATIONS OF NEUTRAL CONSTITUENTS OF THE ATMOSPHERE FOR PERIODS OF VERY LOW SUNSPOT ACTIVITY. The data were taken from CIRA 1965, Model 1, for 0600 local time.

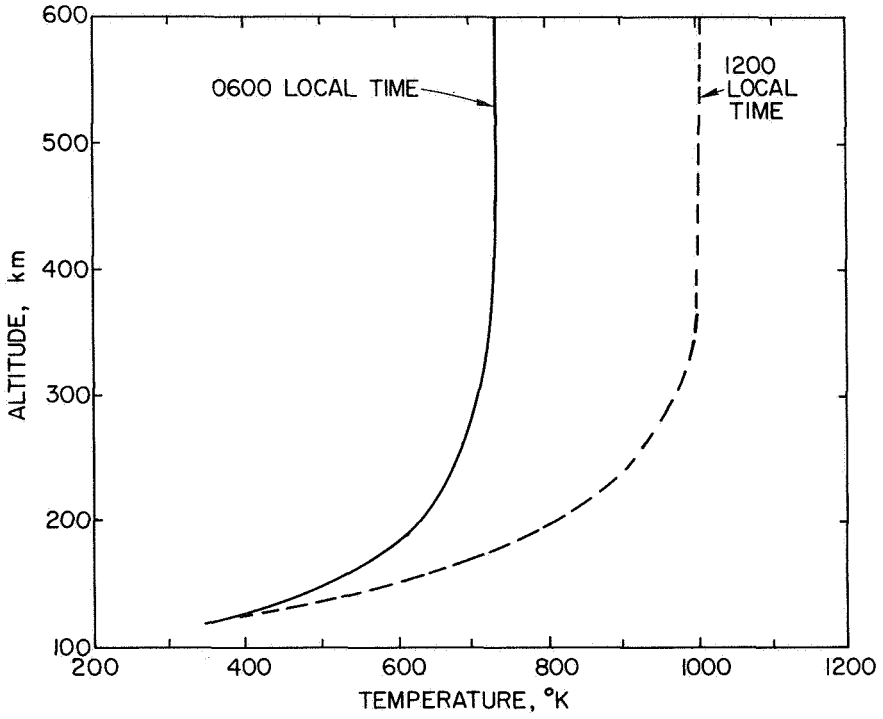

Fig. 4. TEMPERATURE OF THE NEUTRAL ATMOSPHERE FOR PERIODS OF VERY LOW SUNSPOT ACTIVITY. The data were taken from CIRA 1965, Model

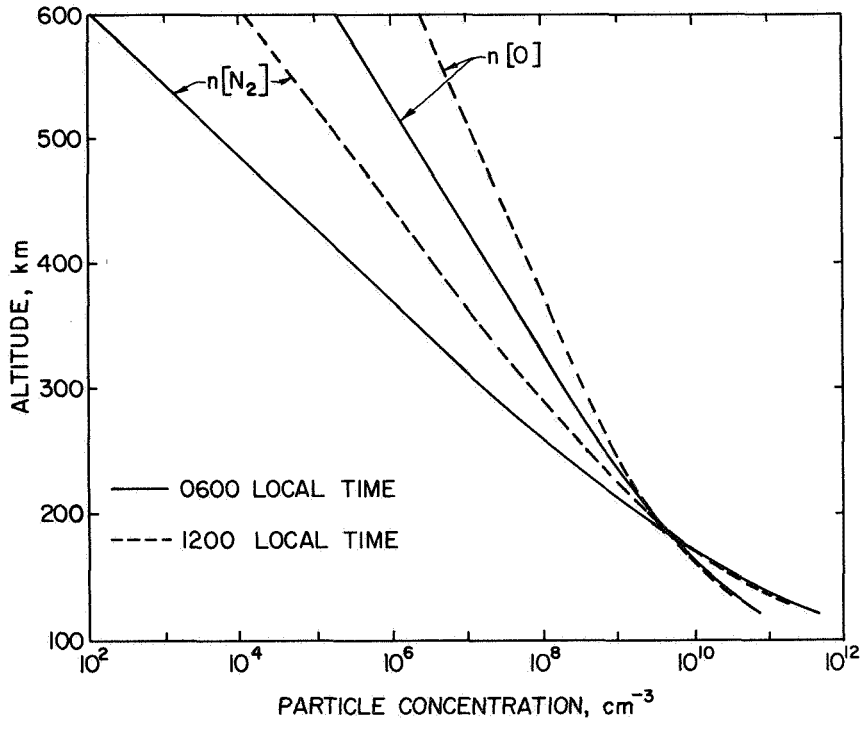

Fig. 5. DIURNAL VARIATION OF THE ATOMIC OXYGEN AND MOLECULAR NITROGEN CONCENTRATIONS. The data were taken from CIRA 1965, Model 1.

are based on this model, and apply in periods of very low sunspot activity. As indicated in Fig. 3, the neutral gas consists mainly of oxygen and nitrogen. Since oxygen is easily dissociated by solar ultraviolet radiation, it exists primarily in the atomic form in the F region. Nitrogen, however, remains almost entirely in the molecular form. The other constituents are all of very minor importance in the F region. The ionization itself is only a minor constituent in the F region. The concentration of electrons is generally less than 0.1 percent of the concentration of neutral species even at the altitude of maximum electron concentration.

Above about 120 km, the neutral gases are all in diffusive equilibrium. Each gas is distributed independently of the others so that its own partial pressure decreases exponentially with altitude. The exponential scale height H for each constituent is given by

$$H = \frac{kT}{mg} \tag{2-2}$$

where k is Boltzmann's constant, T is the absolute temperatue, m is the molecular mass of the constituent, and g is the acceleration of gravity. Despite the fact that H may not be independent of altitude, the partial pressure of any constituent may be expressed as

$$p = p_o e^{-z} \tag{2-3}$$

where z is the so-called reduced height measured from a convenient reference altitude, h_o, and is defined by

$$z = \int_{h_o}^{h} \frac{dh}{H} \tag{2-4}$$

When H can be considered to be independent of altitude, the reduced height is simply

$$z = \frac{h - h_o}{H} \tag{2-5}$$

Figure 4 shows that at sunrise most of the temperature increase with altitude occurs below 200 km. Above 200 km, T is only a slowly varying function of altitude. Since the acceleration of gravity varies even more slowly with altitude, the scale height of any atmospheric constituent is not a rapidly varying function of altitude in, say, the 200 to 600 km range. Below 200 km, the scale height does decrease rapidly due to the decreasing temperature.

Figure 4 also indicates a pronounced diurnal variation in the temperature of the upper atmosphere, which in turn results in a diurnal variation in the distribution of the neutral constituents (Fig. 5). The temperature of the thermosphere ranges from about 700°K at night to about 1000°K in midday during periods of low solar activity. During years of high solar activity, the diurnal variation may be shifted upward to a night to day range of about 1300 to 2000°K.

D. Photoionization

The rate of photoionization of a gas is proportional both to the concentration n of the gas and to the intensity I of the ionizing radiation. The proportionality constant, when the radiation intensity is expressed as a photon flux, is known as the ionization cross section and will be represented by the symbol, σ'. Hence the photoionization rate as a function of altitude for a single constituent of the atmosphere can be expressed as

$$q(h) = \sigma' I(h)\, n(h) \qquad (2\text{-}6)$$

where either radiation of only one wavelength is considered or, equivalently, a band of radiation over which σ' remains constant is considered. The radiation intensity at an altitude h can be conveniently expressed in terms of an optical depth τ as

$$I(h) = I_{\infty} e^{-\tau(h)} \qquad (2\text{-}7)$$

where I_{∞} is the intensity above the atmosphere and τ is a measure of the attenuation due to passage through part of the atmosphere. The optical

depth is a function of the absorption cross section, σ, and the concentrations of the constituents responsible for the absorption along the path of the radiation. When only one constituent is involved, the relation is given by the line integral

$$\tau(h) = \sigma \int_{L_h} n \, ds \tag{2-8}$$

where n is the concentration of the constituent and L_h is the radiation raypath from the sun to a point at altitude h. For the case of an isothermal atmosphere, where n varies as $\exp(-h/H)$, the integral in (2-8) has been evaluated [Chapman, 1931] with the result expressed as

$$\tau(h) = \sigma n(h) \, H \, Ch(\chi,H) \tag{2-9}$$

The Chapman function $Ch(\chi,H)$ closely approximates $\sec \chi$ for $\chi < 70°$ but does not become infinite as χ approaches 90° (Fig. 6). The angle χ is the solar zenith angle.

To be precise, $Ch(\chi,H)$ is not a function of χ and H. Rather it is a function of χ and $H/(R_E + h)$, where R_E is the radius of the earth and h is the altitude. However, R_E (6370 km) is so much larger than h in the F region of the ionosphere (150 to 600 km) that the sum, $(R_E + h)$, can be considered constant for most purposes without leading to significant errors.

A combination of Eqs. (2-6), (2-7), and (2-9) yields the Chapman production formula for a single constituent, isothermal atmosphere, exposed to monochromatic ionizing radiation:

$$q = q_o \exp[1 - z - Ch(\chi,H) \, e^{-z}] \tag{2-10}$$

Here the altitude variations have been expressed in terms of the reduced height of Eq. (2-5). The reference level at which $z = 0$ has been chosen to be the altitude at which $\sigma n H = 1$, that is, the altitude of unit optical depth for an overhead sun ($\chi = 0$). For $\chi = 0$, the peak rate of

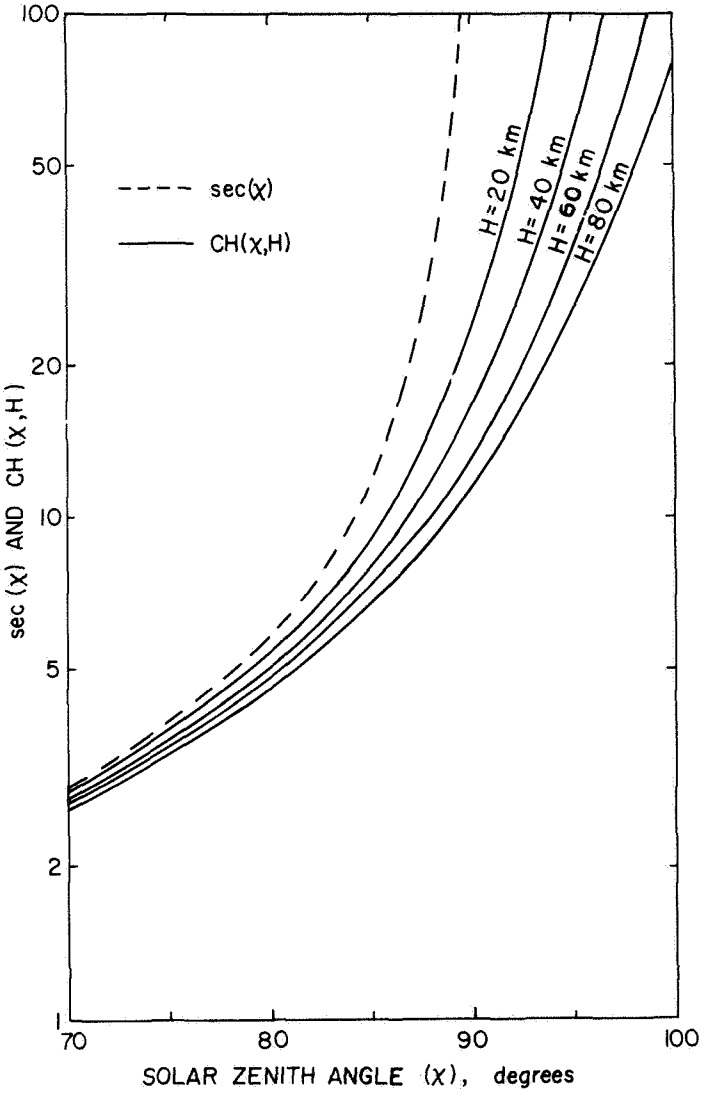

Fig. 6. SEC (χ) AND $CH(\chi,H)$ VS χ FOR SEVERAL SCALE HEIGHTS. The geocentric radius, which also influences the value of $Ch(\chi,H)$, was taken to be 6700 km.

photoionization occurs at the level $z = 0$ and is given by

$$q_o = \frac{\sigma'}{\sigma} \frac{I_\infty}{eH} \tag{2-11}$$

In general, the magnitude of the peak production rate, q_m, and the level of its occurrence, z_m, are given by

$$q_m = \frac{q_o}{Ch(\chi,H)} \tag{2-12}$$

and

$$z_m = \ln [Ch(\chi,H)] \tag{2-13}$$

Substituting $z' = z - z_m$ into (2-10) gives

$$q = q_m \exp(1 - z' - e^{-z'}) \tag{2-14}$$

indicating that the shape of the production profile is independent of χ while the peak value of q varies as $[Ch(\chi,H)]^{-1}$. Figure 7 illustrates the Chapman production profile for four zenith angles.

For accurate calculations of the photoionization rates in the ionosphere, the theory outlined above can be generalized to consider the

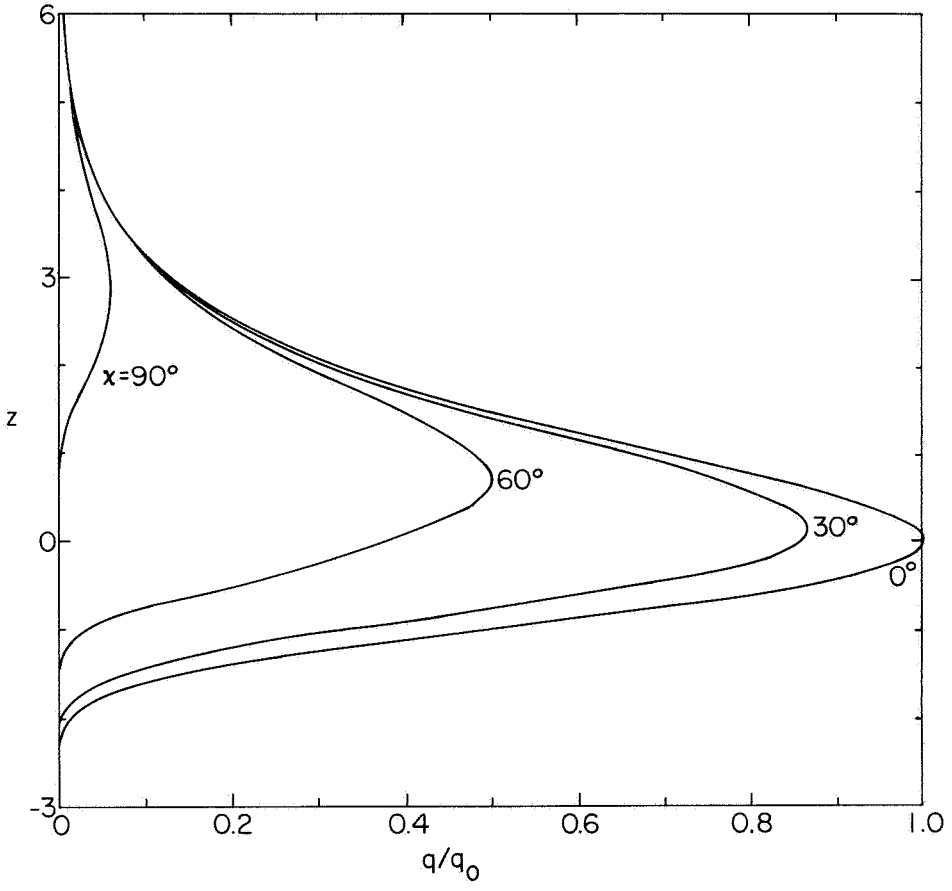

Fig. 7. NORMALIZED CHAPMAN PRODUCTION PROFILES, $\exp[1 - z - Ch(\chi,H)e^{-z}]$ VS z, FOR $H = 40$ km.

effect of several different gases in the atmosphere and to account for the wavelength dependence of σ and σ' for each gas. The entire radiation spectrum that produces the ionization can be divided into numerous bands, each of which covers a range of wavelengths small enough to allow the absorption and ionization cross sections of each constituent to be considered constant across the band. The optical depth for any one of these bands would be given by a sum of terms like that on the right-hand side of Eq. (2-8)--one term for each constituent with a nonzero σ. A substitution of the optical depth into Eq. (2-7), followed by a substitution of the resulting $I(h)$ and an appropriate value for σ' into Eq. (2-6), yields the photoionization rate for one constituent due to the band of radiation considered. To obtain the total photoionization rate, summations over all the constituents and all the bands of radiation are necessary.

Figure 8 shows the results of such calculations, using the radiation flux, absorption cross sections, and ionization cross sections published by Hinteregger et al [1965] and a COSPAR model for the neutral atmosphere. The spectrum between 911 and 165 Å has been divided into 46 bands for the numerical calculations, and the 165 to 1 Å range has been divided into 12 bands. Though the situation is more complicated than that described by the Chapman formula, the results are similar to Chapman production profiles. The absorption cross sections tend to be significantly smaller for X-rays (165 to 1 Å) than for the EUV radiation from 911 to 165 Å. Hence the peak rates of the photoionization due to X-rays occur at lower altitudes where the concentrations of the neutral constituents are greater.

Radiation of wavelengths greater than 911 Å does not have sufficient energy to ionize either O or N_2, though it can produce O_2^+ ions. Since the absorption cross sections of both N_2 and O_2 are highly variable in this part of the spectrum, detailed calculations of the O_2^+ production rates were somewhat difficult and were not performed. However, Hinteregger et al have taken into account those variations. They have shown, using a different but similar model atmosphere, that the peak rate of photoionization of O_2 due to 1027 to 911 Å radiation occurs at virtually the same altitude as the peak rate of production of <u>all</u> ions due to 165 to 1 Å radiation. They also found, and it will be assumed as an approximation in this report, that the total production of O_2^+ ions by 1027 to 911 Å radiation is nearly twice the total production of all ions by 165 to 1 Å radiation.

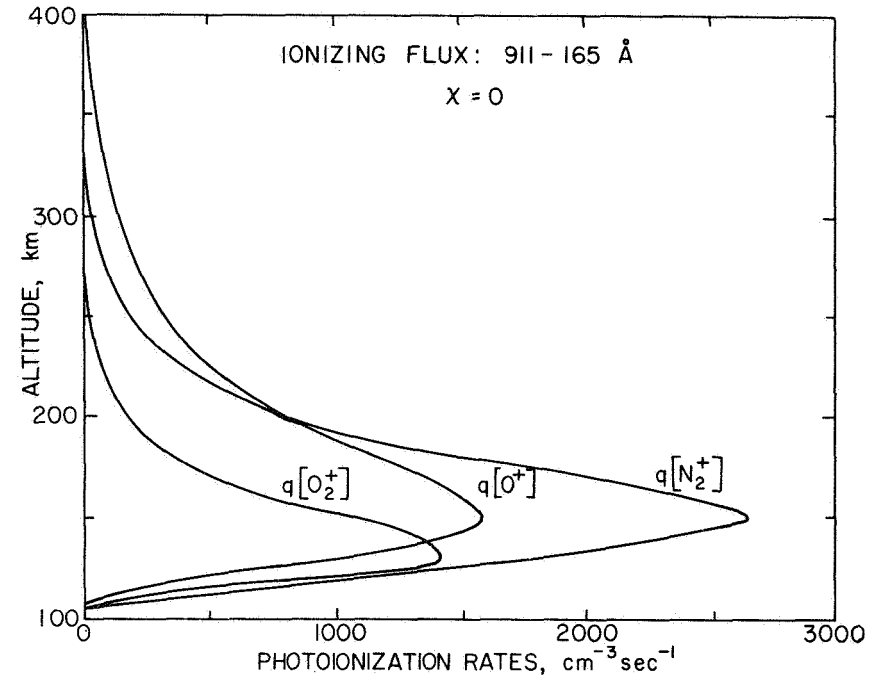

(a)

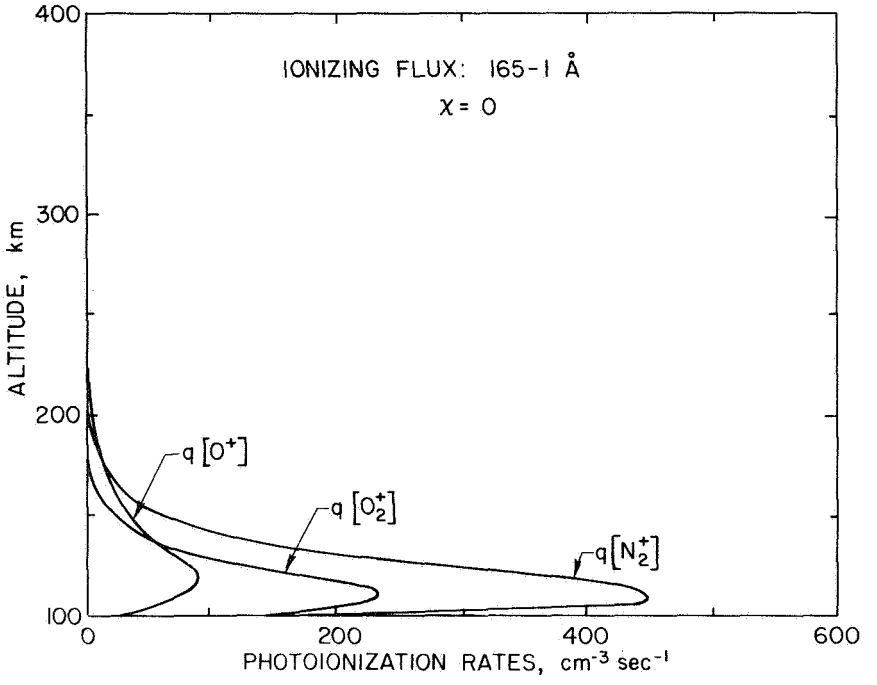

(b)

Fig. 8. PHOTOIONIZATION RATES BASED UPON CIRA 1965, MODEL 1, AND UPON THE SOLAR RADIATION FLUXES, ABSORPTION CROSS SECTIONS, AND IONIZATION CROSS SECTIONS PUBLISHED BY HINTEREGGER ET AL [1965]. At $\chi = 0$, the model atmosphere for 1200 local time was used; at $\chi = 90^{\circ}$, the model for 0600 local time was used.

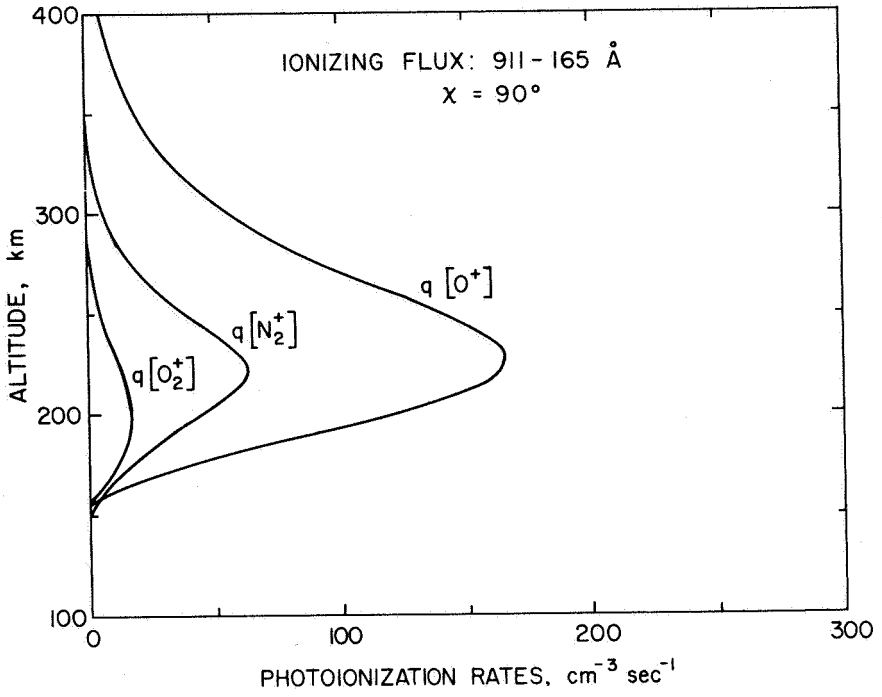

(c)

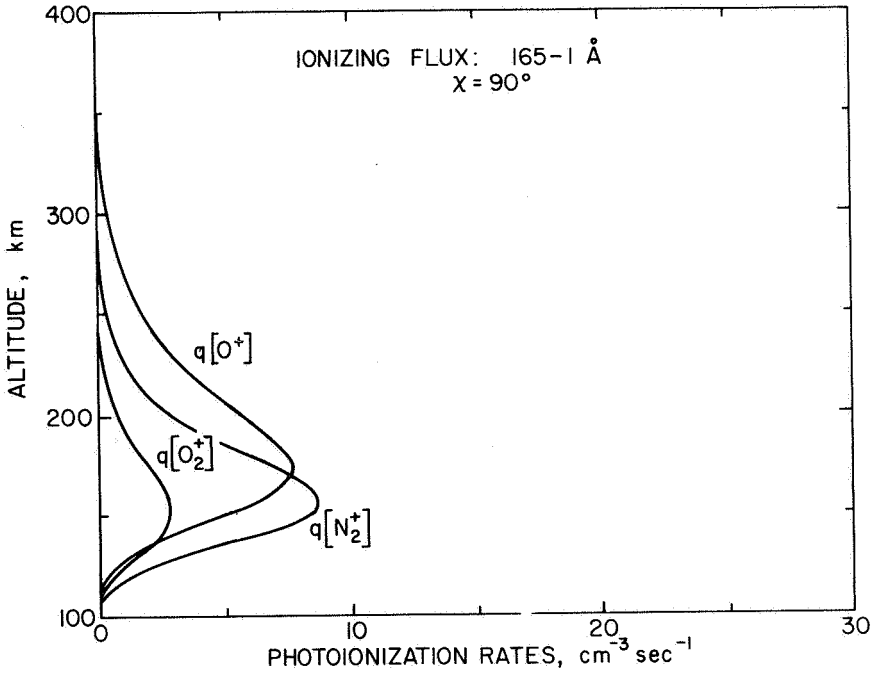

(d)

Fig. 8. CONTINUED.

Tables 2 and 3 present the results of a vertical integration of the production profiles shown in Fig. 8. The figures in these tables give the total number of ions produced per unit time in a vertical column of unit cross-sectional area extending all the way through the atmosphere. The approximate integrated rate of production of O_2^+ ions by radiation in the 1027 to 911 Å range is also included.

The data in Tables 2 and 3 indicate that most of the ionization, especially at sunrise ($\chi = 90°$), but also with an overhead sun ($\chi = 0°$), is produced by EUV radiation with wavelengths ranging from 911 to 165 Å. At sunrise, the peak photoionization rate occurs at a relatively high altitude where atomic oxygen is the dominant neutral constituent (Fig. 3). Hence at $\chi = 90°$, about 67 percent of the ionization produced is O^+. With the sun overhead, the ionizing flux penetrates more deeply into the

Table 2

INTEGRATED PHOTOIONIZATION RATES FOR $\chi = 0$

(10^{13} m^{-2} s^{-1})

Ion Produced	Wavelength Ranges (Å)			Totals
	1027-911	911-165	165-1	
O^+	0	14.2	0.5	14.7
N_2^+	0	17.7	1.7	19.4
O_2^+	6.0	7.3	0.8	14.1
Totals	6.0	39.2	3.0	48.2

Note: Values are based on atmosphere model 1 for 1200 local time from CIRA 1965, and upon the flux and cross sections published by Hinteregger et al [1965]. No secondary ionization is included. The integrated rate of production of O_2^+ ions by 1027 to 911 Å radiation was obtained by doubling the total integrated photoionization rate for 165 to 1 Å radiation (see text).

Table 3

INTEGRATED PHOTOIONIZATION RATES FOR $\chi = 90^{\circ}$
$(10^{13}\ m^{-2}\ s^{-1})$

Ion Produced	Wavelength Ranges (Å)			Totals
	1027-911	911-165	165-1	
O^+	0	1.74	0.06	1.80
N_2^+	0	0.48	0.04	0.52
O_2^+	0.24	0.12	0.02	0.38
Totals	0.24	2.34	0.12	2.70

Note: Values are based upon atmosphere model 1 for 0600 local time from CIRA 1965, and upon the flux and cross sections published by Hinteregger et al [1965]. No secondary ionization is included. The integrated rate of production of O_2^+ ions by 1027 to 911 Å radiation was obtained by doubling the total integrated photoionization rate for 165 to 1 Å radiation (see text).

atmosphere and the three constituents contribute more nearly equal amounts to the total production of ionization.

E. Loss Processes in the F Region

Once a positive ion and a free electron have been formed in the ionosphere, numerous possible reactions could lead to their disappearance. Only those reactions considered to be important at altitudes above 150 km, where virtually all of the photoionization at sunrise takes place, will be considered here.

In the process of recombination, two bodies, an ion and an electron, combine. Conservation of both energy and momentum would be impossible in this process unless two bodies are still present after the recombination. Two bodies may be present afterward, for example, when the recombination is a result of a three-body collision, with the third body some neutral

atom or molecule. However, above 150 km, the gas pressure is so low as to make three-body collisions virtually nonexistent. Three-body interactions cannot account for any significant amount of recombination in the F region.

The problem of conservation of energy and momentum is solved in the case of molecular ions by a dissociation of the molecule accompanying the recombination. The rate coefficient for dissociative recombination, as this process is called, is greater than 10^{-7} cm^3/s for the molecular ions of importance in the F region [Ferguson, 1967].

Radiative recombination, that is, recombination accompanied by the emission of a photon, is the only possibility for atomic ion-electron recombination. The rate coefficient for this process is approximately 10^{-2} cm^3/s [Ratcliffe and Weekes, 1960], or about five orders of magnitude less than that for dissociative recombination. For this reason, radiative recombination does not account for the removal of a significant amount of F region ionization. Atomic ions, such as O^+, are far more likely to be removed through a reaction with a neutral molecule, forming a molecular ion, followed by a dissociative recombination of the molecular ion.

Table 4 contains a list of the reactions believed to be most important in determining the electron and ion densities in the F region. The O^+ ions are removed by an ion-atom interchange with either O_2 or N_2, followed by dissociative recombination reactions (5) or (7). There is still considerable disagreement, however, as to which reactions are important in the removal of N_2^+ ions [Rishbeth, 1967]. Dissociative recombination, reaction (6), is perhaps the most obvious possibility, but reaction (3) followed by (7) is thought to be far more important [Johnson, 1967]. It is also possible that a significant portion of the N_2^+ ions are converted to O^+ ions through the charge transfer reaction (4).

Measurements of the distribution of positive ions between about 130 and 240 km during sunspot minimum conditions have been obtained by Holmes et al [1965]. Data obtained from a rocket flight over White Sands, New Mexico, during February 1963 show that above about 190 km, at 0934 local standard time, over 90 percent of the ionization consists of O^+ ions. The next most abundant ionic species are NO^+ and O_2^+, both of which exist in approximately equal concentrations. Significantly, N_2^+ ions are virtually

Table 4

REACTIONS INVOLVING F REGION IONS

Reaction	Rate Coefficient* at 300°K (cm^3/s)
Ion-atom Interchange:	
(1) $O^+ + N_2 \rightarrow NO^+ + N$	$1 - 5 \times 10^{-12}$
(2) $O^+ + O_2 \rightarrow O_2^+ + O$	$20 - 40 \times 10^{-12}$
(3) $N_2^+ + O \rightarrow NO^+ + N$	2.5×10^{-10}
Charge Transfer:	
(4) $N_2^+ + O \rightarrow N_2 + O^+$	$< 0.1 \times 10^{-10}$
Dissociative Recombination:	
(5) $O_2^+ + e^- \rightarrow O + O$	1.7×10^{-7}
(6) $N_2^+ + e^- \rightarrow N + N$	$\sim 3 \times 10^{-7}$
(7) $NO^+ + e^- \rightarrow N + O$	$\sim 6 \times 10^{-7}$

*The rate coefficients are taken from Johnson [1967]. The appropriate original references are included therein.

nonexistent (less than 1 percent of the total) at all altitudes. Since a substantial portion of the photoionization results in the production of N_2^+ (Fig. 8), the removal of this ion must proceed very rapidly compared with the rate of removal of O^+ ions.

To study in more detail the processes involving O^+, which is by far the dominant F region ion, consider the following pair of reactions:

$$O^+ + XY \rightarrow XO^+ + Y \qquad (2\text{-}15)$$

$$XO^+ + e^- \rightarrow X + O \qquad (2\text{-}16)$$

Here the symbol XY has been used to represent a molecule such as O_2 or N_2. Hence the first of these reactions, (2-15), is equivalent to either (1) or (2) in Table 4, and the second represents either (5) or (7). If γ and α are taken to be the rate coefficients of (2-15) and (2-16), respectively, then the rates of occurrence of the two reactions are given by

$$r_\gamma = \gamma n[O^+]\, n[XY] \tag{2-17}$$

and

$$r_\alpha = \alpha n[XO^+]\, n[e^-] \tag{2-18}$$

where the symbol $n[\ ]$ represents the concentration of the species enclosed within the brackets.

Assume for the moment that O^+ is the only ion produced in the F region. Then under equilibrium conditions the rates r_γ and r_α must be equal. Hence in equilibrium,

$$\frac{n[O^+]}{n[XO^+]} = \frac{\alpha n[e^-]}{\gamma n[XY]} \tag{2-19}$$

It is then apparent that if $\alpha n[e^-] \gg \gamma n[XY]$, O^+ ions account for almost all of the ions present. Under this condition, reaction (2-16) proceeds much more readily than (2-15). It will take some time for an O^+ ion to undergo an ion-atom interchange with XY, but once the reaction occurs, the resulting molecular ion will disappear much more rapidly. The electron concentration will then remain essentially equal to $n[O^+]$ and the rate of loss of electrons, ℓ, will be the same as r_γ. Thus,

$$\ell = \beta n[e^-] \tag{2-20}$$

where

$$\beta = \gamma n[XY]$$

The loss rate is proportional to the electron concentration, with β the proportionality constant or linear loss coefficient. With β proportional to $n[XY]$, the loss coefficient must decrease with altitude. Specifically, if the reduced height is referred to the scale height of atomic oxygen, and if k is used to represent the ratio of the molecular weight of XY to the atomic weight of oxygen, then

$$\beta = \beta_o \, e^{-kz} \tag{2-21}$$

The gas XY could be either N_2 or O_2 [Rishbeth and Setty, 1961], in which case k would be either 1.75 or 2.0.

The case considered above, that is, $\alpha n[e^-] \gg \gamma n[XY]$, is consistent with the observations of Holmes et al [1965], which show that $n[O^+] \approx n[e^-]$ above 190 km. However, proceeding to lower altitudes, $n[e^-]$ decreases and $n[XY]$ increases until a point is eventually reached where $\alpha n[e^-] \ll \gamma n[XY]$. At this point, according to Eq. (2-19), the molecular ions should be more numerous than the O^+ ions. Holmes et al [1965] did indeed find O_2^+ and NO^+ more abundant than O^+ below about 160 km.

When $\alpha n[e^-] \ll \gamma n[XY]$, (2-16) is the limiting reaction that determines the electron loss rate. The loss rate is then essentially equal to r_α and $n[e^-] \approx n[XO^+]$. Thus

$$\ell = \alpha n^2[e^-] \tag{2-22}$$

The loss rate under these conditions is proportional to the square of the electron concentration, and α is the "square law" loss coefficient.

In a transition region between these two extremes, that is, when ℓ is neither proportional to $n[e^-]$ nor to $n^2[e^-]$, the loss rate can be expressed as [Rishbeth, 1967]

$$\frac{1}{\ell} = \frac{1}{\alpha n^2[e^-]} + \frac{1}{\beta n[e^-]} \tag{2-23}$$

The discussion above distinguishing between regions of linear and square-law loss relationships was based upon equilibrium considerations that apply throughout most of the day in the F region. During periods of nonequilibrium, such as at sunrise, the analysis is complicated by the fact that $r_\gamma \neq r_\alpha$. The nonequilibrium case is considered in Section IV-E.

F. Movements of Ionization

The transport term in the continuity equation, (2-1), accounts for variations in the electron density due to the motion of the plasma. The movements of ionization may be due to (1) motions of the neutral atmosphere that tend to carry the ionized gas with it, (2) diffusion of the plasma through the neutral gas, or (3) electromagnetic forces.

The daily temperature variation in the F region, illustrated in Fig. 4, results in thermal expansion and contraction of the neutral atmosphere causing the air to move both horizontally and vertically. The plasma tends to follow these motions, subject to constraints imposed upon it by the earth's magnetic field. In the F region, collision frequencies are low enough that it is a good approximation to assume that such motions of the plasma must be directed along magnetic field lines. At lower altitudes, where collision frequencies are higher, atmospheric winds can move the plasma perpendicular to the magnetic field.

Neutral winds or tidal oscillations may tend to move charged particles across the geomagnetic field below the F region (in the E region) and thereby generate an induced electric field. Since the plasma in the F region is a good electrical conductor in the direction of the magnetic field, the effects of the electric field induced in the E region are in turn felt in the F region. The electric field $\overline{E}$ mapped into the F region is directed normal to the geomagnetic field $\overline{B}$ and can result in a motion of the ionization across the magnetic field lines with a velocity proportional to $\overline{E} \times \overline{B}$. A detailed review of this subject is given by Maeda and Kato [1966].

At altitudes above the level of the peak electron concentration, diffusion is a dominant factor in determining the concentration of electrons. Electrons and ions diffuse through the neutral gas under the

influence of gravity and concentration gradients in the ionosphere. The ions and electrons tend to diffuse together with a velocity whose vertical component, v_z, can be written as [Ratcliffe and Weekes, 1960]

$$v_z = -D \left(\frac{1}{N} \frac{\partial N}{\partial n} + \frac{1}{2H} \right) \sin^2 \Theta \qquad (2\text{-}24)$$

where D is the ambipolar diffusion coefficient given by

$$D = \frac{2kT}{m\nu} \qquad (2\text{-}25)$$

The inclination of the magnetic field with respect to the horizontal is represented by Θ. Here it has been assumed that only one ion species is present with a scale height $H = kT/mg$, where m is the mass of the ion. The symbol ν represents the ion-neutral collision frequency which, since it is proportional to the neutral gas concentration, decreases with altitude as e^{-z}. Hence the diffusion coefficient increases exponentially with altitude and may be expressed in terms of the reduced height as

$$D = D_o e^{z} \qquad (2\text{-}26)$$

The increasing diffusion rates at high altitudes result in a peak in the electron density profile. If the electron density in equilibrium were only due to a balance between production and loss with a loss coefficient decreasing with altitude as in Eq. (2-21), N would increase without limit as a function of altitude, at least until limited by another factor, such as exhaustion of the neutral species.

Chapter III

MEASUREMENT OF FARADAY ROTATION

The experimental data used in this work consisted of measurements of the amount of Faraday rotation imposed on transmissions from a geostationary satellite. This chapter discusses the mechanism leading to Faraday rotation of the plane of polarization of a linearly polarized radio wave. It also contains a description of the satellite whose transmissions were used, a discussion of the technique for measuring the amount of Faraday rotation imposed upon those transmissions, and an estimate of the accuracy of the measurements.

A. The Theory

Consider a linearly polarized electromagnetic wave propagating through a medium containing a static magnetic field and charged particles that can move under the influence of the wave. Provided the direction of propagation does not come too near to being normal to the static magnetic field lines, the wave will have its plane of polarization rotated as it passes through the medium. The phenomenon, known as Faraday rotation, is best explained by considering the linearly polarized wave to be composed of two circularly polarized components. The amplitudes of the two components are equal, but their polarizations are in opposite senses. Lorentz [1906] showed that circularly polarized electromagnetic waves propagating along magnetic field lines in such a medium are characteristic waves in the sense that they will undergo no change in polarization. The waves will, however, propagate with different velocities, depending on whether they are polarized in a clockwise or in a counterclockwise sense. Thus the phase relationship between the circularly polarized components of a linearly polarized wave, and hence the orientation of the plane of polarization, will change as the wave propagates through the medium.

The Lorentz theory was originally applied to the propagation of light through solids. Later it was extended and applied specifically to the

propagation of radio waves through the ionosphere [Appleton, 1932]. According to the theory developed by Appleton, under certain assumptions considered below, the difference between the indices of refraction for the two circularly polarized components of a linearly polarized wave at any point in the ionosphere is proportional to both the electron concentration and the component of the geomagnetic field in the direction of propagation. It follows that the amount of rotation of the plane of polarization per unit distance along the propagation path is also proportional to the electron concentration and to the magnetic field strength. The total Faraday rotation for propagation along a path L_p through the ionosphere is given by [see Browne et al, 1956]

$$\Omega = \frac{K}{f^2} \int_{L_p} N\mathcal{H} \cos\theta \, ds \qquad (3\text{-}1)$$

where Ω is measured in radians, K is a constant with a numerical value of 0.0297 in MKS units, f is the wave frequency, N is the concentration of electrons, $\mathcal{H}$ is the magnetic field intensity, θ is the angle between the magnetic field and the direction of propagation, and ds is an element of length along the path of propagation.

In order for Eq. (3-1) to hold, the wave must be propagating in the so-called quasi-longitudinal mode. Ratcliffe [1959] has shown that this will be the case if

$$\frac{(Y \sin\theta)^4}{4(Y\cos\theta)^2} \ll \left|(1 - X - iZ)^2\right| \qquad (3\text{-}2)$$

where X is the ratio of the plasma frequency to the wave frequency, Y is the ratio of the electron gyrofrequency to the wave frequency, and Z is the ratio of the electron-neutral collision frequency to the wave frequency.

At the wave frequency used in this study (approximately 136 MHz), Z is negligible. Furthermore, X does not become much greater than 0.01 anywhere along the raypath even at noon, and its magnitude is even less at

sunrise. Under these conditions the quasi-longitudinal approximation will hold as long as θ is not between 88° and 92°. For the present study, θ is approximately 30°.

Though the integral in Eq. (3-1) extends over the entire distance from the observer to the satellite, practically all of the Faraday rotation occurs at altitudes below 1000 km since both $\mathcal{H}$ and N are small at higher altitudes. The factor $(\mathcal{H} \cos \theta)$ is a slowly varying function in the region which contributes most to the integral. Hence Ω can be expressed as [Browne et al, 1956]

$$\Omega = \frac{K}{f^2} \overline{(\mathcal{H} \cos \theta \sec \phi)} \int N \, dh \qquad (3\text{-}3)$$

where the weighted mean of $(\mathcal{H} \cos \theta \sec \phi)$ is equal to its value at an altitude of approximately 350 km [Yeh and Gonzalez, 1960]. In Eq. (3-3), ds has been replaced by $(dh \sec \phi)$, where dh is an element of vertical distance and ϕ is the inclination of the path of propagation with respect to the vertical. The integral $\int N \, dh$ is the electron content of the ionosphere below 1000 km. Thus the Faraday rotation imposed on a wave propagating through the ionosphere is a measure of the ionospheric electron content.

The magnitude of the factor $(\mathcal{H} \cos \theta)$ is very nearly (to within 0.1 percent) proportional to R^{-4}, at F region altitudes, along the path of propagation used in this study. (R is the geocentric radius. The R^{-4} variation results from an R^{-3} variation in $\mathcal{H}$ and an approximate R^{-1} variation in $\cos \theta$.) An R^{-4} variation only results in a decrease in $(\mathcal{H} \cos \theta)$ of 5 percent per 100 km increase in altitude in the F region. For this reason, the amount of Faraday rotation is not sensitive to the exact vertical distribution of electrons, though it is a measure of the columnar electron content of the ionosphere.

B. The Satellite

The transmissions used for making Faraday rotation measurements were provided by VHF telemetry transmitters on board Syncom III. This satellite was launched in August 1964 and placed in a geostationary orbit approximately above the intersection of the equator and the international

date line. After its first few months on station, the satellite was allowed to drift slowly westward. Figure 9 shows the longitude of Syncom III over a 2-year period. Discontinuities in the slope of the curve in Fig. 9 occurred on days when small gas jets on the satellite were used to make slight corrections in its orbit. The inclination of the orbit, and hence the satellite's latitude, remained within a fraction of a degree of zero. The azimuth and elevation of Syncom III as viewed from the recording station at the University of Hawaii are shown in Fig. 10.

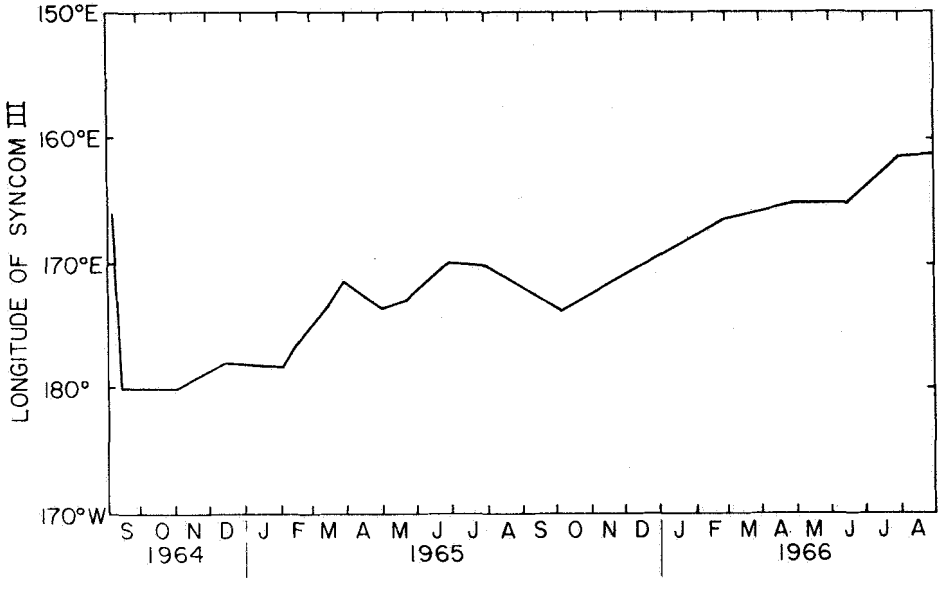

Fig. 9. LONGITUDE OF SYNCOM III VS DATE.

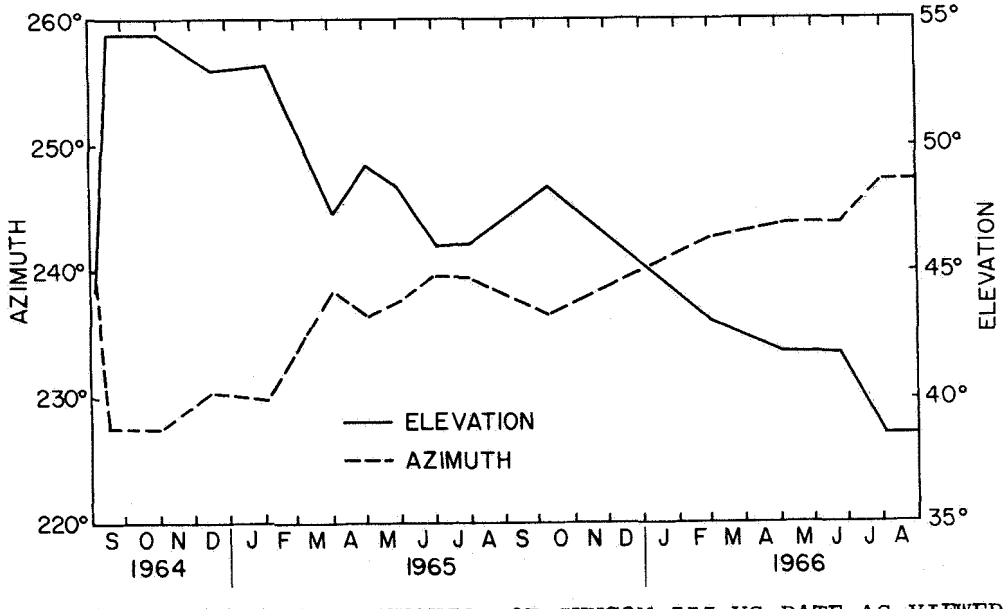

Fig. 10. AZIMUTH AND ELEVATION OF SYNCOM III VS DATE AS VIEWED FROM THE UNIVERSITY OF HAWAII.

The satellite is spin-stabilized with its spin axis parallel to the earth's spin axis. Thus, as viewed from the University of Hawaii, the spin axis of the satellite appears inclined at an angle β_o with respect to the horizontal as indicated in Fig. 11. The angle β_o varies from 46° to 28° as the longitude of the satellite varies from 180° to 161° E, as it did during its first 2 years in orbit.

There are two VHF telemetry transmitters on board the satellite. One transmitter, designated TM1, radiates a wave at 136.980 MHz, which is counterclockwise circularly polarized as viewed toward the south along the satellite's spin axis. The other transmitter, TM2, operates at 136.470 MHz and radiates a clockwise circularly polarized wave toward the south. However, the waves radiated by each transmitter are linearly polarized when viewed from the equatorial plane of the satellite. Since the spin axis is perpendicular to the earth's equatorial plane and since the altitude of the satellite is about 6 earth radii, any observer on the earth will indeed be near the satellite's equatorial plane. Thus the transmissions received at the University of Hawaii were nearly linearly polarized.

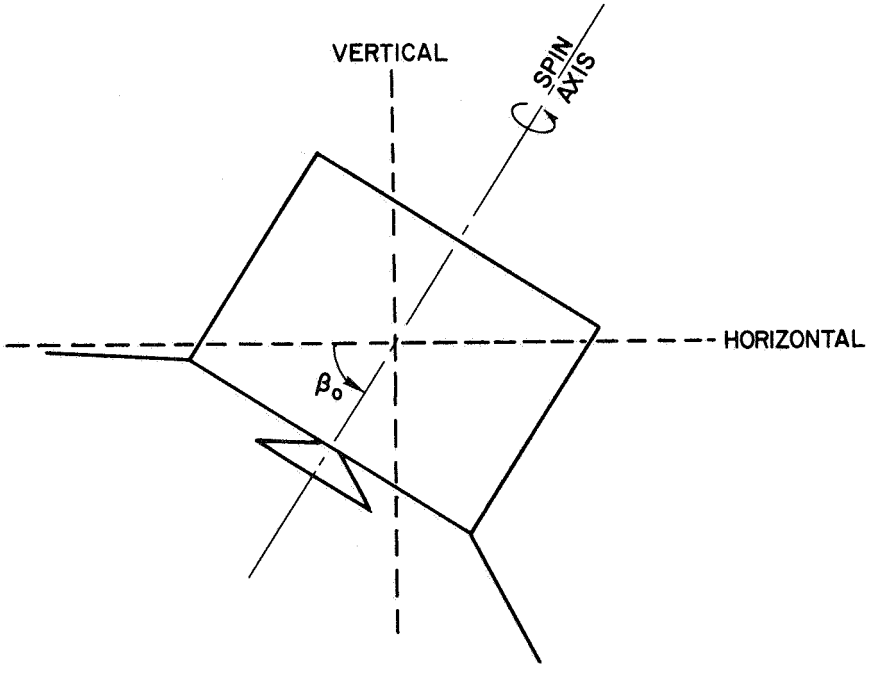

Fig. 11. A SKETCH OF THE SYNCOM III SATELLITE AS VIEWED FROM THE UNIVERSITY OF HAWAII.

A difference in the way the antenna elements are fed by the two transmitters results in the opposite senses of polarization of the circularly polarized waves radiated along the satellite spin axis. It also causes the linearly polarized waves, viewed from the equatorial plane, to be inclined in opposite directions with respect to the spin axis by an angle β_1 (Fig. 12). The angle β_1 was not known before the satellite was launched, but was determined by measuring the change in the received polarization angle that occurred when the transmissions were suddenly switched from transmitter TM1 to transmitter TM2. The total change in polarization angle is of course equal to twice β_1 plus a slight correction due to the difference in the Faraday rotation imposed on the two waves. The correction, which is due to the difference in the frequencies of the waves, is readily determined by Eq. (3-1). It amounts to 0.74 percent. The magnitude of β_1 was found to be 50° [Garriott et al, 1965].

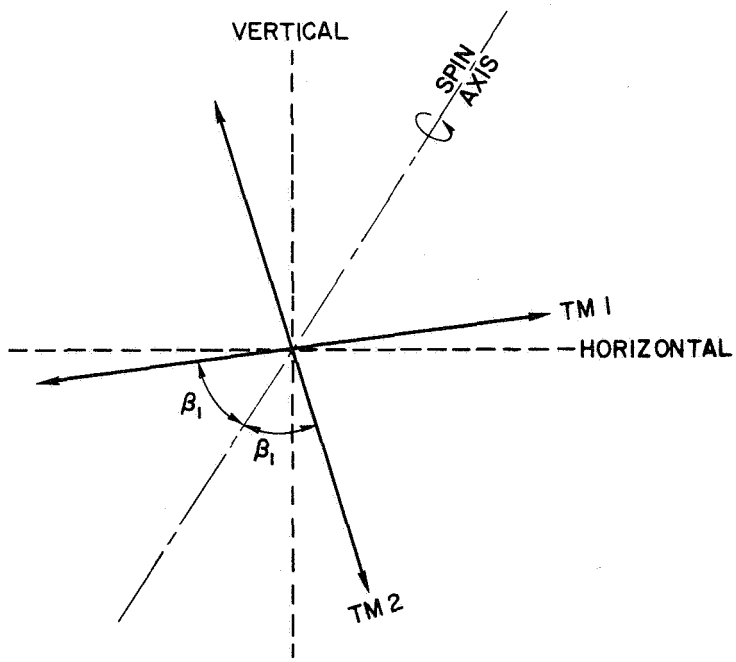

Fig. 12. THE ORIENTATION OF THE TRANSMITTED LINEARLY POLARIZED WAVES FROM TELEMETRY TRANSMITTERS TM1 AND TM2 ON SYNCOM III.

The inclination β of the radiated polarization with respect to the observer's horizon is then given by

$$\beta = \beta_o \pm \beta_1 \qquad (3\text{-}4)$$

The upper sign applied to TM2 and the lower sign to TM1. This angle is then subtracted from the received polarization angle to obtain the total amount of Faraday rotation.

C. The Data

Measurements of the received polarization angle were made at 5 min intervals with a Yagi antenna, which could be rotated about its longitudinal axis. For each measurement, the antenna was rotated first in one direction through an angle of approximately 200°, then back to its original position while both the antenna orientation and received signal strength were being recorded on a strip chart. The antenna passed through a polarization null at least twice. The orientation of the antenna corresponding to each signal strength null was scaled from the chart recording, and an average of the two readings was used to obtain the polarization angle.

The Faraday rotation Ω is computed from

$$\Omega = P_M - \beta + n\pi \qquad (3\text{-}5)$$

where β is given by Eq. (3-4), n is an integer, and P_M is the measured polarization angle obtained as an average of the two separate observations, P_{M1} and P_{M2}, made within a few seconds of the same time. The measurement is ambiguous by $n\pi$ radians as any polarization measurement must be. However, the ambiguity can be resolved at night when the electron content, and hence Ω, is small [Garriott et al, 1965]. The nighttime minimum values of Ω were typically between 50° and 100°. During midday, Ω often exceeded 1000°.

The amount of random error involved in P_M can be estimated from the differences between the two separate measurements, P_{M1} and P_{M2}, which have been averaged. If P_A is taken to be the actual polarization of the wave arriving at the receiving station, then the measurements, which contain random errors, can be expressed as

$$P_{M1} = P_A + \epsilon_1 \qquad (3\text{-}6)$$

and

$$P_{M2} = P_A + \epsilon_2 \tag{3-7}$$

where ϵ_1 and ϵ_2 are the random errors associated with each measurement. Likewise, P_M, which is an average of P_{M1} and P_{M2}, may be written as

$$P_M = P_A + \epsilon \tag{3-8}$$

where

$$\epsilon = \frac{1}{2} (\epsilon_1 + \epsilon_2) \tag{3-9}$$

The individual measurements, P_{M1} and P_{M2}, are assumed to have been made at the same time, so that P_A is the same for each measurement.

If ϵ_1 and ϵ_2 both have the same distribution and are symmetrically distributed about zero, then the standard deviation in $(\epsilon_1 + \epsilon_2)$ is the same as that in $(\epsilon_1 - \epsilon_2)$. Hence the standard deviation in ϵ, $\sigma[\epsilon]$, is given by

$$\sigma[\epsilon] = \sigma \left[\frac{1}{2} (\epsilon_1 - \epsilon_2)\right] \tag{3-10}$$

Since $(\epsilon_1 - \epsilon_2)$ is the difference between P_{M1} and P_{M2}, its standard deviation can readily be obtained.

Figure 13 shows the distribution of ϵ for a representative 2-month interval, including over 17,000 data points. Clearly, the distribution is approximately normal with a standard deviation of 4.7°. Faraday rotation measurements used in this study can thus be expected to include random errors with a root-mean-square value of 4.7°, or somewhat less than 10 percent of the total Faraday rotation during the early morning hours before sunrise. The measurements may also contain slight fixed errors. These errors, however, should amount to less than 10° [Garriott et al, 1965], and are entirely insignificant insofar as the results reported here are concerned.

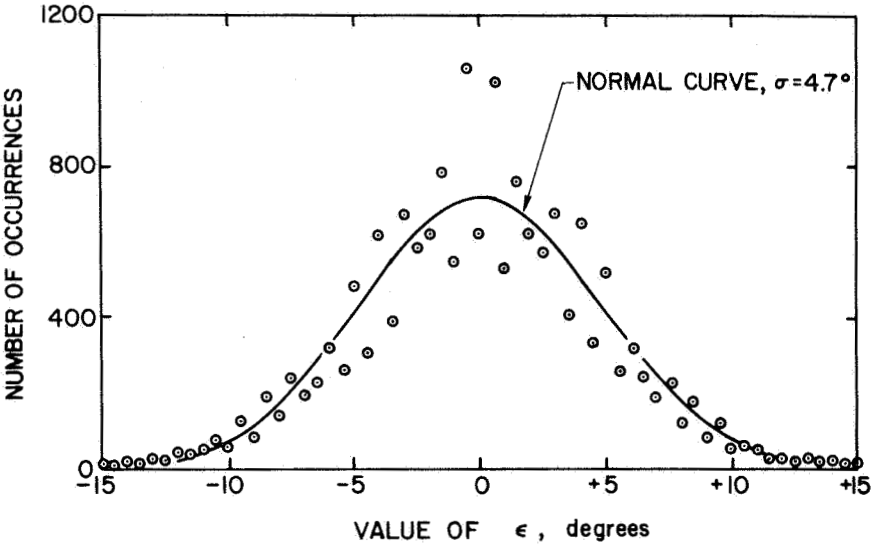

Fig. 13. THE DISTRIBUTION OF THE RANDOM ERROR, ϵ, IN THE FARADAY ROTATION MEASUREMENTS MADE DURING OCTOBER AND NOVEMBER 1965. The total number of data points represented by this figure is 17,002.

Chapter IV

ANALYSIS

As indicated in Chapter I, observations of the Faraday rotation imposed upon radio transmissions from Syncom III were compared with a theoretical model in order to determine $Q_{90}[O^+]$, the integrated rate of production of O^+ ions at sunrise, and β_{300}, the magnitude of the linear loss coefficient at an altitude of 300 km. The present chapter describes the model and the method used for determining the values of $Q_{90}[O^+]$ and β_{300} that best fit the observations. In Section B, a series of block diagrams are used to present an overall outline of the analysis. The remaining sections elaborate on specific steps in that analysis.

A. Symbols

The following is a list of symbols used in this chapter, some of which are needed for the interpretation of diagrams in Section B:

$Ch(\chi,H)$	Chapman function; actually a function of χ and $H/(R_E + h)$, but $(R_E + h)$ is assumed constant at 6700 km in the ionosphere
D	ambipolar diffusion coefficient
D_{300}	value of D at an altitude of 300 km
E	columnar electron content of the ionosphere, defined as the total number of free electrons in a vertical column of unit cross-sectional area extending through the ionosphere
e^-	electron
$\underline{F}$	calculated amount of Faraday rotation imparted to a radio wave passing through an ionosphere with an electron density profile specified by $\underline{N}_i(z)$
f	wave frequency
$\mathcal{H}$	magnitude of the geomagnetic field intensity
H	scale height
H_1, H_2	scale heights of atomic oxygen and molecular nitrogen, respectively
H_m	mean of H_1 and H_2

h	altitude
I	photon flux of solar ionizing radiation as a function of altitude in the earth's atmosphere; measured per unit area in a plane perpendicular to the radiation raypath
I_∞	photon flux of solar ionizing radiation incident on the top of the earth's atmosphere; measured per unit area in a plane perpendicular to the radiation raypath
K_D	diffusion parameter defined as $K_D = (D \sin^2 \Theta)/H_1$
K_{Do}	value of K_D at the altitude where $z = 0$
L_p	path of propagation of a radio wave
ℓ	rate of loss of electrons
$\ell[O^+]$	rate of loss of O^+ ions
N	concentration of electrons; equivalent to $n[e^-]$
$\underline{N}_i(z)$	electron density profile at time t_i, computed by summing over all $\underline{n}_j(z, t_i - t_j)$ for $1 \leq j \leq i$
$n[\ ]$	concentration of a particular constituent of the atmosphere, where the chemical symbol for the constituent is enclosed within the brackets
$\underline{n}_i(z)$	incremental ionospheric electron density profile $= \underline{q}_i(z)\ \Delta t$
$\underline{n}_i(z, t-t_i)$	specifies the time behavior, for $t > t_i$, of an ionospheric electron density profile given by $\underline{n}_i(z)$ when $t = t_i$ and subject to diffusion and recombination for $t > t_i$
n_1, n_2	concentrations of atomic oxygen and molecular nitrogen, respectively; equivalent to $n[O]$ and $n[N_2]$
n_{10}, n_{20}	values of n_1 and n_2 at the altitude where $z = 0$
$Q[O^+]$	rate of production of O^+ ions, integrated with respect to height through the ionosphere
$Q_{90}[O^+]$	value of $Q[O^+]$ when $\chi = 90°$
$Q[N_2^+]$	rate of production of N_2^+ ions, integrated with respect to height through the ionosphere
$Q[O^+ + N_2^+]$	rate of production of O^+ and N_2^+ ions, integrated with respect to height through the ionosphere
$Q_o[O^+ + N_2^+]$	value of $Q[O^+ + N_2^+]$ when $\chi = 0$
q	rate of production of ion-electron pairs
$q_i(z)$	rate of production of electrons as a function of reduced altitude at time t_i
$\underline{q}_i(z)$	$q_i(z)$ normalized with respect to $Q_{90}[O^+]$
q_m	maximum value of q as a function of altitude
R	geocentric radius

R_E	radius of the earth
T	absolute temperature
t	time
t_i	time when $t = t_o + i\Delta t$
t_o	time when $\chi = 100^\circ$
$\bar{v}$	total velocity of ionization, including both drift and diffusion
v_x, v_y, v_z	components of $\bar{v}$ in the east, north, and up directions, respectively
X, Y	arbitrary atomic elements
x	a measure of distance to the east in a horizontal plane
y	a measure of distance to the north in a horizontal plane
z	reduced altitude; a measure of vertical distance defined, for an isothermal atmosphere, as $(h - h_o)/H$, where h_o is a reference altitude (unless otherwise noted, the scale height of atomic oxygen is always used for H, and h_o is defined to make $\sigma_1 n_{10} H_1 = 1$)
z_m	reduced altitude where the rate of production of electrons is maximum

α	rate coefficient of a dissociative recombination reaction
β	linear loss coefficient; fractional loss per second for electrons in the region where the rate of loss of electrons is proportional to the electron concentration
β_o	value of β at the altitude where $z = 0$
β_{300}	value of β at an altitude of 300 km
γ	rate coefficient of an ion-atom interchange reaction
η	rate of change of the Faraday rotation imposed upon Syncom III transmissions during the 1 hour period ending when $\chi = 100^\circ$
Θ	inclination of the geomagnetic field with respect to the horizontal
θ	angle between the direction of propagation of a radio wave and the geomagnetic field
κ	Measures the magnitude of $Q[N^+]$ relative to $Q[O^+]$; defined in detail in Section D3
ν	ion-neutral collision frequency
ρ	root-mean-square difference between the computed and observed Faraday rotation angle for $100^\circ \geq \chi \geq 87^\circ$

σ	absorption cross section
σ_1, σ_2	absorption cross sections for atomic oxygen and molecular nitrogen respectively
σ'	ionization cross section
σ_1', σ_2'	ionization cross sections for atomic oxygen and molecular nitrogen, respectively
τ	optical depth
Φ	latitude of the ionospheric point (ionospheric point defined in footnote, page 53)
χ	solar zenith angle, defined as the angle of incidence of solar ionizing radiation on the atmosphere; measured at ionospheric point unless otherwise noted (ionospheric point defined in footnote, page 53)
χ_i	value of χ at time t_i
Ω	Faraday rotation angle
Ω_M	measured value of Ω after adjusting for the effects of the nighttime ionosphere
Ω_m	measured value of Ω
Ω_T	theoretical value of Ω

B. An Outline of the Analysis

The scheme for deriving $Q_{90}[O^+]$ and β_{300} from the experimental data is summarized in Fig. 14. The data consist of Faraday rotation measurements that are proportional to the columnar electron content of the ionosphere over Hawaii [Section III-A]. A model for the ionosphere is constructed that, when given values for $Q_{90}[O^+]$ and β_{300}, allows for the computation of a theoretical Faraday rotation vs time function. The model is observed to be valid during the time interval when $100^\circ \geq \chi \geq 87^\circ$. A curve-fitting process is used to determine the values of $Q_{90}[O^+]$ and β_{300} that make the model best fit the data during this interval.

The model for the ionosphere is based upon the continuity equation for electrons, which is repeated here for convenience:

$$\frac{\partial N}{\partial t} = q - \ell - \mathrm{div}(N\bar{v}) \qquad (2\text{-}1)$$

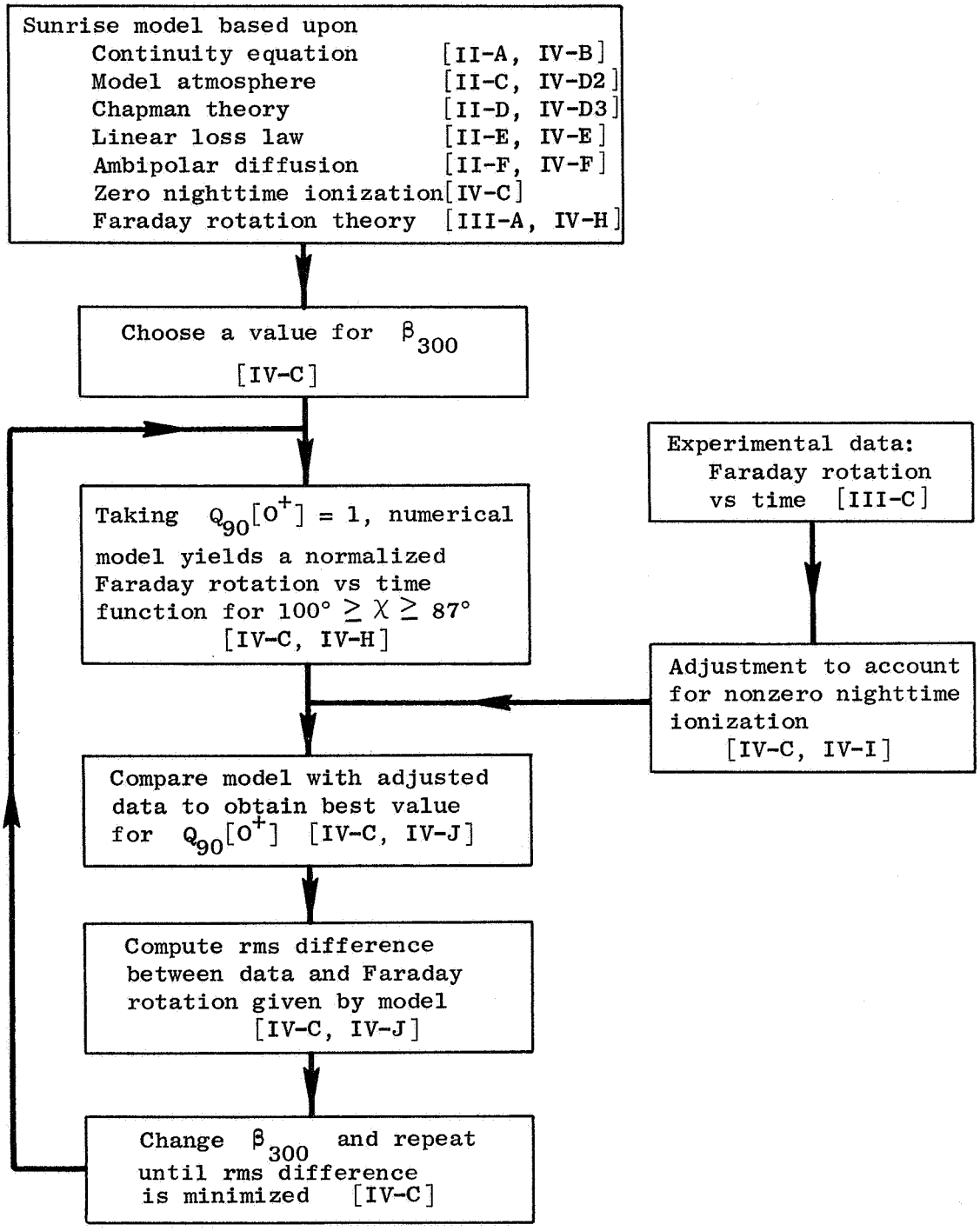

Fig. 14. SCHEME FOR DERIVING THE INTEGRATED O^+ PRODUCTION RATE AND THE LINEAR LOSS COEFFICIENT AT SUNRISE FROM FARADAY ROTATION MEASUREMENTS. References enclosed in brackets refer to sections of the text. For definitions of symbols, see Section A of the text.

Figures 15, 16, and 17 outline the basic assumptions and reasoning used to obtain expressions for the production, loss, and transport terms in this equation. The resulting expressions, discussed in more detail later in this chapter (see section references in Figs. 15, 16, and 17), are the following:

$$\text{Production:} \qquad q = q_m \exp[1 - (z - z_m) - \exp(z_m - z)] \qquad (4\text{-}1)$$

$$\text{Loss:} \qquad \ell = \beta_o N e^{-1.75z} \qquad (4\text{-}2)$$

$$\text{Transport:} \quad \operatorname{div}(N\bar{v}) = -K_{Do}\left(\frac{\partial^2 N}{\partial z^2} + \frac{3}{2}\frac{\partial N}{\partial z} + \frac{1}{2}N\right)e^z \qquad (4\text{-}3)$$

Equations (2-1) and (4-1)-(4-3) yield the electron concentration N as a function of t, z, z_m, q_m, β_o, and K_{Do}. The parameters z_m and q_m are in turn functions of σ_1, σ_2, n_{10}, n_{20}, H_1, H_2, I_∞, and χ (see Fig. 15). A number of these quantities, however, are either known accurately, or do not have a strong influence on the analysis presented here. The scale heights, H_1 and H_2, for example, can be specified with sufficient accuracy (Section D2), and the angle χ is known as a function of time. The columnar electron content, obtained by integrating N with respect to altitude through the ionosphere, is independent of z. It is also observed to be largely independent of the diffusion parameter K_{Do}, at least for $100^\circ \geq \chi \geq 87^\circ$ (see Section F). Furthermore, if the production term given by Eq. (4-1) is normalized with respect to the parameter $Q_{90}[O^+]$, the electron content derived from a solution of the continuity equation will also be normalized, and consequently will be independent of I_∞. It is further observed (Section D3) that the electron content normalized with respect to $Q_{90}[O^+]$ is not critically dependent upon the values of σ_1, σ_2, n_{10}, and n_{20}. The only remaining parameters that have a significant bearing upon the electron content, and hence Faraday rotation, as a function of time when $100^\circ \geq \chi \geq 87^\circ$ are $Q_{90}[O^+]$ and β_o, or equivalently β_{300}. (The altitude where $z = 0$ lies below the F region [Section D3], where the linear loss relationship does not apply.

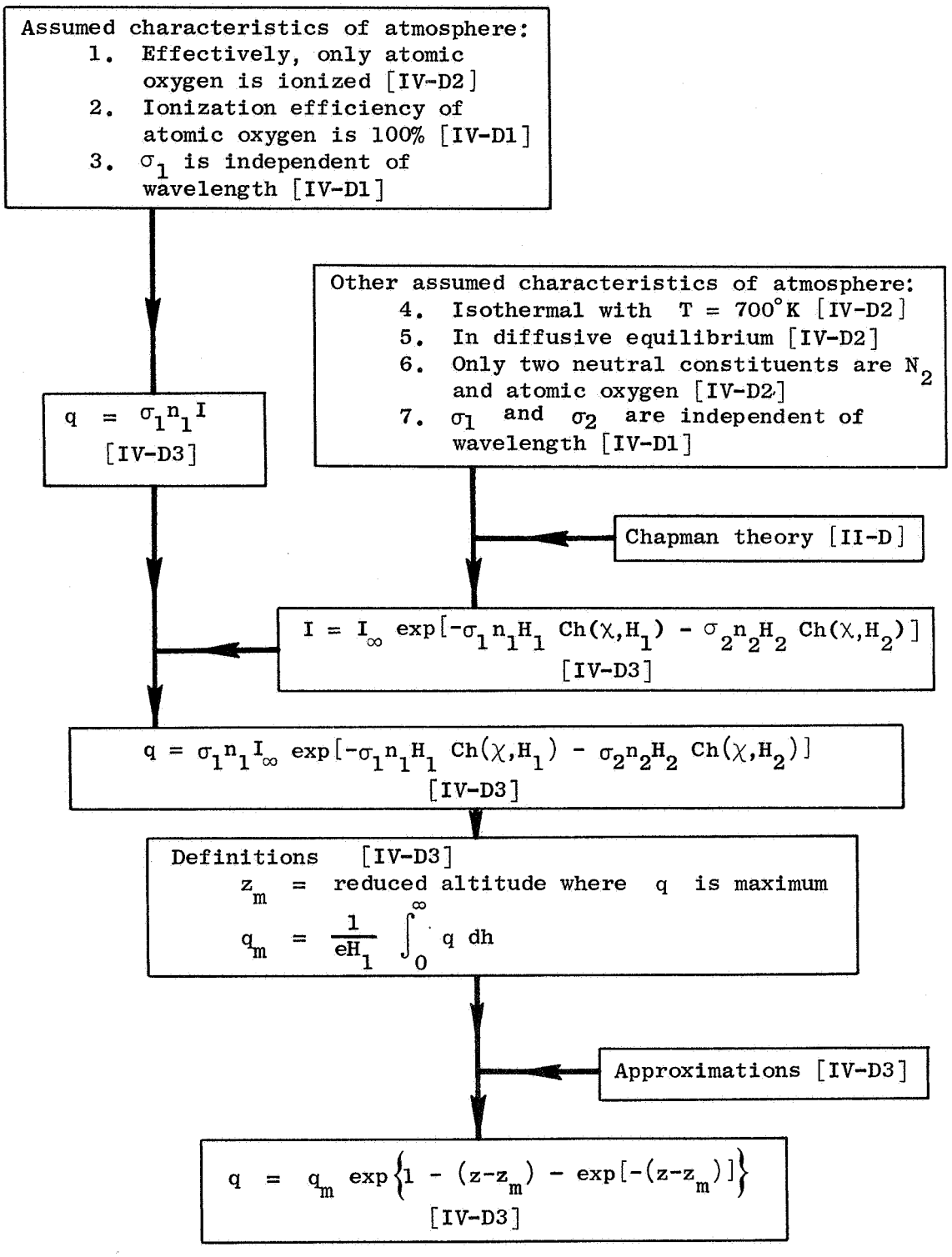

Fig. 15. THE DERIVATION OF AN EXPRESSION FOR THE PRODUCTION TERM IN THE ELECTRON CONTINUITY EQUATION. References enclosed in brackets refer to sections of the text. For definitions of symbols, see Section A of the text.

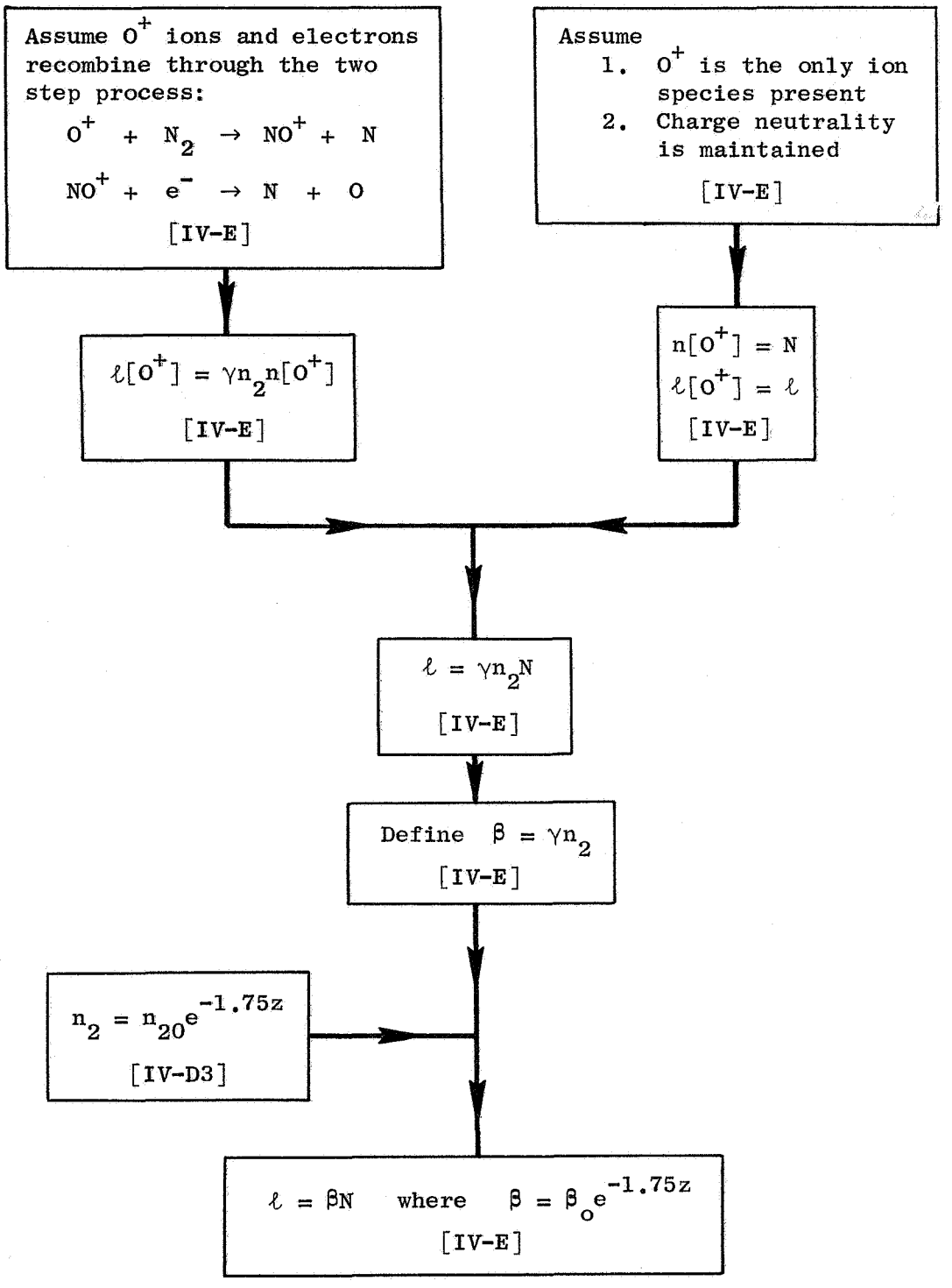

Fig. 16. THE DERIVATION OF AN EXPRESSION FOR THE LOSS TERM IN THE ELECTRON CONTINUITY EQUATION. References enclosed in brackets refer to sections of the text. For definitions of symbols, see Section A of the text.

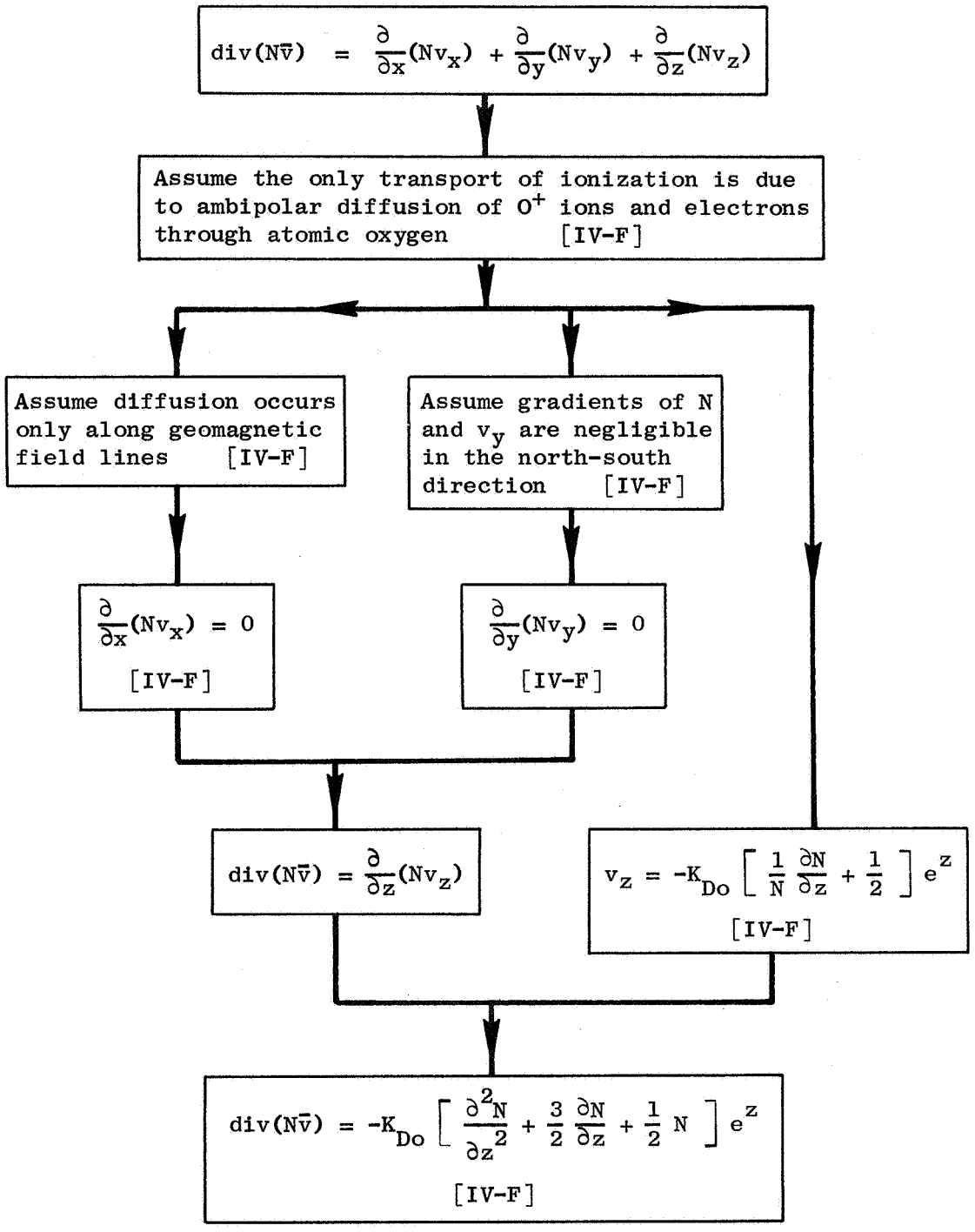

Fig. 17. THE DERIVATION OF AN EXPRESSION FOR THE TRANSPORT TERM IN THE ELECTRON CONTINUITY EQUATION. References enclosed in brackets refer to sections of the text. For definitions of symbols, see Section A of the text.

Hence β_o has little physical significance, though β_{300} is a significant parameter.)

The solution of the continuity equation is directly proportional to $Q_{90}[O^+]$, but depends in a complicated manner upon β_{300}. Assuming a value for β_{300}, it is not difficult to solve for the value of $Q_{90}[O^+]$ that best fits the experimental data in a least-mean-square sense. The assumed β_{300} can be iterated until the best pair of values for $Q_{90}[O^+]$ and β_{300} is found. This is the procedure used in the analysis presented here.

C. The Numerical Procedure

This section outlines the computational steps involved in the data reduction process illustrated in Fig. 14. Discussions of the details of most of the steps are postponed to later sections of this chapter.

The data reduction scheme is based upon a numerical solution of Eq. (2-1), the continuity equation for electrons, with the production, loss, and transport terms given by Eqs. (4-1), (4-2), and (4-3), respectively. This equation is an inhomogeneous, linear, partial differential equation. Its linearity allows the total electron concentration to be viewed as a linear superposition of several components, each of which may be treated separately.

The principle of linear superposition is used first in order to justify treating the nighttime ionization separately. For simplicity, the nighttime residual ionization is treated in the model for the ionosphere by assuming that it does not exist. That is, it is assumed that $N = 0$ in Eq. (2-1) before the effects of sunrise are felt. Since in reality residual ionization does exist before sunrise, the experimental data obtained after sunrise, that are to be compared to the calculations, must first be adjusted to take out the effects of the nighttime ionization. Section I discusses the method of treating the effects of nighttime ionization on the sunrise data.

A numerical time integration of the continuity equation is accomplished by first dividing time into equal increments of length Δt. The linearity of the equation allows the electrons produced within each time increment to be treated separately.

Let t_o be the time at which the solar zenith angle χ reaches 100°, and let t_i represent the time i intervals after t_o. Thus,

$$t_i = t_o + i\Delta t \tag{4-4}$$

When the subscript i is attached to any other quantity in this report it will refer to time t_i and will indicate that the quantity is a function of time. The time when $i = 0$ was chosen to correspond to $\chi = 100^\circ$ since observable production of ion-electron pairs by solar EUV radiation begins shortly thereafter (normally within 10 min). For the purposes of this analysis, it is assumed that

$$q = 0 \qquad \text{for} \quad t < t_o \tag{4-5}$$

and, as noted in Section D3,

$$\Delta t = 1.0 \text{ minutes} \tag{4-6}$$

Let $q_i(z)$ be the production profile given by Eq. (4-1) at time t_i [remember that both q_m and z_m in Eq. (4-1) are functions of χ and hence of t], and let $\underline{q}_i(z)$ be this same profile normalized with respect to $Q_{90}[O^+]$. Define $\underline{n}_i(z)$ to be an <u>incremental</u> electron density profile that would contain all the electrons resulting from maintaining the normalized production profile $\underline{q}_i(z)$ for a time interval equal to Δt. By definition,

$$\underline{n}_i(z) = \underline{q}_i(z)\,\Delta t \tag{4-7}$$

To carry out the numerical integration, it is assumed that the sum of all electrons actually produced within the time interval $t_{i-1} \leq t \leq t_i$ is, when normalized with respect to $Q_{90}[O^+]$, represented by $\underline{n}_i(z)$ for $i > 0$. The total, normalized, electron density profile (neglecting nighttime residual ionization present before time t_o), at a time t_j, where $j \geq 1$, can be determined from the incremental profiles, $\underline{n}_i(z)$. It is only necessary to sum over all the $\underline{n}_i(z)$'s for $0 \leq i \leq j$, <u>after</u> first

taking into account the effects of the loss and transport terms in Eq. (2-1) on each $\underline{n}_i(z)$. The effects of loss and transport on the incremental electron density profiles are determined by solving a homogeneous version of the continuity equation. That is, Eq. (2-1) is solved using $\underline{n}_i(z)$ as an initial condition, and using the loss and transport terms given by Eqs. (4-2) and (4-3), but with $q \equiv 0$. The result is a time-varying, electron density profile, $\underline{n}_i(z, t-t_i)$, where by definition

$$\underline{n}_i(z,0) = \underline{n}_i(z) \tag{4-8}$$

The numerical solution of the homogeneous continuity equation that yields $\underline{n}_i(z, t-t_i)$ is straightforward and is discussed in Section G.

It is shown in Section F that the electron content of $\underline{n}_i(z, t-t_i)$, and hence the contribution of $\underline{n}_i(z, t-t_i)$ to the Faraday rotation imparted to satellite transmissions passing through the model ionosphere, is relatively independent of the magnitude of the diffusion parameter K_{Do}. For the purposes of this discussion, it may be considered that the solution $\underline{n}_i(z, t-t_i)$ of the homogeneous continuity equation, with $\underline{n}_i(z)$ as an initial condition, is dependent only upon the initial condition itself and upon the choice of β_{300}. To emphasize its dependence upon β_{300}, the solution could be written as $\underline{n}_i(z, t-t_i, \beta_{300})$ instead of $\underline{n}_i(z, t-t_i)$, but that notation is cumbersome and should not be necessary at this point. A similar notation, however, will be used later [see Eq. (4-13)].

Now let $\underline{N}_i(z)$ be an electron density profile at time t_i that accounts for all the electrons remaining from those produced for $t \leq t_i$. That is,

$$\underline{N}_i(z) = \sum_{j=1}^{i} \underline{n}_j(z, t_i-t_j) \tag{4-9}$$

$\underline{N}_i(z)$ contains all of the ionization produced in the t_o to t_i time interval and still present at time t_i.

The amount of Faraday rotation imposed on a VHF radio wave passing through an ionosphere composed of these profiles is computed. First, however, a brief look at the pertinent geometry will be helpful.

At time t_i, χ_i is, by definition, the solar zenith angle at the ionospheric point.* It is also, however, the zenith angle anywhere along a vertical surface running approximately north and south in the neighborhood of the ionospheric point. The surfaces of constant χ are actually conical with apexes at the center of the earth, but they approach plane surfaces as χ approaches 90°. The intersection of the $\chi = 90°$ plane with the surface of the earth will be designated the sunrise line. Surfaces of constant χ for $100° \geq \chi \geq 87°$ shall be considered in this work to be vertical planes parallel to the sunrise line in the vicinity of the ionospheric point. Figure 18 shows the orientation of these planes near the summer and winter solstices. The dashed lines represent edge views of some of the planes, with the earth considered flat over the limited region covered by the diagrams.

The angle δ in Fig. 18, which represents the inclination of the sunrise line with respect to the north-south line, is very nearly equal to the solar declination. On the equator, δ would in fact be equal to the solar declination. For other latitudes, the solution of a simple spherical trigonometry problem shows δ to be given by

$$\cos \delta = f(\Phi,d) \cos d \qquad (4\text{-}10)$$

where Φ is the latitude, d is the solar declination, and

$$f(\Phi,d) = 2 \frac{\cos (d + \Phi) \cos (d - \Phi)}{\cos (d + \Phi) + \cos (d - \Phi)} \qquad (4\text{-}11)$$

The function $f(\Phi,d)$ remains near unity for $\Phi = 20°$ (see Fig. 19), corresponding to the location of the ionospheric point in this study.

*The ionospheric point is defined to be the point where the transmission path between the University of Hawaii and Syncom III reaches an altitude of 300 km.

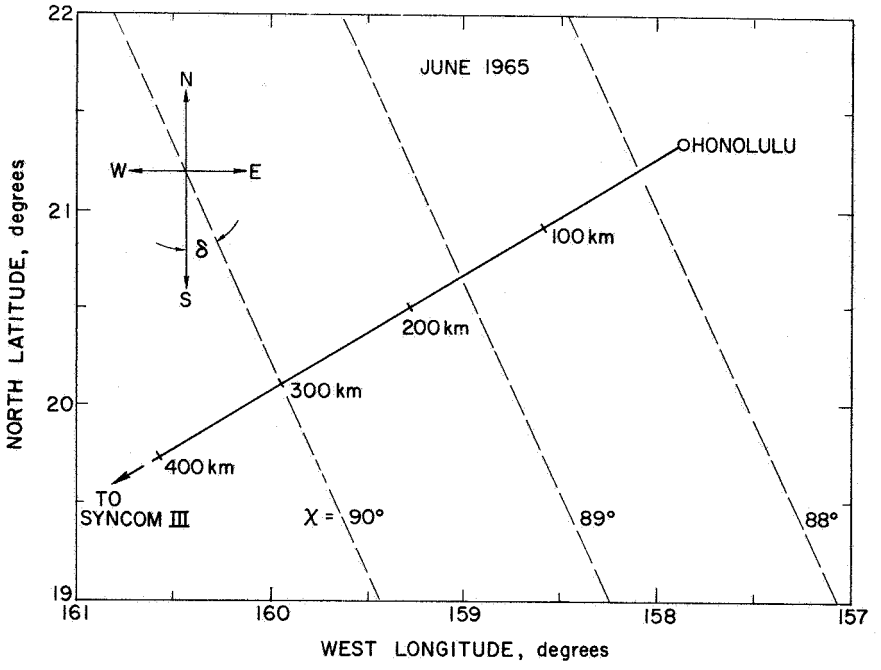

(a)

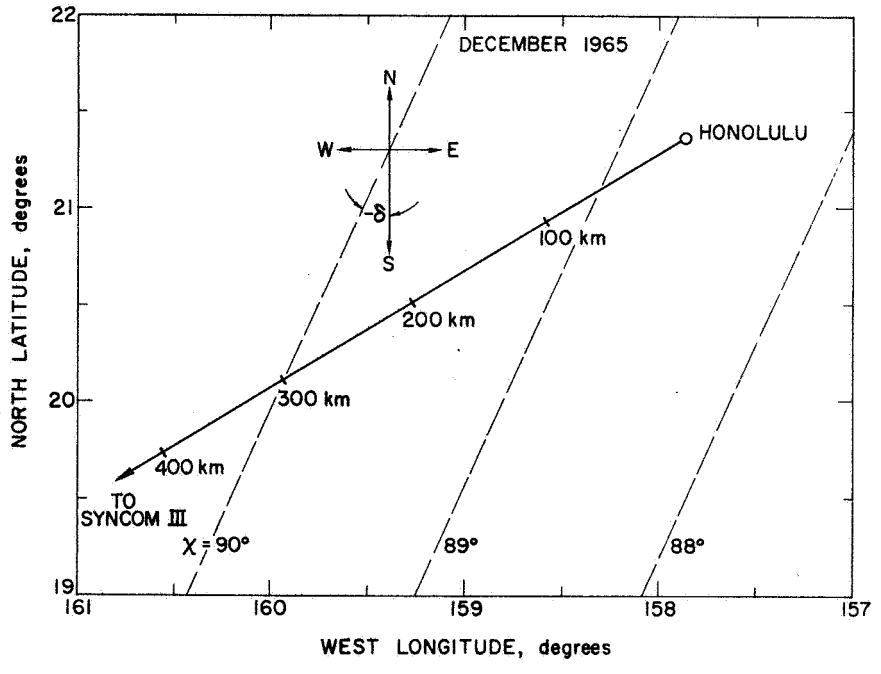

(b)

Fig. 18. THE RELATIONSHIP BETWEEN PLANES OF CONSTANT χ AND THE PROPAGATION PATH BETWEEN HONOLULU AND SYNCOM III DURING JUNE AND DECEMBER 1965. The altitude in 100 km increments is indicated along the propagation path.

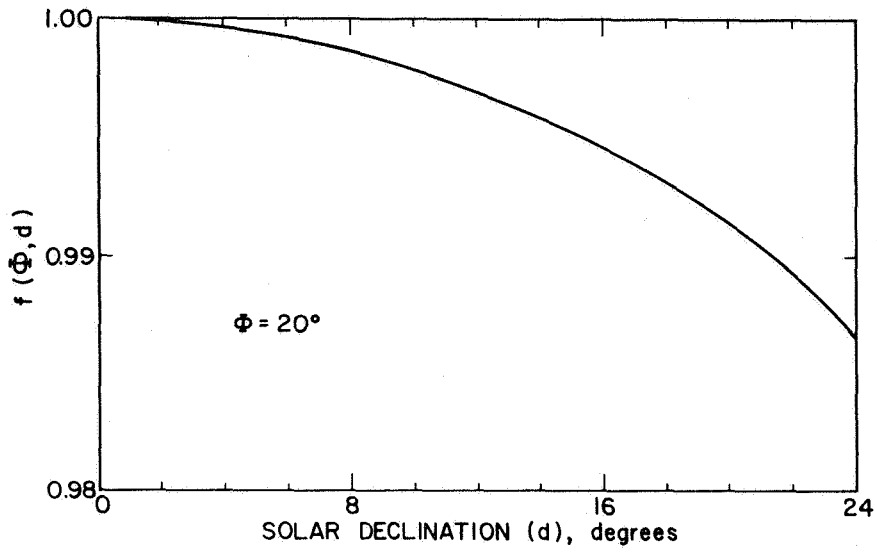

Fig. 19. PLOT OF $f(\Phi,d)$ VS SOLAR DECLINATION AT A LATITUDE OF 20°. The function is symmetric in both Φ and d.

Thus far electron density profiles have been computed only for the latitude and longitude of the ionospheric point. However, it is apparent that $\underline{N}_i(z)$ would also specify the electron concentration along any vertical line in the plane where $\chi = \chi_i$ at time t_i. The profile $\underline{N}_{i+1}(z)$ applies either in this same plane at time t_{i+1} or in a plane displaced a distance Δs to the east at time t_i, where

$$\Delta s = 2\pi R_E \cos \Phi \frac{\Delta t}{T_d} \qquad (4\text{-}12)$$

and where R_E is the radius of the earth, Φ is the latitude of the ionospheric point, and T_d is one day. The calculation of $\underline{N}_i(z)$ for each i, such that $100^\circ \geq \chi_i \geq 87^\circ$ is therefore equivalent to the calculation of electron density profiles in a series of planes like those illustrated in Fig. 20. As time increases, the series of planes may be viewed as moving to the west with a velocity equal to $\Delta s/\Delta t$.

The line integral in Eq. (3-1), $\int_{Lp} N\mathcal{H} \cos\theta \, ds$, is evaluated numerically along the raypath shown in Fig. 20 to determine the amount of Faraday rotation produced by a normalized ionosphere made up of the $\underline{N}_i(z)$

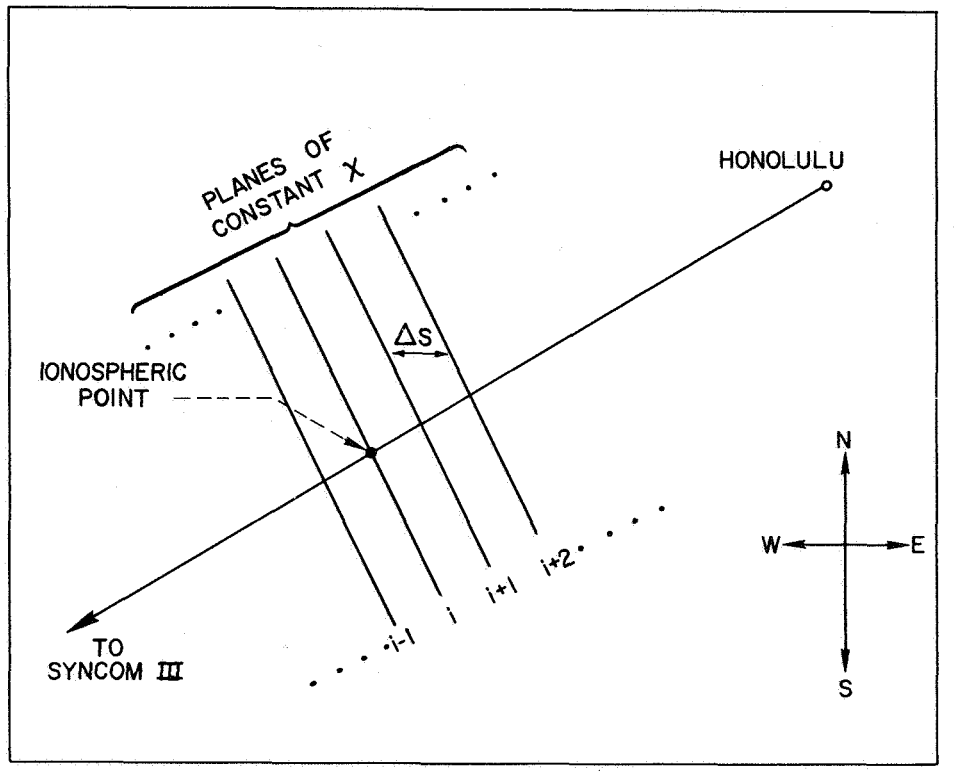

Fig. 20. AN EXAMPLE OF THE PLANES OF CONSTANT χ ALONG WHICH ELECTRON DENSITY PROFILES SPECIFIED BY $\underline{N}_i(z)$ APPLY.

profiles. For evaluating the integral, values of the electron concentration are obtained both in the planes containing known profiles and, by interpolation, between these planes. To obtain the Faraday rotation angle corresponding to a particular time, it is only necessary to shift the set of planes along the east-west direction until the ionospheric point lies in the plane corresponding to the desired time. For example, to compute the Faraday rotation angle at $t = t_k$, the line integral should be evaluated when the ionospheric point lies in the plane corresponding to $i = k$.

Let the Faraday rotation due to the normalized ionosphere be denoted by $\underline{F}(t,\beta_{300})$ to indicate that its value is a function of both time and the particular β_{300} used earlier in solving the continuity equation. $\underline{F}$ is a normalized value of the Faraday rotation, but the value of the normalization constant $Q_{90}[0^+]$ is not at this point known.

Define $\Omega_T(t)$ as

$$\Omega_T(t) = Q_{90}[O^+]\ \underline{F}(t,\beta_{300}) \qquad (4\text{-}13)$$

The subscript T is used to indicate that this function is a theoretical representation of the Faraday rotation angle, based upon the numerical analysis outlined above. Let $\Omega_M(t)$ be the measured Faraday rotation imparted to the VHF transmissions from Syncom III <u>after</u> effectively correcting for variations due to residual nighttime ionization. (The method of handling the nighttime ionization is discussed in Section I.) Then if $Q_{90}[O^+]$ and β_{300} are chosen correctly, $\Omega_T(t)$ should match $\Omega_M(t)$ throughout the sunrise period for which the theoretical model is valid.

The initial value of β_{300}, say $\beta_{300}^{(1)}$, used to obtain the incremental time-varying electron density profiles, $\underline{n}_i(z,\ t\text{-}t_i)$, is intentionally chosen abnormally low. Using the resulting $F\left(t,\beta_{300}^{(1)}\right)$, a $Q_{90}^{(1)}[O^+]$ is determined as that value of $Q_{90}[O^+]$ that minimizes the root-mean-square difference between $\Omega_T(t)$ and $\Omega_M(t)$ in the time interval where $100^\circ \geq \chi \geq 87^\circ$. (Photoionization by solar EUV radiation does not begin before $\chi = 100^\circ$; and after $\chi = 87^\circ$, the data often do not agree well with the theoretical model.) The symbol $\rho^{(1)}$ is used to denote the corresponding root-mean-square difference between $\Omega_T(t)$ and $\Omega_M(t)$. The loss coefficient $\beta_{300}^{(1)}$ is increased to a new value, $\beta_{300}^{(2)}$, and the process is repeated to obtain $Q_{90}^{(2)}[O^+]$ and $\rho^{(2)}$. The analysis is continued, increasing β_{300} with each iteration, until a minimum is obtained in ρ. Assuming that a well-defined minimum in ρ exists and that the minimum is indeed low, the values of $Q_{90}[O^+]$ and β_{300} corresponding to the minimum are considered the correct values for those quantities.

The parameters thus obtained are those desired in the beginning, namely, the integrated rate of production of O^+ ions at sunrise, $Q_{90}[O^+]$, and the magnitude of the linear loss coefficient at the reference altitude, β_{300}. The steps in the computational process may be reviewed briefly as follows:

(1) Compute normalized production profiles, $q_i(z)$.

(2) Using the production rates obtained in (1), compute incremental electron density profiles, $\underline{n}_i(z)$.

(3) Choose a value for β_{300} and solve the homogeneous continuity equation to obtain $\underline{n}_i(z, t-t_i)$.

(4) Sum over the $\underline{n}_i(z, t-t_i)$'s to get total (normalized) electron density profiles, $\underline{N}_i(z)$.

(5) Compute the Faraday rotation $\underline{F}(t,\beta_{300})$ due to the normalized ionosphere obtained in (4).

(6) Match the results of (5) to observed Faraday rotation data to yield values of $Q_{90}[O^+]$ and ρ.

(7) Increment β_{300} and repeat (3) through (6) until a minimum in ρ is found. The magnitude of $Q_{90}[O^+]$ and β_{300} corresponding to the minimum are the best values.

The remaining sections of this chapter describe the details involved in each step of the analysis. The results of applying this procedure to the data and implications of those results are presented in Chapter V.

D. Production

1. Solar Flux and Ionization Cross Sections

The solar ionizing radiation is effectively assumed to be monochromatic with a total flux equal to the actual flux in the 911 to 165 Å band. This assumption is equivalent (a) to neglecting ionization produced by both X-rays and radiation in the 1027 to 911 Å range, and (b) to assuming the ionization and absorption cross sections to be constant between 911 and 165 Å.

At sunrise, almost all of the ionization does result from production by radiation in the 911 to 165 Å range. Table 3 in Chapter II shows that about 87 percent of the total production is attributable to flux in this band. The remaining 13 percent, which is divided between X-ray production and the production of O_2^+ ions by 1027 to 911 Å flux, occurs at substantially lower altitudes where the loss rates are much greater. (The peak of production is about 60 km lower than the peak due

to radiation in the 911 to 165 Å range.) The remaining 13 percent of the total production, therefore, accounts for much less than 13 percent of the total rate of increase of the electron content. It can be neglected without introducing significant errors.

That absorption cross sections are sufficiently constant in the 911 to 165 Å band to allow the radiation to be considered monochromatic can be seen by observing that the production profiles in Fig. 8c closely resemble Chapman production profiles. The value of the absorption cross section for a particular emission line affects only the altitude of the peak of production resulting from that line, not the magnitude of the peak or the shape of the profile. A wide variation in the absorption cross sections over a band of wavelengths results in a wide variation in altitudes of the peaks of production due to different emission lines within the band. The production profile for the entire band would thus be much broader than a Chapman profile and would probably contain several secondary peaks. This is not the case for the production due to 911 to 165 Å radiation. Notice, however, that the abrupt decrease in the cross sections for wavelengths shorter than 165 Å is reflected in decreased altitudes of the peaks of production for all constituents in the 165 to 1 Å range (Fig. 8d).

A further assumption is that the ionization efficiency of atomic oxygen is 100 percent, that is, $\sigma_1 = \sigma_1'$, in the 911 to 165 Å band. Actually, the efficiencies at the longer wavelength end of the band (λ greater than about 300 Å) are probably somewhat less than 100 percent. Electrons freed by radiation of shorter wavelengths, however, have sufficient energy to produce secondary ionization, and hence ionization efficiencies greater than 100 percent. Over the entire band, the effective ionization efficiency is probably close to 100 percent, though an exact figure is not known. For reasons noted in Section D2, the ionization efficiency for N_2 is assumed to be zero.

The solar spectrum between 911 and 165 Å has been divided into 46 bands, and values of the cross sections of the major atmospheric constituents have been published for each band by Hinteregger et al [1965]. Where cross sections are needed in this work, an effective value is used; this value is obtained by taking weighted means of the logarithms of the

published absorption cross sections. The weights are determined by the total flux in each of the 46 bands. These cross sections result in approximate production profiles with peaks at the same altitude as the peak of the exact profiles. Table 5 shows the effective cross sections used for the two major constituents.

Table 5

ABSORPTION CROSS SECTIONS

Atom or Molecule	Absorption Cross Sections (cm^2)
Atomic oxygen (O)	5.7×10^{-18}
Nitrogen (N_2)	7.4×10^{-18}

2. Atmosphere

The atmosphere is assumed to be isothermal and composed of two constituents, atomic oxygen and molecular nitrogen. The two constituents are assumed to be in diffusive equilibrium with the scale height of atomic oxygen taken to be 40 km, corresponding to a temperature of 700°K. The concentrations of atomic oxygen and molecular nitrogen are chosen to correspond to the COSPAR model atmosphere of Fig. 3 at a 200 km altitude. Atomic oxygen atoms are subject to ionization by solar EUV flux, but molecular nitrogen is considered only to absorb radiation without contributing to the observable ionization.

The atmosphere may be assumed to be isothermal since at sunrise practically all of the production takes place above a 200 km altitude (Fig. 8c). Above 200 km, the temperature at sunrise is only a slowly varying function of altitude (Fig. 4). The COSPAR model atmosphere shows the temperature above 200 km to be about 700°K and shows all constituents to be in diffusive equilibrium above 120 km.

A two-constituent model atmosphere is justified since O_2^+ production accounts for only about 5 percent of the total production due to EUV flux in the 911 to 165 Å range (see Table 3). Neglecting the presence

of O_2 simply means that about 5 percent additional flux will be available for the ionization of O and N_2.

The assumption that N_2 does not contribute to the observable ionization is based upon observations of the ion composition, which show N_2^+ ions to be virtually absent throughout the ionosphere. Holmes et al [1965], for example, show that N_2^+ accounts for less than 0.5 percent of the total ionization in the F region. The ionization of N_2 does account for a significant fraction of the total ion production, but N_2^+ ions disappear much more rapidly than do O^+ ions. According to Johnson [1967], about 20 percent of the N_2^+ ions are removed through a dissociative recombination. The ion-atom interchange reaction with atomic oxygen, however, apparently proceeds rapidly enough to allow the following two-step process to remove the rest (the reaction rates are listed in Table 4, Chapter II):

$$\begin{aligned} N_2^+ + O &\rightarrow NO^+ + N \\ NO^+ + e^- &\rightarrow N + O \end{aligned} \qquad (4\text{-}14)$$

In either case, N_2^+ disappears rapidly without contributing to the observable electron content.

One other reaction could possibly be important in the removal of N_2^+, namely, a charge exchange with atomic oxygen:

$$N_2^+ + O \rightarrow N_2 + O^+ \qquad (4\text{-}15)$$

Recent measurements of the rate coefficients for the ion-atom interchange, (4-14), and the charge exchange, (4-15), reactions show that the latter rate is at least an order of magnitude smaller [Ferguson, 1967]. Thus it will be assumed that (4-15) is not an important mechanism for the removal of N_2^+. To the extent that it is important, however, N_2^+ does contribute to the observable ionization, since N_2^+ ions would simply be converted by this reaction to O^+ ions.

3. Calculations

Let the subscripts 1 and 2 represent the neutral constituents O and N_2, respectively. Using the Chapman theory referred to in Section II-D [see Eq. (2-9)], the optical depth may be expressed as

$$\tau = \sigma_1 n_1 H_1 \, Ch(\chi, H_1) + \sigma_2 n_2 H_2 \, Ch(\chi, H_2) \tag{4-16}$$

The photoionization rate, keeping in mind the fact that only the production of O^+ ions is being counted, is given by

$$q = \sigma_1 n_1 I \tag{4-17}$$

where

$$I = I_\infty e^{-\tau} \tag{4-18}$$

Thus

$$q = \sigma_1 n_1 I_\infty \exp[-\sigma_1 n_1 H_1 \, Ch(\chi, H_1) - \sigma_2 n_2 H_2 \, Ch(\chi, H_2)] \tag{4-19}$$

Both n_1 and n_2 are, of course, functions of altitude and may be written, for an isothermal atmosphere, as

$$n_1 = n_{10} e^{-z} \tag{4-20}$$

and

$$n_2 = n_{20} e^{-1.75z} \tag{4-21}$$

where the reduced altitude z is based on the atomic oxygen scale height. The factor 1.75 in Eq. (4-21) is the ratio H_1/H_2.

Equation (4-19) is used to compute the normalized production profiles needed for the analysis. At each time t_i, the solar zenith angle χ_i is computed and substituted into (4-19). The production rate

is evaluated in steps of $\Delta z = 0.1$ from two scale heights below to six scale heights above the peak of production, a range which accounts for over 99 percent of the photoionization. The normalization factor $Q_{90}[O^+]$ is determined by numerically evaluating $\int_0^\infty q\ dh$ for $\chi = 90°$. The symbol $Q_{90}[O^+]$ indicates the integrated rate of production of O^+ ions at sunrise. After normalization, the production profiles are independent of the factor $\sigma_1 I_\infty$ in Eq. (4-19). Their dependence upon the relative magnitudes of n_1 and n_2 is discussed below. New profiles are computed at 1 min increments in time throughout the period when $100° \geq \chi \geq 87°$ (that is, $\Delta t = 1.0$ min). A more frequent evaluation of the production profile only results in an increased use of computer time without noticeably improving the accuracy of the results.

Equation (4-19) may be reduced to a more convenient form for studying the effects of variations in the concentrations of O and N_2. The only additional approximation needed is that the Chapman function may be evaluated at the mean scale height, $H_m = (H_1 + H_2)/2$, without a significant loss of accuracy. Let $z = 0$ at the altitude where

$$\sigma_1 n_{10} H_1 = 1 \tag{4-22}$$

With the neutral atmosphere assumed (see Section D2), Eq. (4-22) is satisfied at an altitude of about 89 km, well below the F region of the ionosphere.

Now let

$$\kappa = \frac{\sigma_2 n_{20}}{\sigma_1 n_{10}} \tag{4-23}$$

Then the production rate reduces to [Garriott and Smith, 1965]

$$q(z) = \frac{I_\infty}{eH_1} \exp\left[1 - z - Ch(\chi, H_m)\ e^{-z}\right] \left\{\exp\left[\frac{-\kappa}{1.75} Ch(\chi, H_m)\ e^{-1.75z}\right]\right\} \tag{4-24}$$

If the concentration of N_2 is set to zero, $\kappa = 0$ and Eq. (4-24) reduces to the Chapman formula for a single constituent atmosphere [Eq. (2-10)]. The effect of the presence of N_2 is contained entirely in the right-hand exponential term and results in an attenuation of q, particularly at low altitudes. Figure 21 shows the O^+ production profile derived from Eq. (4-24) for three values of κ and three solar zenith angles.

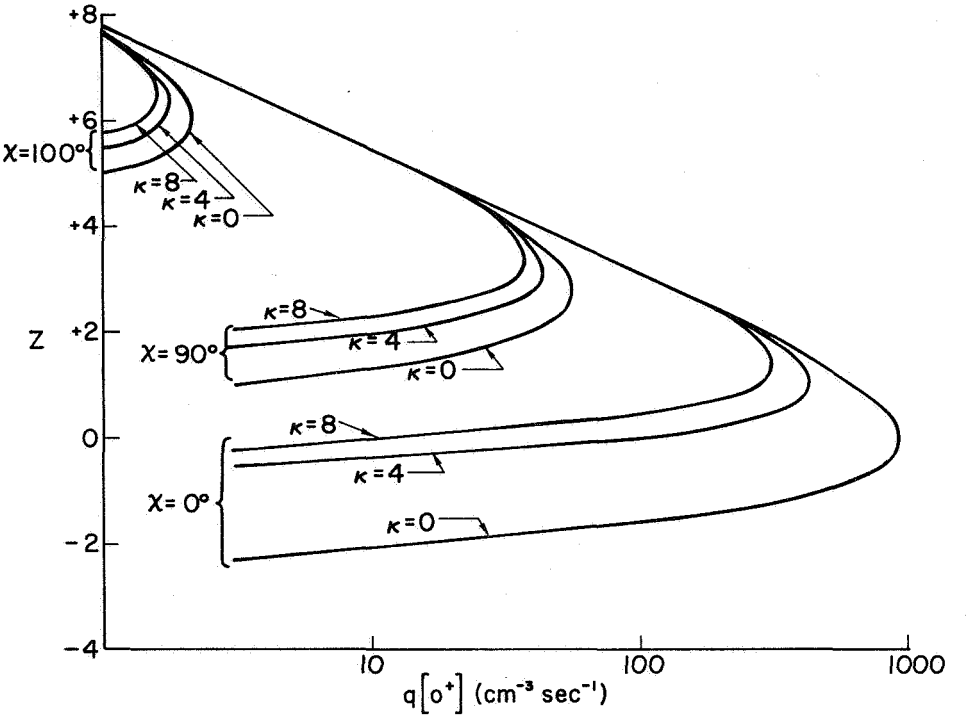

Fig. 21. THE RATE OF PRODUCTION OF O^+ IONS AS A FUNCTION OF REDUCED HEIGHT FOR THREE SOLAR ZENITH ANGLES AND THREE VALUES OF κ. The incident photon flux I_∞ has been taken to be 10^{10} photons/cm^2/s [after Garriott and Smith, 1965].

The parameter κ is convenient to use in developing an expression for the production profile, though its physical significance may not be readily apparent. It can be related to more directly observable quantities by combining Eq. (4-23) with Eqs. (4-20) and (4-21). For example, the same information contained in κ can also be specified by giving the altitude at which $n[O] = n[N_2]$ and simultaneously the concentration of either constituent at a convenient fixed altitude. Figure 22 provides a means of determining κ for a model atmosphere when the crossover altitude,

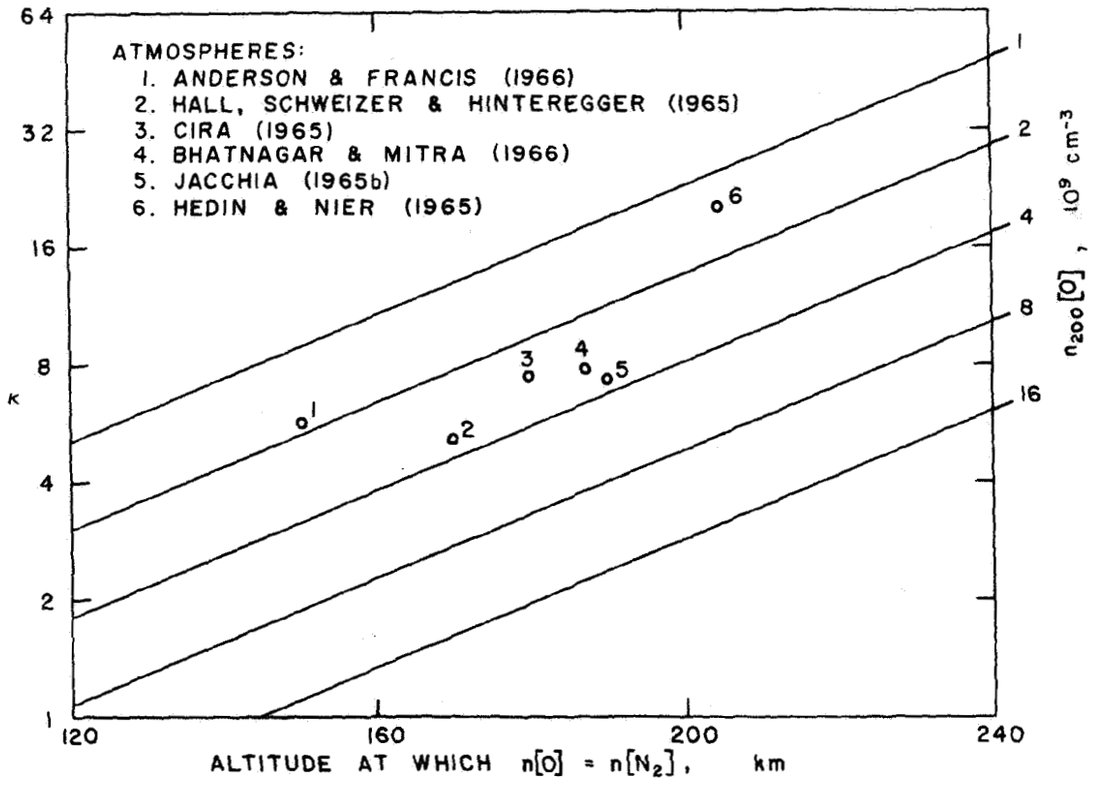

Fig. 22. A DIAGRAM WHICH WILL GIVE κ FOR AN ATMOSPHERE IF THE CONCENTRATION OF ATOMIC OXYGEN AT 200 km IS KNOWN AS WELL AS THE CROSSOVER ALTITUDE AT WHICH THE CONCENTRATIONS OF ATOMIC OXYGEN AND MOLECULAR NITROGEN ARE EQUAL. The diagram assumes the scale height of atomic oxygen to be 40 km.

where $n[O] = n[N_2]$, and the concentration of atomic oxygen at an altitude of 200 km, are known. The assumptions that $\sigma_1/\sigma_2 = 1.3$ (from Table 5 in this chapter) and $H_1 = 40$ km are built into Fig. 22. Note that though the characteristics of the recently published atmospheres referenced in Fig. 22 vary significantly in some respects, κ is nearly the same for five of the six models.

According to the definition given by Eq. (4-23), κ increases if either the cross section or concentration of N_2 increases relative to the cross section or concentration of atomic oxygen. An increase in κ would result in an increase in $Q[N_2^+]$, the integrated rate of production of N_2^+ ions, compared to $Q[O^+]$. The parameter κ is thus a measure of the relative magnitudes of $Q[O^+]$ and $Q[N_2^+]$. As κ increases, more

of the EUV radiation goes into the production of N_2^+ ions, which contribute very little to the observable ionization, and less goes into the production of O^+ ions, which account for almost all of the observable ionization.

Figure 21 shows that a variation in κ affects the shape of the production profile and the altitude of the peak of production. But when normalized, the integrated production rates are virtually unaffected by a variation in κ or nearly one order of magnitude (Fig. 23). As a result, the experimental values of $Q_{90}[O^+]$, to be determined by comparing the data to calculations based on this theoretical model, are essentially independent of the value of κ assumed in the model. Particular magnitudes for the concentrations of atomic oxygen and molecular nitrogen are assumed in order to use Eq. (4-19) in computing the normalized production profiles. The final results, however, are almost independent of those original assumptions, at least, according to Fig. 23, as long as κ lies between 2 and 16. Figure 22 suggests that κ is almost certainly near the center of the range.

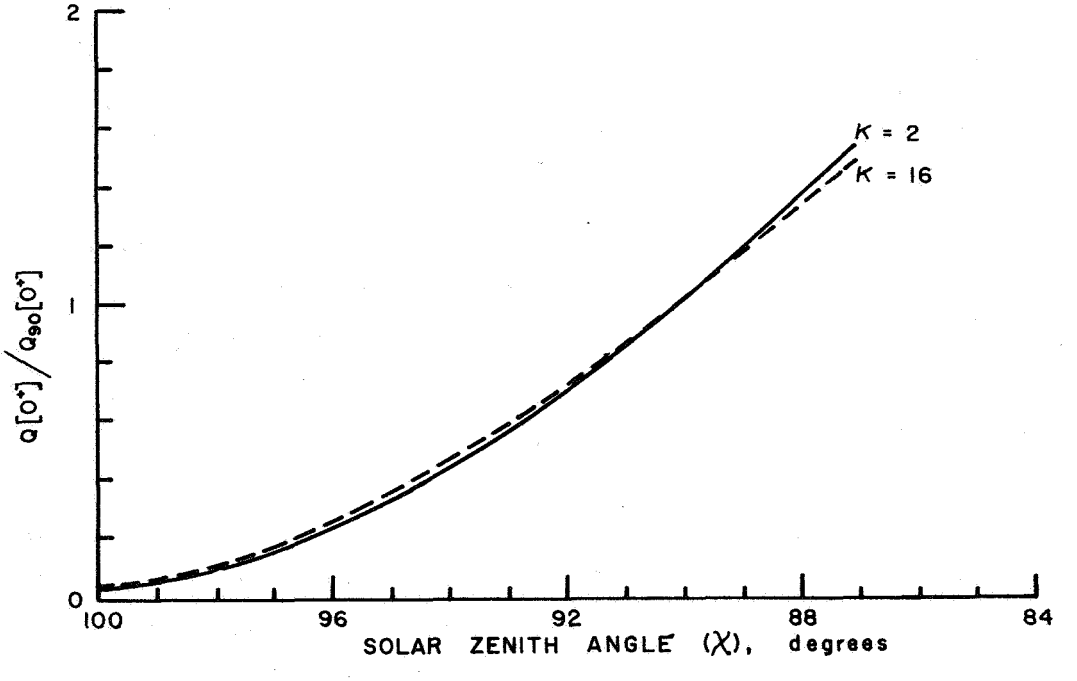

Fig. 23. THE INTEGRATED RATE OF PRODUCTION OF O^+ IONS, NORMALIZED WITH RESPECT TO $Q_{90}[O^+]$, AS A FUNCTION OF THE SOLAR ZENITH ANGLE FOR $\kappa = 2$ AND 16. This figure shows that the normalized values, $Q[O^+]$, are essentially independent of κ.

As mentioned in the previous section, the concentrations of the atmospheric constituents have been chosen to correspond to the COSPAR model atmosphere for these calculations. Thus it has been assumed that $\kappa = 7$ in this analysis.

Before closing this section, it must be noted that though Eq. (4-19) is evaluated to determine the desired normalized production profiles, the exact profiles thus obtained are not used as the $\underline{q}_i(z)$'s. Vast simplification in the computational process can be realized by assuming that all the production profiles have the same functional form. It is then only necessary to keep track of the altitude and magnitude of the peak of production for each $\underline{q}_i(z)$ rather than the entire profile. Since the production profiles, even for $\kappa \neq 0$, resemble Chapman profiles, $\underline{q}_i$ is assumed to have the form

$$\underline{q}_i(z) = \underline{q}_{im} \exp\left\{1 - (z-z_i) - \exp[-(z-z_i)]\right\} \tag{4-25}$$

The reduced altitude of the peak of production, z_i, is chosen to correspond to the peak of production derived on the basis of Eq. (4-19). The peak rate of production, $\underline{q}_{im}$, is chosen to make $\int_0^\infty \underline{q}_i \, dh$ the same as the vertical integral of the normalized production profile computed from Eq. (4-19). With $\underline{q}_i$ given by Eq. (4-25),

$$\int_0^\infty \underline{q}_i \, dh = \underline{q}_{im} e H_1 \tag{4-26}$$

Let $\underline{Q}_i$ be the true, normalized, integrated production rate, found by numerically integrating Eq. (4-19). Then $\underline{q}_{im}$ is chosen as

$$\underline{q}_{im} = \frac{\underline{Q}_i}{eH_1} \tag{4-27}$$

The production profiles chosen in this manner approximate the exact production profiles, but what is more important for this analysis, the vertical integrals of the approximate profiles are exactly correct.

Furthermore, correct placement of the altitude of the peak of production assures that the electron density profiles resulting from the approximate $\underline{q}_i$'s will be subject to loss rates nearly the same as if the exact production profiles had been used.

E. Loss

Atomic oxygen ions recombine with electrons through the two-step process considered in Chapter II:

$$O^+ + XY \rightarrow XO^+ + Y \qquad \text{(rate coefficient} = \gamma) \tag{4-28}$$

$$XO^+ + e^- \rightarrow X + O \qquad \text{(rate coefficient} = \alpha) \tag{4-29}$$

The molecule XY represents either N_2 or O_2.

Two limiting cases for the electron loss rate in equilibrium were considered in Chapter II. In one case, for $\alpha N \gg \gamma n[XY]$, reaction (4-29) proceeds so rapidly that (4-28) becomes the limiting reaction and

$$\ell = \beta N \tag{4-30}$$

where

$$\beta = \gamma n[XY] \tag{4-31}$$

If $\alpha N \ll \gamma n[XY]$, the loss rate is limited by (4-29) and

$$\ell = \alpha N^2 \tag{4-32}$$

At sunrise, when the ionosphere is not in equilibrium, the electron concentration and its rate of change must in general be determined by a simultaneous solution of three partial differential equations, one continuity equation each for the concentrations of electrons, XO^+ ions, and O^+ ions. The rate of loss of electrons is the rate for reaction (4-29),

$$\ell = \alpha n[XO^+]\, N \qquad (4\text{-}33)$$

But, except for very special cases, $n[XO^+]$ cannot be readily determined.

Suppose, however, that during the sunrise period, composition measurements show virtually all of the ions at a certain altitude to be XO^+. Then $N[XO^+] \approx N$ and $\ell \approx \alpha N^2$ as in Eq. (4-32) for an equilibrium ionosphere. Similarly, if observations show that $n[O^+] \approx N$, the electron loss rate must be essentially the same as the rate of loss of O^+ ions so that $\ell \approx \beta N$ as in Eq. (4-30). Thus the same limiting approximations apply as in the equilibrium case; but in a nonequilibrium situation, it is not possible in general to state where the approximations are valid in terms of simple conditions like $\alpha N \gg \gamma n[XY]$ or $\alpha N \ll \gamma n[XY]$. The conditions determining whether either Eq. (4-30) or Eq. (4-32) is valid depend in a complicated manner upon the production rate, rate coefficients, and concentrations. Though it may be difficult to predict theoretically which, if either, loss expression applies at a particular altitude, composition measurements showing a large predominance of either atomic or molecular ions indicate that either (4-30) or (4-32), respectively, does apply.

As indicated by Eq. (4-2), it is assumed for this analysis that the rate of loss of electrons is directly proportional to the electron concentration, so that Eq. (4-30) applies. To see the validity of this assumption, consider first the mass spectrometer ion composition measurements reported by Holmes et al [1965]. Their nighttime measurements show that at 230 km, which is the altitude of the peak of the O^+ ion production rate in a COSPAR model atmosphere at sunrise (Fig. 8c), $n[O^+]$ equals 70 percent of the total ion concentration. Results obtained on two earlier nighttime rocket flights reported by Johnson et al [1958] confirm these results at 230 km. The percent of O^+ ions increases above this altitude and decreases rapidly below. Thus it should be reasonably accurate to say $\ell \approx \beta N$ at night down to about 230 km but not much below this altitude.

Furthermore the nighttime electron concentration observed by Holmes et al [1965] was only 1.0×10^{10} m^{-3} at an altitude of 230 km. As the electron concentration increases, αN^2 increases more rapidly than βN. Reaction (4-28) becomes to an even larger extent the limiting reaction and $\ell = \beta N$ is an even better approximation. It would be expected that

as N increases, the linear loss law could be applied at lower and lower altitudes. A daytime rocket flight, made at 0934 local time and also reported by Holmes et al [1965], shows this to be the case. The electron concentration at 230 km at this time was 4×10^{11} m^{-3}, an increase by a factor of 40 over the nighttime concentration. The O^+ concentration had increased to over 98 percent of the total ion concentration, and the level at which $n[O^+]$ was 70 percent of the total had been lowered from 230 to 180 km. The region where $\ell = \beta N$ had, as expected, been substantially lowered.

As a final consideration, the electron content at the time when $\chi = 87°$ (this analysis is not applied beyond the time when $\chi = 87°$) is usually found to be about 3×10^{16} m^{-2} above its predawn level (from results presented in Chapter V). Assuming that all the electrons added since sunrise are contained within a profile shaped like a Chapman production profile with a scale height of 40 km, an electron content of 3×10^{16} m^{-2} corresponds to a peak concentration at about 230 km (the peak of production is actually located at 215 km when $\chi = 87°$) of 3×10^{11} m^{-3}, about thirty times that observed on the nighttime rocket flight of Holmes et al. Thus it is expected that all of the new electrons and ions created up to the time when $\chi = 87°$ are contained in a region where the linear loss law is applicable.

The molecule XY involved in the loss process is assumed to be N_2. The concentration $n[XY]$ is thus given by [see Eq. (4-21)]

$$n[XY] = n_2 = n_{20} e^{-1.75z} \tag{4-34}$$

Thus

$$\beta = \beta_o e^{-1.75z} \tag{4-35a}$$

or equivalently

$$\beta = \beta_{300} \exp[-1.75(z - z_{300})] \tag{4-35b}$$

where z_{300} is the value of z at an altitude of 300 km.

It is probable that an ion-atom interchange reaction with O_2 also accounts for a significant fraction of the loss [Ferguson, 1967]. Fortunately, however, the scale heights of O_2 and N_2 are approximately the same so that the altitude dependence of β is not greatly affected by neglecting one or the other of these gases.

F. Transport

The velocity $\bar{v}$ in the continuity Eq. (2-1) is assumed to be due only to the ambipolar diffusion of O^+ ions and electrons through a background gas composed principally of atomic oxygen. Hence the vertical component of $\bar{v}$ may be written as [follows directly from Eq. (2-24)]

$$v_z = -K_D \left(\frac{1}{N} \frac{\partial N}{\partial z} + \frac{1}{2} \right) \tag{4-36}$$

where

$$K_D = \frac{D \sin^2 \Theta}{H_1} \tag{4-37}$$

All horizontal and vertical drift velocities are neglected in this analysis. The effects of this assumption on the final results are discussed in Sections V-E2 and V-E3. It is not a necessary assumption, but is convenient in view of the lack of accurate information concerning the magnitudes of drift velocities in the ionosphere.

Collision frequencies in the F region are sufficiently low to cause the diffusion of ionization to be limited to the direction of geomagnetic field lines. Thus diffusion is effectively blocked in an east-west direction, resulting in near zero values for v_x and $\partial v_x / \partial x$. In the north-south direction, gradients are small enough to allow

$$\left(v_y \frac{\partial N}{\partial y} + N \frac{\partial v_y}{\partial y} \right)$$

to be neglected in computing $\mathrm{div}(N\bar{v})$. With these considerations, the transport term in the continuity equation reduces to

$$\text{div}(N\bar{v}) = v_z \frac{\partial N}{\partial z} + N \frac{\partial v_z}{\partial z} \tag{4-38}$$

Substituting Eq. (4-37) into Eq. (4-38), and using the fact that D in Eq. (4-37) varies exponentially with altitude [see Eq. (2-26)], gives

$$\text{div}(N\bar{v}) = -K_{Do} \left(\frac{\partial^2 N}{z^2} + \frac{3}{2} \frac{\partial N}{\partial z} + \frac{1}{2} N \right) e^z \tag{4-39}$$

The inclination of the geomagnetic field at the ionospheric point Θ is 37°, which gives the following value for $\sin^2 \Theta$ in Eq. (4-37):

$$\sin^2 \Theta = 0.362 \tag{4-40}$$

A value for the ambipolar diffusion coefficient D is taken from the work of Dalgarno [1964]. He finds the diffusion coefficient for O^+ ions in atomic oxygen at 700°K to be given by $Dn_1 = 5.7 \times 10^{18}$ cm^{-1} s^{-1}. Using the concentration of atomic oxygen at 300 km specified by the COSPAR model atmosphere of Fig. 3, $n_1 = 1.8 \times 10^8$ cm^{-3}, the value of D at 300 km is then

$$D_{300} = 3 \times 10^{10} \text{ cm}^2/\text{s} \tag{4-41}$$

The parameter K_{Do} in Eq. (4-39) is chosen on the basis of the values for $\sin^2 \Theta$ and D_{300} given in Eqs. (4-40) and (4-41). It should be noted, however, that the exact value used for K_{Do} is rather unimportant insofar as this work is concerned. This is due to the fact that the experimental data (Faraday rotation measurements) are proportional to the columnar electron content. Vertical movements of the ionization, due to diffusion or any other cause, do not directly affect the electron content. They do have a secondary effect on the electron content, though, due to the fact that the loss coefficient varies with altitude.

Consider, for example, the time behavior of an electron density profile which at $t = 0$ has the shape of a Chapman profile [given by Eq. (2-14) or (4-25)] with its peak at 240 km. For the purpose of this example, the

loss coefficient was chosen to make its value at 300 km, β_{300}, equal to 1.6×10^{-5} s^{-1}, and the homogeneous continuity equation was solved numerically as discussed in Section G. Figure 24 shows this profile after being subjected to loss and diffusion for 15 minutes with three separate diffusion coefficients--the one quoted above, together with one larger by a factor of 5 and one smaller by a factor of 5. The resulting profiles do differ, but the columnar electron content after 15 minutes is substantially the same regardless of which diffusion coefficient is used. When D_{300} was decreased by a factor of 5, the resulting electron content was increased by 1 percent; it was decreased by 6 percent when D_{300} was increased by a factor of 5. The differences, of course, increase with time, but the electron content of the ionosphere increases rapidly enough near sunrise so that at any instant within the interval of interest more than half of the "new" ionization present will have been produced during the

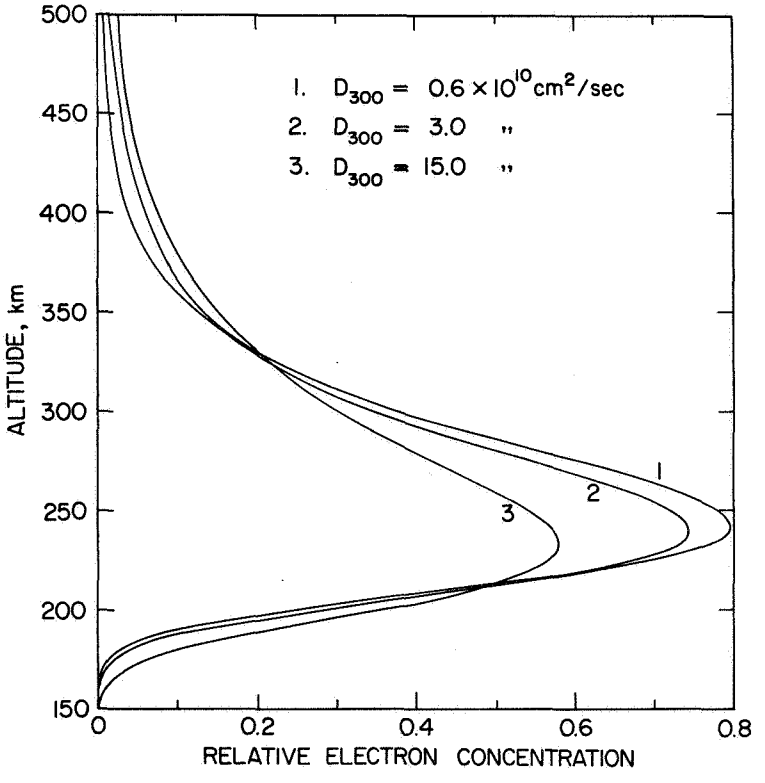

Fig. 24. ELECTRON DENSITY PROFILES AFTER BEING SUBJECTED TO DIFFUSION AND A LINEAR RECOMBINATION LAW FOR 15 MINUTES. In each case $\beta_{300} = 1.6 \times 10^{-5}$ s^{-1}, but three different values of D_{300} were used. Initially each profile had the shape of a Chapman production profile with a peak of 1.0 at an altitude of 230 km.

preceding 15 minutes. Furthermore the columnar electron content, rather than the exact electron density profile, is important here. Thus an exact value of D_{300}, or K_{Do}, is not needed.

G. Solution of Homogeneous Continuity Equation

The time-varying incremental electron density profiles, $\underline{n}_i(z, t-t_i)$, are determined from a numerical solution of the homogeneous continuity equation that results from setting $q \equiv 0$ in Eq. (2-1) and using the loss and transport expressions given by Eqs. (4-2) and (4-3). The equation can be written as

$$\frac{\partial N}{\partial t} = \left(K_{Do} e^{z}\right)\left(\frac{\partial^2 N}{\partial z^2} + \frac{3}{2}\frac{\partial N}{\partial z} + \frac{1}{2} N\right) - \beta_o e^{-1.75z} N \tag{4-42}$$

Consider $N \equiv \underline{n}_i(z, t-t_i)$ in Eq. (4-42). In a more compact form the equation can be expressed as

$$\frac{\partial N}{\partial t} = A \frac{\partial^2 N}{\partial z^2} + B \frac{\partial N}{\partial z} + CN \tag{4-43}$$

where

$$A = K_{Do} e^{z} \tag{4-44}$$

$$B = \frac{3}{2} K_{Do} e^{z} \tag{4-45}$$

$$C = \frac{1}{2} K_{Do} e^{z} - \beta_o e^{-1.75z} \tag{4-46}$$

To obtain a numerical solution, Eq. (4-43) is replaced by the difference equation,

$$\frac{N_{u,v+1} - N_{u,v}}{\Delta t} = A \frac{N_{u-1,v+1} - 2N_{u,v+1} + N_{u+1,v+1}}{(\Delta z)^2} + B \frac{N_{u+1,v+1} - N_{u-1,v+1}}{2(\Delta z)} + CN_{u,v+1} \tag{4-47}$$

where u is the order of the height step, v is the order of the time step, and $N_{u,v} = N(u\Delta z, v\Delta t)$. A system of equations composed of an equation like (4-47) for each altitude step and two boundary conditions is solved for values of N at time step $v+1$ in terms of values of N at time step v. The exact technique used to obtain the solution was described in detail by da Rosa [1965].

For one boundary condition, the electron concentration was taken to be zero at 100 km. The other boundary condition comes from considering the ionization to be in diffusive equilibrium (that is, $v_z = 0$) above 600 km. The resulting upper boundary condition, from Eq. (4-36), is

$$\frac{\partial N}{\partial z} = -\frac{1}{2} N \qquad (4\text{-}48)$$

The value used for K_{Do} is discussed in Section F.

A detailed solution of Eq. (4-42) for each of the $\underline{n}_i(z)$ profiles would be a rather extravagant use of computer time; it is also unnecessary. Since a Chapman profile has been used for each $\underline{n}_i(z)$ [see Eqs. (4-7) and (4-25)], it is sufficient to solve the equation for only a representative sample of such profiles. For each β_{300} to be used in attempting to find a best fitting value, a numerical solution of Eq. (4-42) is obtained for several initial conditions. Each of the initial profiles used to derive representative solutions is a Chapman profile with unit columnar electron content. The altitude of the peaks of these profiles at $t = 0$ is varied between 200 and 400 km. Detailed information regarding the time-varying shape of each profile is not needed, as discussed above. The only information retained from each solution is the time variation of both the electron content and the altitude of the peak. These results form a set of solutions for each assumed value of β_{300}, like the set shown in Figs. 25 and 26 for $\beta_{300} = 1.6 \times 10^{-5}\ s^{-1}$.

Each of the incremental electron density profiles, taken to be Chapman profiles at $t = 0$, is assumed to retain its Chapman shape with the altitude of its peak varying, for $\beta_{300} = 1.6 \times 10^{-5}$, as in Fig. 25. Its electron content and hence its peak concentration vary according to Fig. 26. In practice, information like that in Figs. 25 and 26, but in numerical

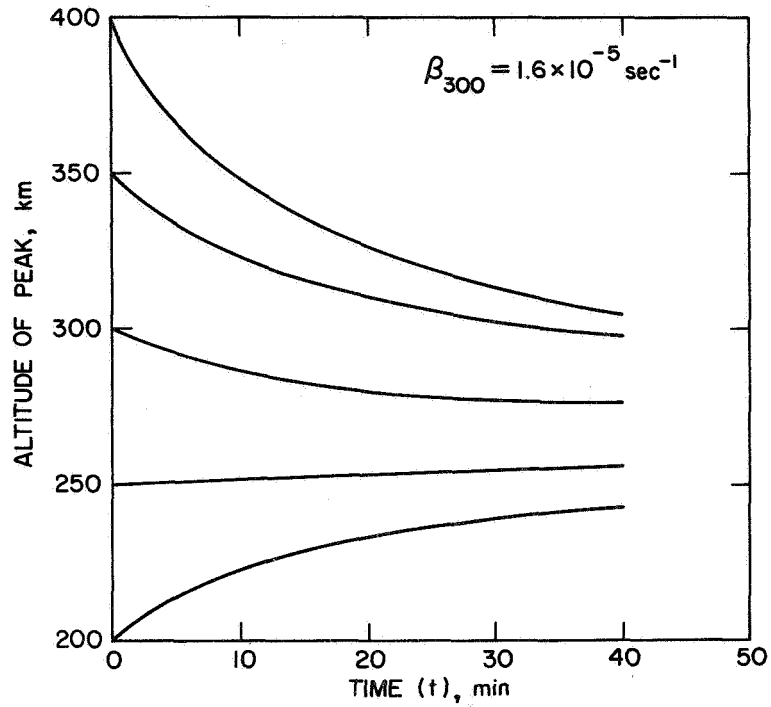

Fig. 25. THE ALTITUDE OF THE PEAK OF AN ELECTRON DENSITY PROFILE VS TIME, WHERE THE IONIZATION IS SUBJECT ONLY TO VERTICAL DIFFUSION ($D_{300} = 3 \times 10^{10}$ cm^2/s AND $\sin^2 \Theta = 0.362$) AND A LINEAR RECOMBINATION LAW. The graph applies to electron density profiles which at $t = 0$ are shaped like a Chapman production profile.

form, is fed into a computer for each β_{300} to be considered. By interpolation, the peak concentration and altitude of the peak of any $\underline{n}_i(z, t-t_i)$ may be determined from these data for $t > t_i$ if these quantities are known at $t = t_i$.

Several investigators have presented analytical solutions of the continuity equation with characteristics similar to those shown in Figs. 25 and 26. Duncan [1956] and Martyn [1956], for example, investigated the solution of Eq. (4-42) but with the assumption that the loss coefficient varies as e^{-z} rather than $e^{-1.75z}$. They both found that a Chapman alpha layer--an electron density profile whose functional form is the square root of the Chapman production profile--will decay under the influence of diffusion and recomination without any change in shape. The layer moves as it decays until its peak is situated at an equilibrium altitude where $\beta = 0.25\ (D/H^2)\ \sin^2 \Theta$. Still assuming $\beta \sim e^{-z}$, Rishbeth

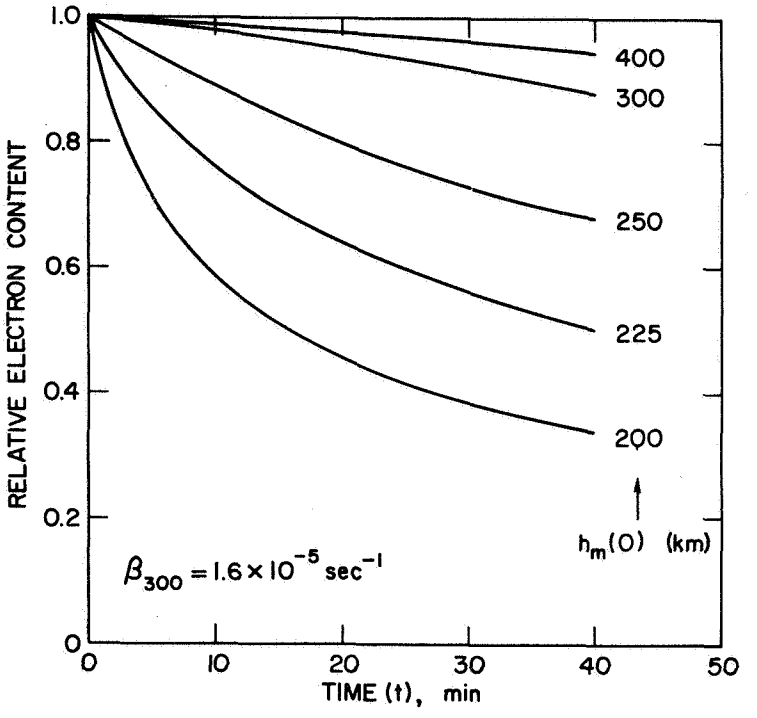

Fig. 26. THE RELATIVE ELECTRON CONTENT VS TIME FOR ELECTRON DENSITY PROFILES WHICH AT $t = 0$ ARE SHAPED LIKE CHAPMAN PRODUCTION PROFILES, AND WHICH FOR $t > 0$ ARE SUBJECT ONLY TO VERTICAL DIFFUSION ($D_{300} = 3 \times 10^{10}$ cm^2/s AND $\sin^2 \Theta = 0.362$) AND A LINEAR RECOMBINATION LAW. The altitude of the peak at $t = 0$ is represented by $h_m(0)$.

[1961] showed that an electron density profile like the $\underline{n}_i(z, t-t_i)$ profiles used here--a Chapman beta layer--could also decay without changing its shape. He found that its peak would approach an equilibrium altitude where $\beta = (D/H^2) \sin^2 \Theta$. The numerical solutions obtained in the present analysis, with $\beta \sim e^{-1.75z}$, show that the electron density profiles do not strictly maintain their shape, but they do tend to move to an equilibrium altitude where $\beta \approx 0.13\ (D/H^2) \sin^2 \Theta$. According to a solution given by Dungey [1956], the $\underline{n}_i(z, t-t_i)$ profiles also will not exactly maintain their shape when $\beta \sim e^{-2z}$, but they will move to an equilibrium level where $\beta \approx 0.11\ (D/H^2) \sin^2 \Theta$.

H. Faraday Rotation Calculations

Let $\underline{N}$ represent the electron concentration in the model ionosphere composed of the $\underline{N}_i(z)$ profiles given by Eq. (4-9). The amount of Faraday rotation, in radians, due to this ionosphere is [see Eq. (3-1)]

$$\underline{F} = \frac{0.0297}{f^2} \int_{L_p} \underline{N} \mathcal{H} \cos \theta \, ds \qquad (4\text{-}49)$$

where rationalized MKS units are used.

The line integral in Eq. (4-49) is evaluated numerically in a straightforward manner. Values for $\underline{N}$ are obtained at points where the raypath intersects the planes of constant χ (Fig. 20) along which the $\underline{N}_i(z)$ profiles apply. Between these planes a linear interpolation yields values of $\underline{N}$.

The integral is evaluated along the raypath only between altitudes of 100 and 500 km. Virtually all of the 0^+ ions are produced within this range (Fig. 8c) and remain within these limits.

The factor $(\mathcal{H} \cos \theta)$ in the integral is very nearly (to within 0.1 percent) proportional to R^{-4} along the raypath at F region altitudes, where R is the geocentric radius. (The R^{-4} variation results from an R^{-3} variation in $\mathcal{H}$ and an approximate R^{-1} variation in $\cos \theta$.) Its magnitude at an altitude of 300 km is computed from a set of 48 gaussian coefficients published by Jensen and Cain [1962]. Typical values are shown in Table 6. The values used at other altitudes are derived from the 300 km

Table 6

VALUES OF $(\mathcal{H} \cos \theta)$ AT THE IONOSPHERIC POINT

Longitude of Syncom III	$\mathcal{H} \cos \theta$ (A/m)
180°	21.4
170° E	20.1
160° E	18.1

value, extrapolated according to an R^{-4} variation. The R^{-4} variation only amounts to a decrease in $(\mathcal{H} \cos \theta)$ of 5 percent per 100 km increase in altitude in the F region. For this reason, as mentioned in Section III-B, the amount of Faraday rotation is not sensitive to the exact vertical distribution of electrons, though it is a measure of the columnar electron content of the ionosphere.

I. Treatment of Nighttime Ionization

Let Ω_m represent the observed Faraday rotation angles before applying any corrections. The data consist of a set of measurements taken at 5 min intervals, a sample of which is shown in Fig. 27. There is no evidence of increased ionization due to the rising sun prior to the time when $\chi = 100°$, but shortly afterward the ionospheric electron content and the observed Faraday rotation angle begin increasing rapidly.

Generally during the last 3 or 4 hours of the night, before $\chi = 100°$, the electron content observed over Hawaii remains nearly constant [Garriott

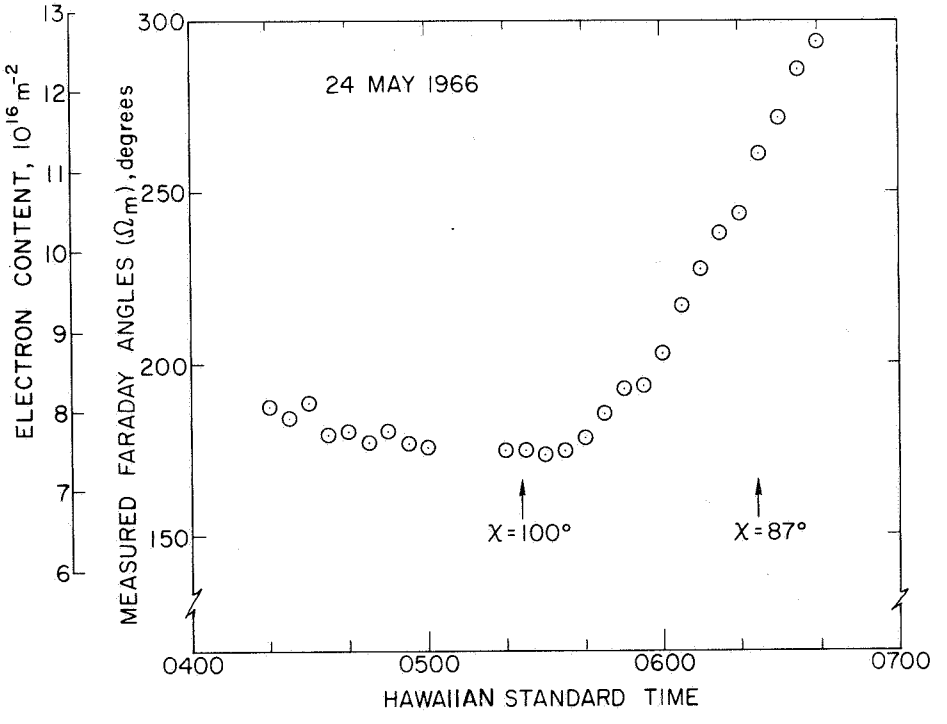

Fig. 27. THE FARADAY ROTATION ANGLES, AND CORRESPONDING VALUES OF ELECTRON CONTENT, OBSERVED FROM HONOLULU DURING THE MORNING OF 24 MAY 1966.

et al, 1965; Yuen and Roelofs, 1967]. The effects of the nighttime ionization are taken into account in the analysis essentially by assuming that the electron content of the body of ionization present at $\chi = 100^\circ$ continues to behave during the following 1 hour exactly as it did during the hour prior to $\chi = 100^\circ$. The straight line that best fits, in a least-mean-square sense, the observed data during the 1 hour interval ending when $\chi = 100^\circ$ is computed. The symbol η is used to represent the slope of this line. Then, adjusted values Ω_M of the observed Faraday rotation angles Ω_m are obtained by letting

$$\Omega_M = \Omega_m - \eta(t - t_o) \qquad (4\text{-}50)$$

which has the effect of making the slope of the nighttime data equal to zero. Data for any day on which the nighttime electron content is disturbed, so that a meaningful value of η cannot be obtained, are omitted from the analysis. The magnitude of the adjustment is normally rather small. For 80 percent of the data used in the final analysis, the nighttime rate of change, η, was less than that for the data shown in Fig. 27.

The method of accounting for the effects of the nighttime ionization is reasonable, although at present, prediction of the exact behavior of this body of ionization after sunrise in detail would be difficult. Even the mechanism for maintaining the ionization at night is by no means fully understood [da Rosa and Smith, 1967]. Certainly sunrise is accompanied by an increasing temperature, which in turn leads to a vertical redistribution of the ionization. However, a vertical redistribution of the nighttime layer will not in itself alter its total electron content.

The body of ionization present at $\chi = 100^\circ$ is usually observed to have been maintained for several hours prior to the time when $\chi = 100^\circ$ with a small but approximately constant rate of change in its electron content. It is being assumed that the rate of change of the electron content of this body of ionization does not vary significantly from the nighttime rate of change within approximately 1 hour after $\chi = 100^\circ$.

That this treatment of the nighttime ionization is likely to be correct can be seen from the data in Figs. 28 and 29. Figure 28 shows

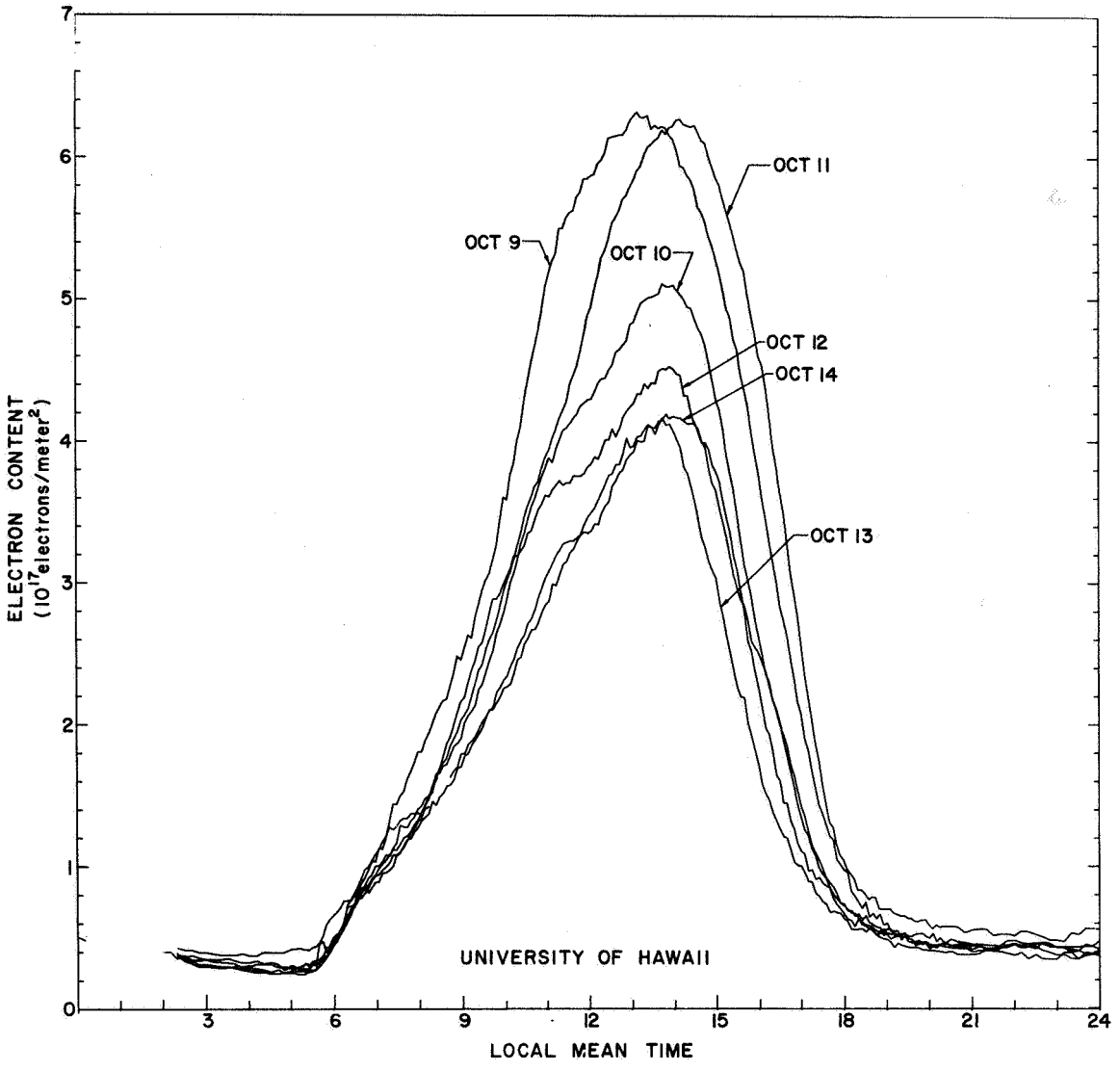

Fig. 28. THE DIURNAL VARIATION OF THE ELECTRON CONTENT OVER HONOLULU ON A SERIES OF DAYS IN OCTOBER 1964. (After Garriott et al, 1965.)

the electron content over Hawaii for several days in October 1964. Figure 29 shows for the same days the "slab thickness" of the ionosphere, a parameter defined as the ratio of electron content to the maximum electron concentration. Notice the pronounced peak in the slab thickness curves between 0300 and 0600 local mean time. The peak is due to a rather sudden decrease in the maximum electron concentration, by more than a factor of 2, which is not accompanied by a change in the electron content. The layer of ionization must, therefore, have undergone a substantial vertical redistribution

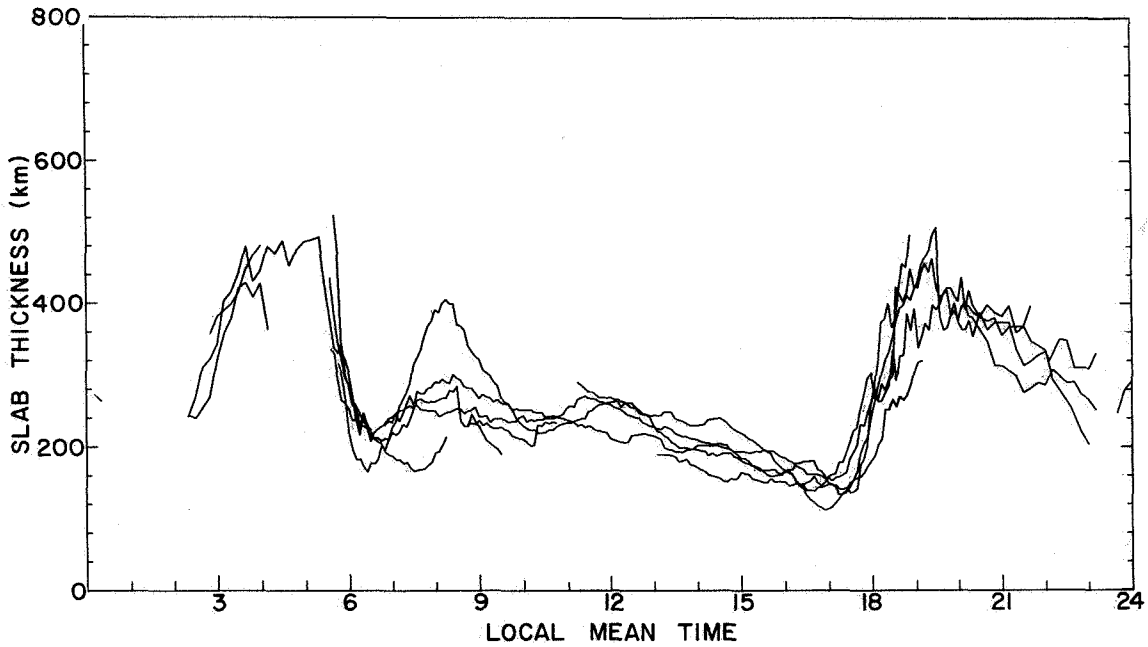

Fig. 29. THE DIURNAL VARIATION OF SLAB THICKNESS OBSERVED AT THE UNIVERSITY OF HAWAII FOR THE SAME DATES AS GIVEN IN FIG. 28. (After Garriott et al, 1965.)

during the interval, but the electron content change was minimal. Yuen and Roelofs [1967] have presented, on a monthly average basis, data like those in Figs. 28 and 29, which show that the same type of behavior was typical over Hawaii during the entire year of 1965.

J. Curve Fitting

The result of the Faraday rotation calculations in Section H is a function $\underline{F}$ such as that shown in Fig. 30. The problem here is to match this function to a set of experimental observations, after adjusting the observations according to Eq. (4-50). The function $\underline{F}$ is compared to the data between $\chi = 100^\circ$ and $\chi = 87^\circ$. Shortly after $\chi = 87^\circ$, the data often do not agree well with the theoretical model, perhaps because the production of ionization moves to lower altitudes where the linear loss law no longer applies.

Let Ω_{M_j} represent the adjusted data points occurring between $\chi = 100^\circ$ and $\chi = 87^\circ$. The first data point occurring after $\chi = 100^\circ$

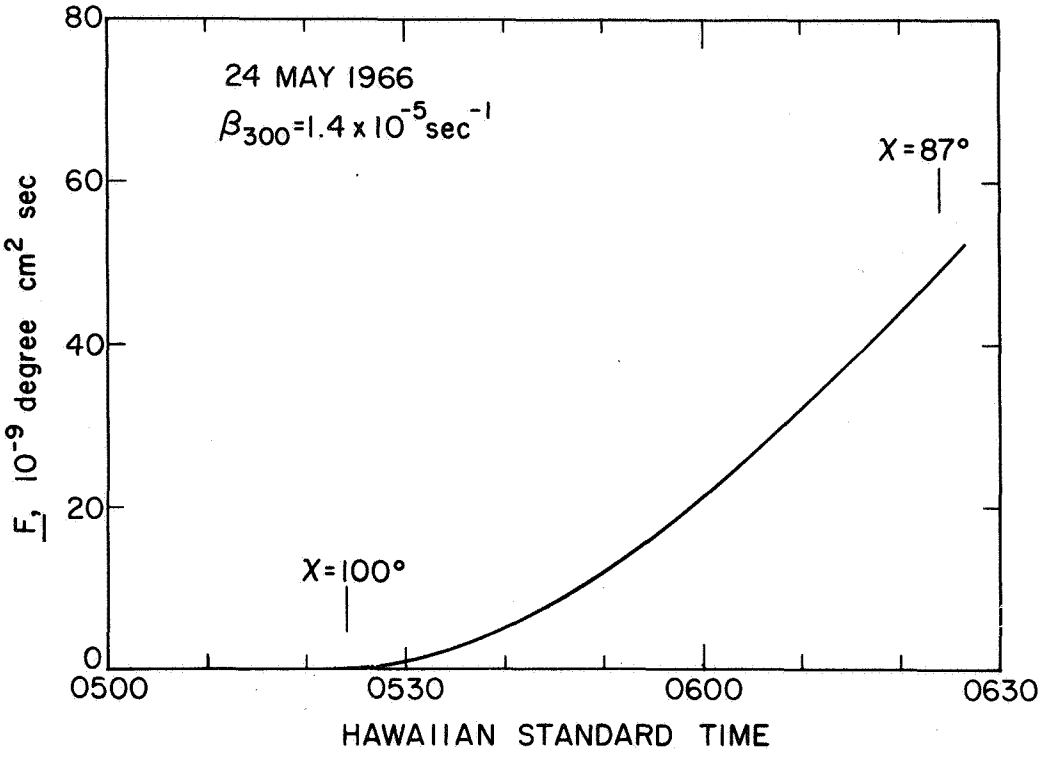

Fig. 30. THE FUNCTION $\underline{F}$ SHOWING THE FARADAY ROTATION DUE TO AN IONOSPHERE COMPOSED OF NORMALIZED ELECTRON DENSITY PROFILES, $\underline{N}_i(z)$, FOR 24 MAY 1966. The units of $\underline{F}$ arise from the normalization with respect to $Q_{90}[0^+]$.

is designated by $j = 1$. The total number of points in the interval is J. Time t_j is the time associated with Ω_{M_j}.

Consider the function

$$\gamma(t) = \mu + \lambda \underline{F}(t) \tag{4-51}$$

The theoretical function will be matched to the data by computing the constants μ and λ that will minimize the mean-square difference between $\gamma(t)$ and Ω_{M_j} for $1 \leq j \leq J$. The resulting value of μ is the Faraday rotation angle due to the nighttime ionization present at $\chi = 100°$. The value of λ is the best fitting value of $Q_{90}[0^+]$ associated with the particular β_{300} assumption upon which $\underline{F}$ is based.

Let ρ be the root-mean-square difference between $\gamma(t)$ and Ω_{M_j} for $1 \leq j \leq J$. Then,

$$\rho^2 = \frac{1}{J} \sum_{j=1}^{J} \left[\Omega_{M_j} - \gamma(t_j) \right]^2 \qquad (4\text{-}52a)$$

or

$$\rho^2 = \frac{1}{J} \sum_{j=1}^{J} \left[\Omega_{M_j} - \mu - \lambda F(t_j) \right]^2 \qquad (4\text{-}52b)$$

Squaring the term under the summation sign in Eq.(4-52b) and summing each of the resulting terms separately gives

$$\rho^2 = \mu^2 + 2\mu\lambda K_1 - 2\lambda K_2 - 2\mu K_3 + \lambda^2 K_4 + K_5 \qquad (4\text{-}53)$$

where

$$K_1 = \frac{1}{J} \sum_{j=1}^{J} \underline{F}(t_j) \qquad (4\text{-}54)$$

$$K_2 = \frac{1}{J} \sum_{j=1}^{J} \underline{F}(t_j)\, \Omega_{M_j} \qquad (4\text{-}55)$$

$$K_3 = \frac{1}{J} \sum_{j=1}^{J} \Omega_{M_j} \qquad (4\text{-}56)$$

$$K_4 = \frac{1}{J} \sum_{j=1}^{J} \underline{F}^2(t_j) \qquad (4\text{-}57)$$

$$K_5 = \frac{1}{J} \sum_{j=1}^{J} \Omega_{M_j}^2 \qquad (4\text{-}58)$$

When ρ^2 is minimized with respect to μ and λ,

$$\frac{\partial \rho^2}{\partial \mu} = 0 \tag{4-59}$$

and

$$\frac{\partial \rho^2}{\partial \lambda} = 0 \tag{4-60}$$

Conditions (4-59) and (4-60) applied to Eq. (4-53) lead to the following pair of equations:

$$\mu + K_1 \lambda = K_3 \tag{4-61}$$

and

$$K_1 \mu + K_4 \lambda = K_2 \tag{4-62}$$

Solving Eqs. (4-61) and (4-62) simultaneously for μ and λ yields

$$\mu = \frac{K_1 K_2 - K_3 K_4}{K_1^2 - K_4} \tag{4-63}$$

and

$$\lambda = \frac{K_1 K_3 - K_2}{K_1^2 - K_4} \tag{4-64}$$

If the function $\underline{F}$ is based upon the assumed loss coefficient $\beta_{300}^{(1)}$, the integrated rate of production of O^+ ions at sunrise implied by this particular $\underline{F}$ is

$$Q_{90}^{(1)}[O^+] = \lambda \tag{4-65}$$

Using the same day's data but theoretical Faraday functions based upon different assumed values of β_{300}, other values are computed for $Q_{90}[0^+]$ until the pair of numbers for β_{300} and $Q_{90}[0^+]$ resulting in the lowest possible ρ is found.

Chapter V

RESULTS

Chapter IV described a method for determining $Q_{90}[O^+]$, the integrated rate of production of O^+ ions at sunrise, and β_{300}, the magnitude of the linear loss coefficient at an altitude of 300 km, from Faraday rotation observations. The present chapter presents the results of an application of the analysis to data obtained at the University of Hawaii during a period extending from September 1964 through August 1966. Values of $Q_o[O^+ + N_2^+]$, the integrated rate of production of both O^+ and N_2^+ ions for $\chi = 0$, and values of the solar EUV photon flux implied by the results are also discussed.

A. Loss Coefficient

The data reduction process outlined in Chapter IV was only applied in its entirety to monthly averaged Faraday rotation measurements rather than to each individual day's data. A value of the loss coefficient was thus obtained for each month. Later the loss coefficient was fixed at its average value and the necessary $\underline{F}$'s were computed in order to determine $Q_{90}[O^+]$ on a day-to-day basis as described in Section B.

Figure 31 indicates the quality of the fit between the computed Faraday rotation angles and the monthly averaged data as a function of the assumed magnitude of the loss coefficient at 300 km. The figures show the root-mean-square difference between computed and observed data, expressed as a percentage of the total increase in the Faraday rotation angle between $\chi = 100°$ and $\chi = 87°$. In most cases a well defined value of β_{300} was found, which resulted in the best possible agreement between theory and the data. Furthermore, the minimum ρ associated with the optimum value of β_{300} is usually about 1 percent; the agreement is indeed very good. Figure 32 shows the monthly averaged data, expressed in terms of the ionospheric electron content, together with the best fitting theoretical curves.

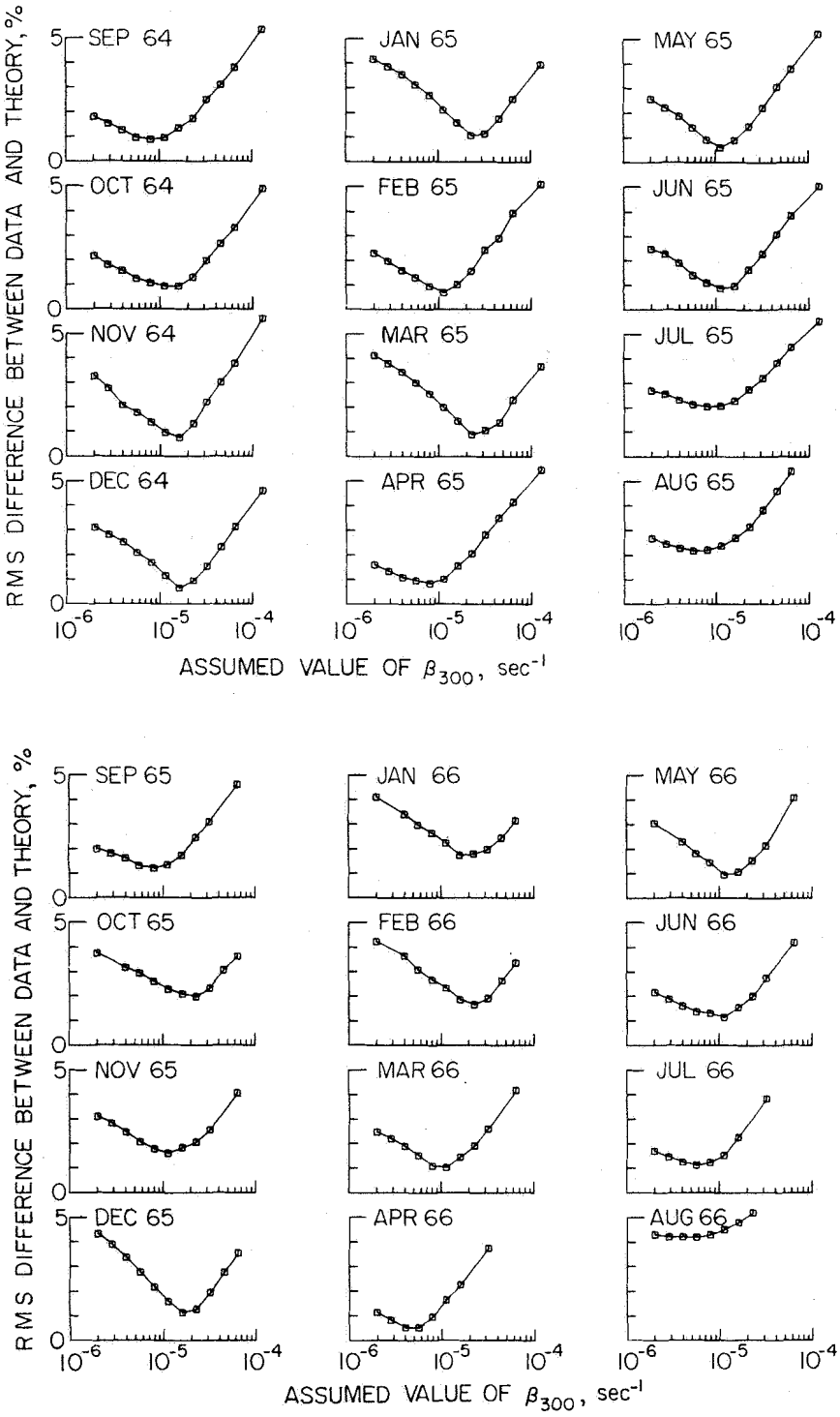

Fig. 31. THE ROOT-MEAN-SQUARE DIFFERENCE BETWEEN COMPUTED FARADAY ROTATION ANGLES AND MONTHLY AVERAGED DATA, FOR $100° \geq \chi \geq 87°$, AS A FUNCTION OF THE ASSUMED VALUE OF THE LOSS COEFFICIENT AT 300 km. The rms difference is expressed as a percent of the total increase in the Faraday rotation angle between $\chi = 100°$ and $\chi = 87°$. No value for the loss coefficient was taken from the August 1966 data.

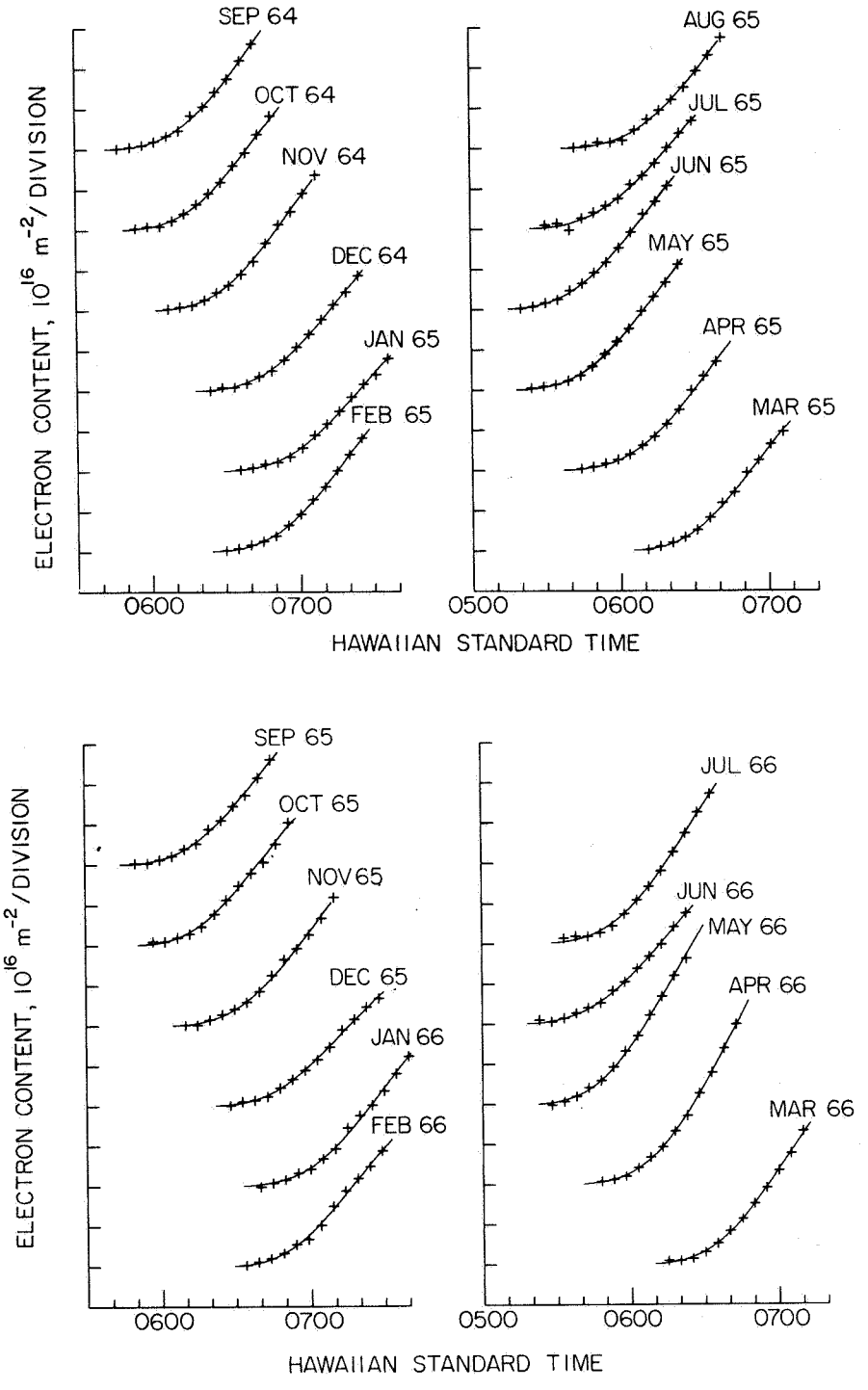

Fig. 32. MONTHLY AVERAGED DATA (CROSSES), EXPRESSED IN TERMS OF THE ELECTRON CONTENT, SUPERIMPOSED UPON THEORETICAL CURVES (SOLID LINES) THAT CORRESPOND TO THE OPTIMUM VALUES OF β_{300} OBTAINED FROM FIG. 31.

Figure 33 summarizes the results derived from Fig. 31. On the average, during the 2-year interval covered, the loss coefficient at 300 km is found to be

$$\text{Average } \beta_{300} = 1.4 \times 10^{-5} \text{ s}^{-1} \qquad (5\text{-}1)$$

A seasonal variation of about 2:1 is also observed, with higher loss coefficients occurring in the winter.

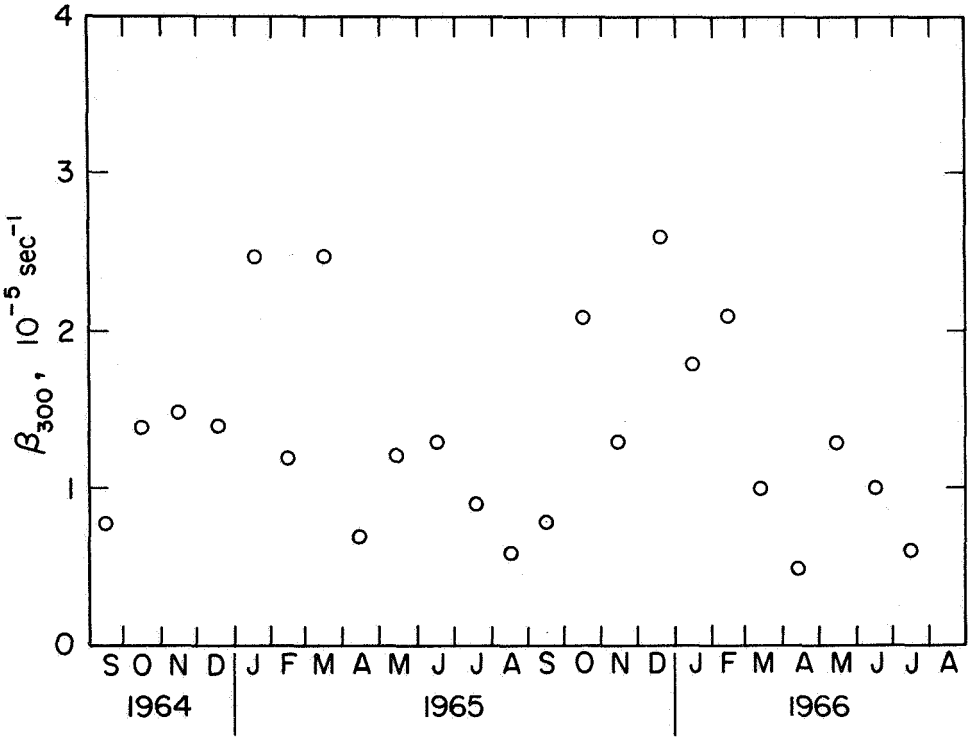

Fig. 33. THE LOSS COEFFICIENT AT 300 km VS DATE. The points plotted represent the optimum values obtained from Fig. 31.

The effect of the observed loss coefficient [Eq. (5-1)] on the sunrise electron content is shown in Figs. 34 and 35. The total increase in electron content by the time that $\chi = 87°$ is 32 percent less with $\beta_{300} = 1.4 \times 10^{-5}$ s^{-1} than it would be if there were no recombination of the freshly produced O^+ ions. It is the effect of loss on the rate of change of electron content, or on the shape of the electron content vs time curve, that leads to the determination of β_{300} by the present method. With $\beta_{300} = 0$, the time derivative of the electron content

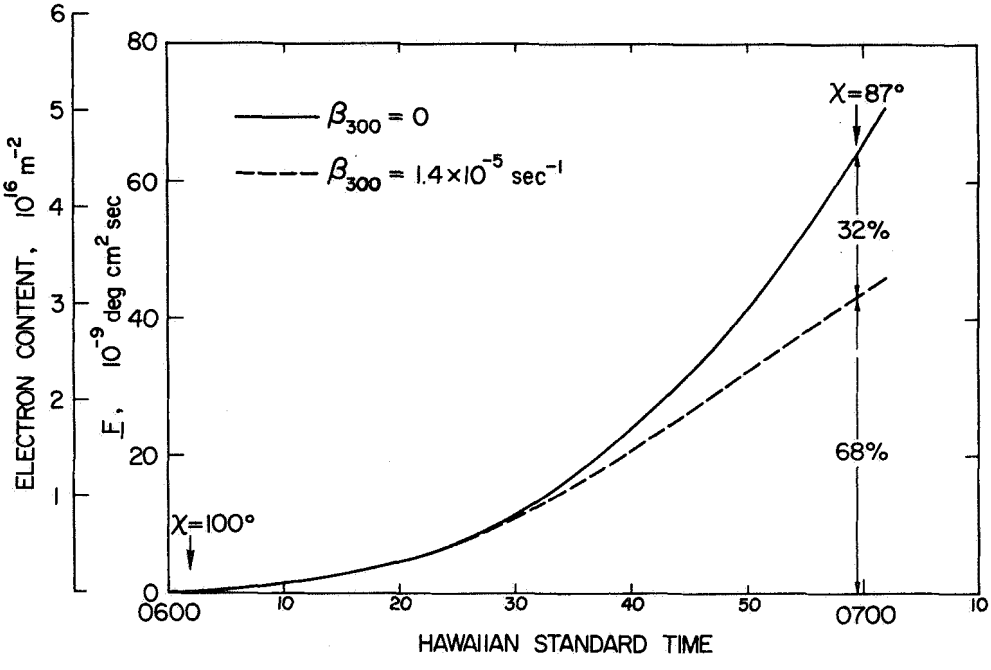

Fig. 34. THE EFFECT OF RECOMBINATION ON THE SUNRISE FARADAY ROTATION ANGLES AND ELECTRON CONTENT. The electron content prior to $\chi = 100°$ is taken to be zero. These curves were computed specifically for 1 November 1965.

would continue increasing throughout the sunrise period since the integrated rate of production of O^+ ions continues increasing. But this is not the case when $\beta_{300} \neq 0$ (Fig. 35).

Because the determination of β_{300} is dependent upon the exact shape of the electron content or Faraday rotation curves, monthly averaged data were used. If the loss coefficient had been determined on a day-to-day basis, random errors in the individual data points would have lead to large, and erroneous, daily fluctuations in the values obtained for β_{300}. Computing β_{300} on a day-to-day basis, therefore, was not justified, especially in view of the extra computer time that would have been required.

The magnitude of the loss coefficient is a difficult quantity to determine accurately because the effects of loss on the electron concentration are, in general, difficult to separate from the effects of production, diffusion, and drift. In the present case, it is the availability of nearly continuous data through a period when the effects of

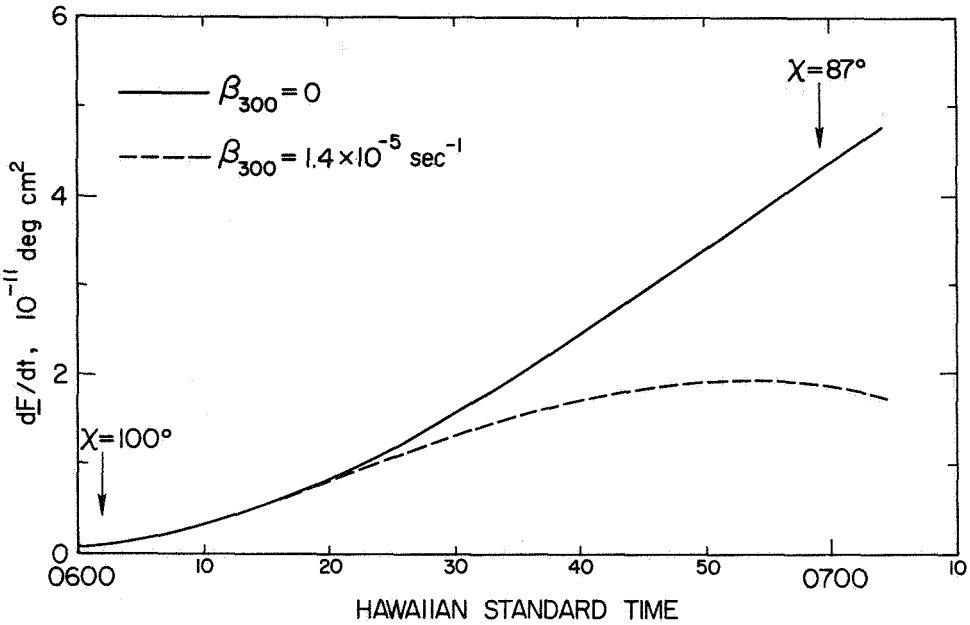

Fig. 35. THE EFFECT OF RECOMBINATION ON THE RATE OF CHANGE OF THE SUNRISE FARADAY ROTATION ANGLES. These curves are derivatives of those in Fig. 34.

loss on the electron content are varying rapidly in a predictable manner that allows for the determination of β_{300}. Other investigators have used a variety of techniques in an effort to measure the same quantity.

Recently Prasad [1967] published a method for computing β_{300} from the shape of a nighttime electron density profile. His results are based upon data taken at Arecibo, Puerto Rico, one night in November 1965. He found the loss coefficient β_{300} to be 1.07×10^{-5} s^{-1}, a value which agrees reasonably well with Eq. (5-1).

Earlier Mitra et al [1964] used another method of analysis based upon electron density profiles at a time during the night when dN/dt was found to be zero at all altitudes. Their method is only applicable near the geomagnetic equator where vertical diffusion can be neglected. The results published show $\beta_{300} = 1 \times 10^{-4}$ s^{-1} over Huancayo, Peru, on October 11, 1958, and $\beta_{300} = 2 \times 10^{-4}$ s^{-1} over Delhi, India, on September 12, 1958. These coefficients are approximately 10 times larger than those obtained in this work. However, 1958 was a year of very high solar activity when, according to Nicolet [1963], the nighttime temperature of the atmosphere was about 1300°K. The COSPAR model for the neutral

atmosphere [CIRA 1965] shows the concentration of N_2 at 300 km under these conditions to be 20 times greater than during periods of minimum solar activity, such as 1965. Thus, since β_{300} is proportional to $n[N_2]$ [see Eqs. (4-31) and (4-34)] the results here are consistent (within a factor of 2) with those reported by Mitra et al.

Ratcliffe et al [1956] found β_{300} to be 1×10^{-4} s^{-1} during a period of high solar activity, a value which is also consistent with the present results if the variation of $n[N_2]$ with solar activity is taken into account. Their results were derived from the rate of decay of the electron concentration at fixed altitudes at night. It was assumed that at night the loss term in the continuity equation completely dominated the production and transport terms. The authors noted that this assumption appeared to be valid during periods of high solar activity but definitely was not valid during solar minimum conditions.

Quinn and Nisbet [1965] used measurements of the nighttime electron density profile below the height of the peak electron concentration, and a model above that altitude, to derive nighttime values of β_{300}. Their results scatter considerably, but on the average they found $\beta_{300} = 2 \times 10^{-5}$ s^{-1} during periods of low solar activity.

Rishbeth [1964] compared values of β_{300} obtained by several other authors under widely varying conditions. He found most of the values to be consistent with $\beta_{300} \approx 1 \times 10^{-5}$ s^{-1} during periods of low solar activity.

The seasonal variation in β_{300} (Fig. 33) is still puzzling. If a seasonal variation in the loss coefficient is to be invoked as an explanation for the seasonal anomaly (higher electron contents in winter than in summer), β_{300} would have to decrease in the winter rather than increase. At this point, neither the seasonal anomaly nor the observed seasonal variation in β_{300} is understood.

B. Integrated Production Rates

1. Production of O^+ at Sunrise

With the loss coefficient determined on the basis of monthly averaged data, the value of β_{300} is fixed at 1.4×10^{-5} s^{-1} as in Eq. (5-1). Daily measurements of the Faraday rotation are then matched

to theoretical curves computed on the basis of this loss coefficient to determine $Q_{90}[O^+]$ on a day-to-day basis. The loss coefficient could be allowed to vary on a month-to-month basis in line with the data in Fig. 33, but resulting values of $Q_{90}[O^+]$ would not be substantially different. Values obtained during June and July would tend to be about 10 percent lower, and those for December and January would be about 10 percent higher corresponding to the ±50 percent variation is β_{300}. This shows the degree to which the computations of $Q_{90}[O^+]$ are "decoupled" from the results of the loss coefficient calculations.

Figure 36 indicates the degree to which the daily experimental data agreed with the theory. Plotted is the root-mean-square difference

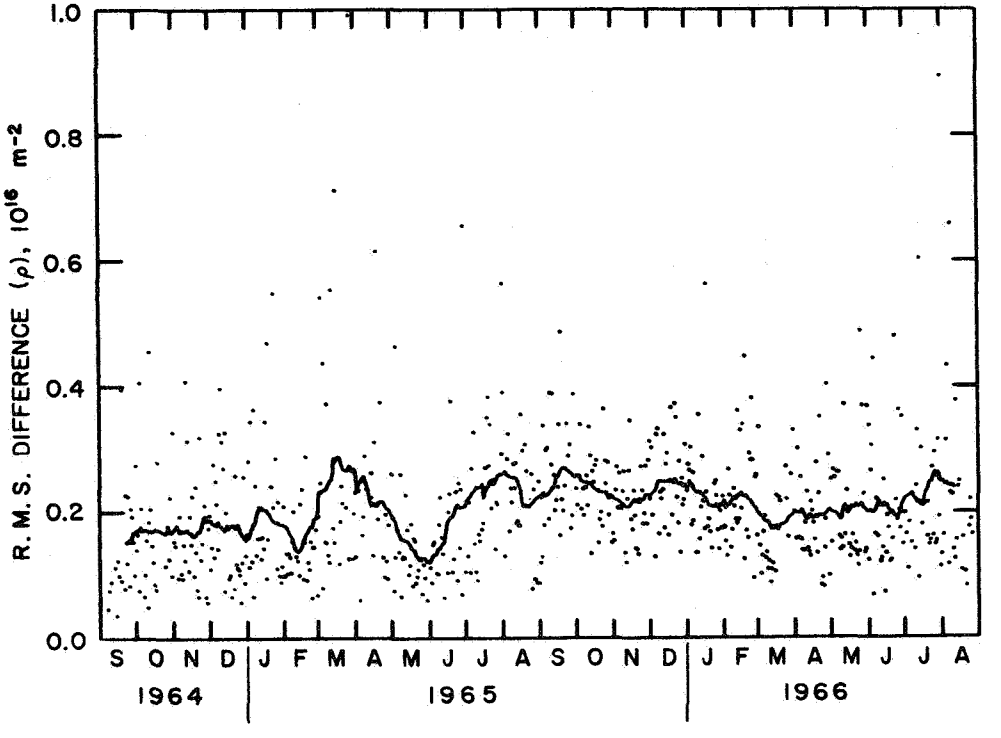

Fig. 36. THE ROOT-MEAN-SQUARE DIFFERENCE BETWEEN COMPUTED FARADAY ROTATION ANGLES AND DAILY MEASUREMENTS FOR $100° \geq \chi \geq 87°$. Data on all days when ρ, expressed in terms of electron content, was greater than 0.3×10^{16} m^{-2} were discarded.

between the measurements and computed curves. Most of the difference is simply due to random scatter in the measured data. The random error itself has an rms value of about 4.7° of Faraday rotation (see Section III-C)

or about 0.20×10^{16} electrons m^{-2} when expressed in terms of electron content. On the average, ρ is not much greater than what would be expected on the basis of the random errors alone. For the purposes of obtaining values for $Q_{90}[0^+]$, all days on which ρ exceeds 0.3×10^{16} electrons m^{-2} were ignored.

The actual data, together with the best fitting theoretical curves for several days, are shown in Fig. 37. Data for the 1-hour interval preceding $\chi = 100°$ are included in the figure. A straight

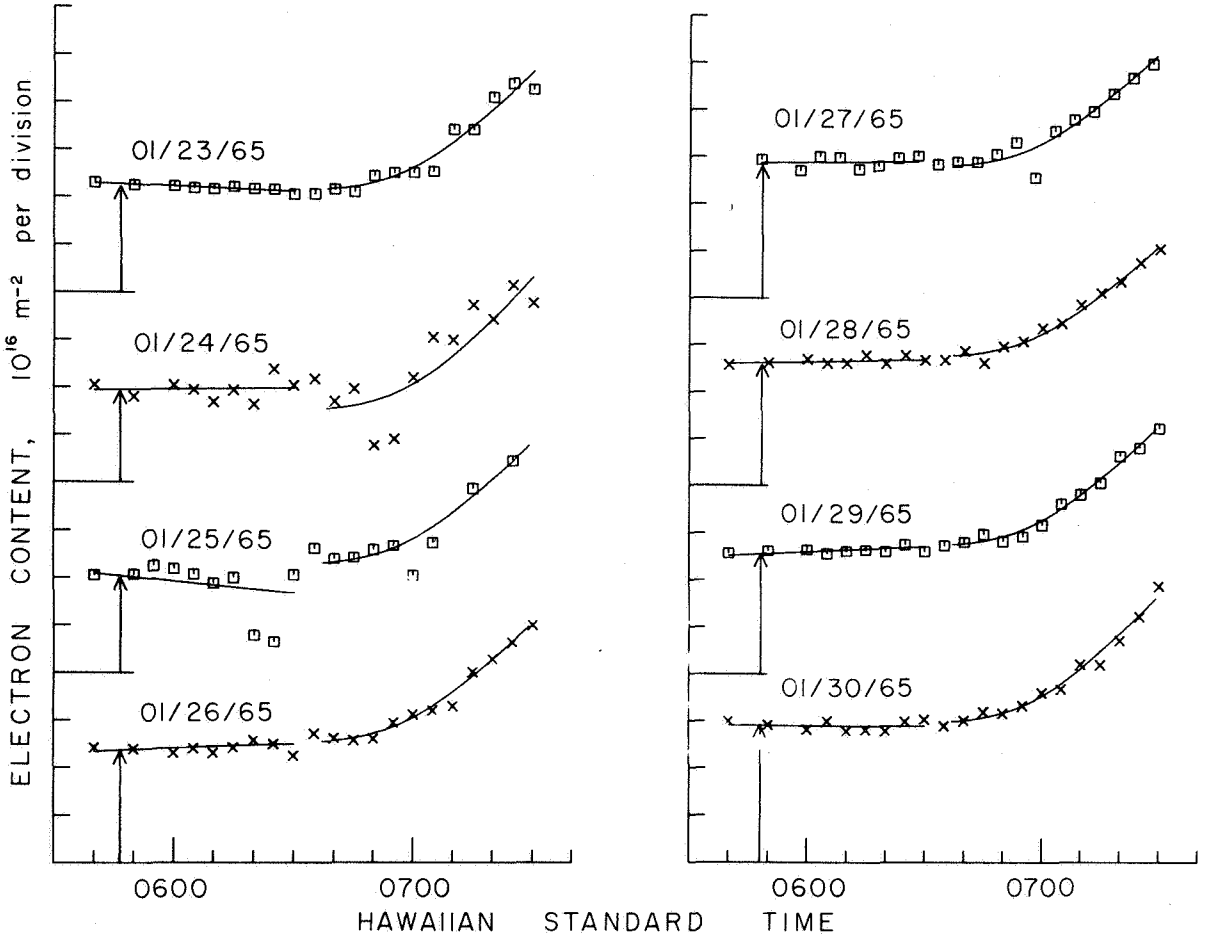

Fig. 37. THE MEASURED DATA TOGETHER WITH THE BEST FITTING THEORETICAL CURVES FOR SEVERAL DAYS IN JANUARY 1965. The straight line which best fits the data during the 1-hour interval prior to $\chi = 100°$ is shown, as well as the best fitting theoretical function for $100° \geq \chi \geq 87°$.

line was fit to the nighttime data in order to determine its slope (see Section IV-I). After correcting the data for the nighttime slope, a function, F, was fit to the sunrise data to determine $Q_{90}[O^+]$ as described in Section IV-J. If everything was in order, the straight line that was fit to the nighttime data should match F at $\chi = 100°$. The data are discarded for days such as January 24 and 25, 1965, when this matching does not occur.

Daily values and a 30-day running mean of $Q_{90}[O^+]$ are plotted in Fig. 38. The daily values of $Q_{90}[O^+]$ plotted in the figure are also

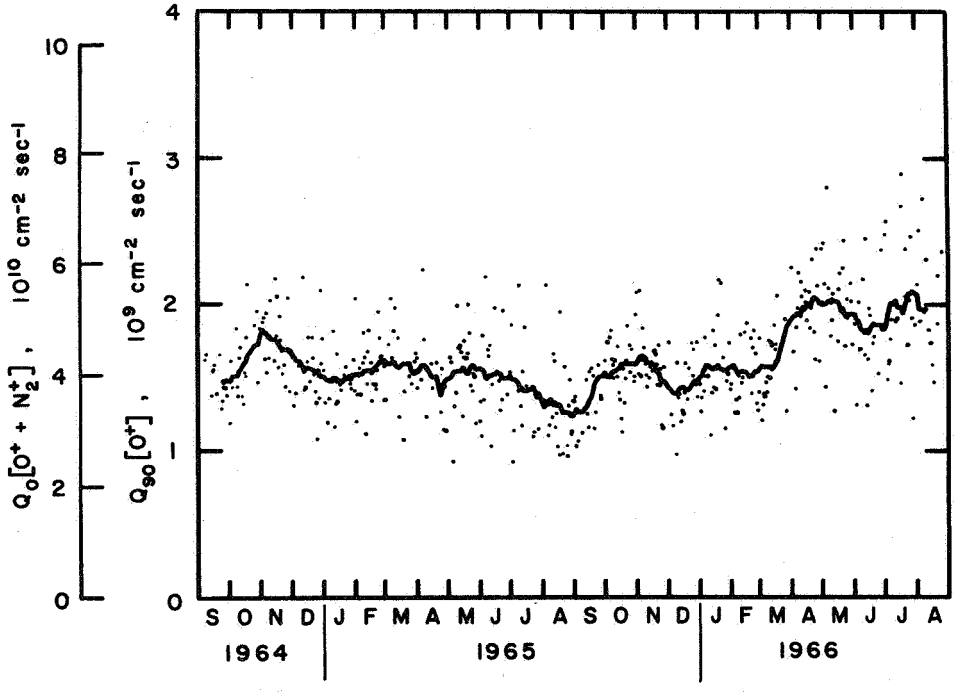

Fig. 38. PLOT OF $Q_{90}[O^+]$ AND $Q_o[O^+ + N_2^+]$ VS DATE. The solid line is a 30-day running mean.

tabulated in the appendix. On the average, $Q_{90}[O^+]$ was about 1.7×10^9 cm^{-2} s^{-1} during the 2-year interval, with considerable day-to-day fluctuations but no clear seasonal variation. (No seasonal variation in excess of a few percent, due to the change in the Earth-Sun distance, is expected.) Values plotted in Fig. 38 are distributed about the running mean with a standard deviation of ±15 percent. The lowest production rates are obtained during the summer of 1965.

Rishbeth and Setty [1961] suggested that an increase in the percent of molecular nitrogen in the atmosphere at F region altitudes during the summer could at least partly account for the lower electron concentrations observed in the summer months. They observed that the rate of increase of the electron concentration at fixed heights at sunrise was about twice as great in winter as in summer during sunspot minimum conditions. The seasonal variation was attributed to a seasonal variation in the rate of production of observable ions, which they indicated could at least be partly due to a possible seasonal variation in atmospheric composition.

An increase in $n[N_2]$ relative to $n[O]$ would show up in Fig. 38 as a decrease in $Q_{90}[O^+]$. No pronounced decrease was in fact observed, but the so-called seasonal anomaly was not very pronounced during this period of low solar activity either [Yuen and Roelofs, 1967].

2. Production of O^+ and N_2^+ with an Overhead Sun

Figure 38 also contains a scale for $Q_o[O^+ + N_2^+]$, the integrated rate of production of both O^+ and N_2^+ ions for an overhead sun. Once a model atmosphere is fixed, $Q_o[O^+ + N_2^+]$ is proportional to $Q_{90}[O^+]$. To determine the proportionality constant, first note that $Q_o[O^+ + N_2^+] = I_\infty$ for a two-constituent model atmosphere where the ionization efficiency is 100 percent; that is, each incident photon produces one ion. The relationship between $Q_{90}[O^+]$ and $Q_o[O^+ + N_2^+]$ is determined by computing the former in terms of I_∞ through a numerical integration of Eq. (4.19). Results for a two-constituent model atmosphere are shown in Fig. 39, where the parameter κ, as derived from either Eq. (4-23) or Fig. 22, is used to provide a measure of the relative concentrations of O and N_2. As κ increases (with I_∞, and hence $Q_o[O^+ + N_2^+]$, remaining constant), $Q_{90}[O^+]$ decreases since a smaller portion of the incident ionizing flux is then available for producing O^+ ions. The ratio $Q_o[O^+ + N_2^+]/Q_{90}[O^+]$ must therefore increase as κ increases.

The $Q_o[O^+ + N_2^+]$ scale in Fig. 38 is based upon a $\kappa = 7$ assumption, corresponding to the COSPAR model atmosphere of Fig. 3. This scale does depend upon the choice of κ, to the extent indicated by Fig. 39, but the values shown for $Q_{90}[O^+]$ are virtually independent of the assumed κ. The rate of production of O^+ ions is, to be sure, a

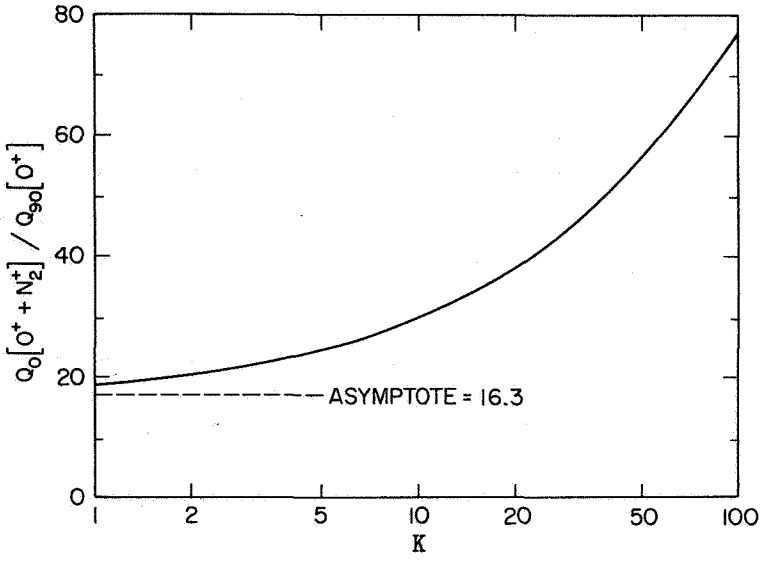

Fig. 39. THE RATIO $Q_o[O^+ + N_2^+]/Q_{90}[O^+]$ VS κ. It has been assumed that the scale height H_1 of atomic oxygen is 40 km. The asymptotic value of the ratio as κ approaches zero is $Ch(\chi, H_1)$ evaluated at $\chi = 90°$.

function of the relative concentrations of O and N_2, but it is not necessary to know the atmospheric composition accurately to determine $Q_{90}[O^+]$. This follows because $Q_{90}[O^+]$ is derived directly from the measured increase of observable ionization at sunrise. Figure 22, however, indicates that κ is, in fact, fairly well known.

Garriott and Smith [1965], studying production rates in the F region, applied a somewhat different technique of analysis to the September, October, and November 1964 data used in this work. A quantity Q_o was defined as the integrated rate of production of O^+ ions for an overhead sun if the atmosphere were composed only of atomic oxygen. Neglecting the effects of loss, Q_o was found to be 1.4×10^{10} cm^{-2} s^{-1}. The present study indicates that this value should be increased by about 30 percent to account for the recombination of O^+ ions (see Fig. 34). Hence Q_o should be about 1.8×10^{10} cm^{-2} s^{-1}. To compare Q_o to the results in Fig. 38, consider Fig. 40. With an overhead sun, the integrated rate

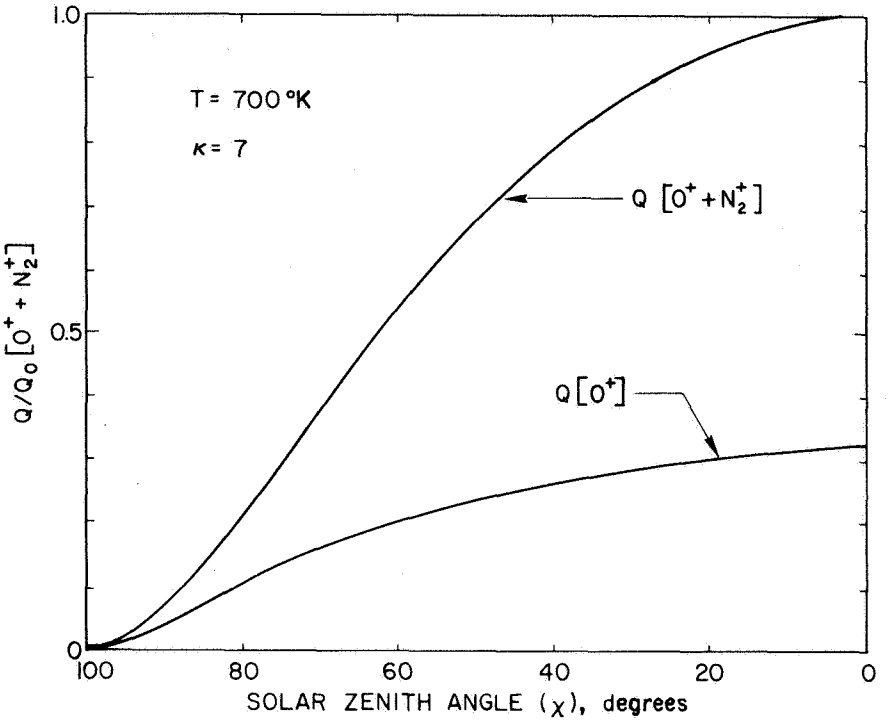

Fig. 40. THE TOTAL ION PRODUCTION, $Q[O^+ + N_2^+]$, AND THE O^+ ION PRODUCTION, $Q[O^+]$, VS SOLAR ZENITH ANGLE. A two-constituent atmosphere is assumed with a temperature of 700°K and $\kappa = 7$.

of production of O^+ ions in a two-constituent atmosphere with $\kappa = 7$ is only about one-third of the total production. Since $Q_o[O^+ + N_2^+]$ averages 4.5×10^{10} cm^{-2} s^{-1} for September through November 1964, $Q_o[O^+]$ must therefore average about 1.5×10^{10} cm^{-2} s^{-1}. The quantity $Q_o[O^+]$ should, and in fact does, approximately agree with Q_o as determined by the earlier work in 1965.

C. Solar EUV Flux

To the extent that the ionization efficiencies are 100 percent, $Q_o[O^+ + N_2^+]$ is equal to the total ionizing photon flux in the 165 to 911 Å range. Figure 38 would thus indicate that, on the average, the total solar EUV flux was about 4.5×10^{10} photons/cm^2/s. According to Hinteregger et al [1965], the flux in this range during periods of low solar activity is about 5×10^{10} photons/cm^2/s (see Table 1 in Chapter II).

In a review paper, Allen [1965] published a table of solar flux values obtained by averaging data from several other authors. He found the total flux between 165 and 911 Å to be 4.1×10^{10} photons/cm^2/s. Other published data show the EUV photon flux in this band to be 2.4×10^{10} photons/cm^2/s [Norton et al, 1963] and 4.73×10^{10} photons/cm^2/s [Watanabe and Hinteregger, 1962]. All of these values are within the day-to-day variation in $Q_o[O^+ + N_2^+]$ shown in Fig. 38.

Sunrise measurements of the ionospheric electron content cannot provide a detailed picture of the solar EUV spectrum such as can be obtained with a rocket-borne spectrometer. With the advent of geostationary satellites, however, these measurements do provide a convenient and inexpensive means of observing day-to-day variations in the total EUV flux. Unfortunately, at present no other data are available against which the measurements of $Q_o[O^+ + N_2^+]$ can be checked to determine their validity as daily measures of the EUV flux.

Neupert et al [1964] did obtain continuous measurements of the flux of the 170 to 300 Å range for 2 months in 1962 from the OSO-I satellite. They found that though the intensities of different emission lines varied differently as a function of solar activity, there was an overall correlation between the total flux in this part of the spectrum and the solar radio flux at 10.7 cm. Presumably there is also at least a rough correlation between 10.7 cm solar flux and the total flux between 165 and 911 Å. Figure 41 shows the results of a crosscorrelation between $Q_{90}[O^+]$, or $Q_o[O^+ + N_2^+]$, and the 10.7 cm flux, $S_{10.7}$, after a 30 day running mean had been subtracted from each. A significant, though not large, correlation is observed. Notice that the correlation coefficient is periodic, with a period roughly corresponding to the sun's 27 day period of rotation. On a long-term basis, Fig. 42 shows the integrated production rates to be increasing at about the same rate as $S_{10.7}$ during 1966.

The correlation between $Q_{90}[O^+]$ and $S_{10.7}$ indicates that variations in the production rate tend to lag variations in $S_{10.7}$ by 1-1/2 days. If the lag is real, it would indicate that fluctuations in the EUV flux lag corresponding fluctuations in the 10.7 cm flux, a situation which would certainly be interesting, though somewhat difficult, to explain. Other similar observations have been reported, however. MacDonald [1963]

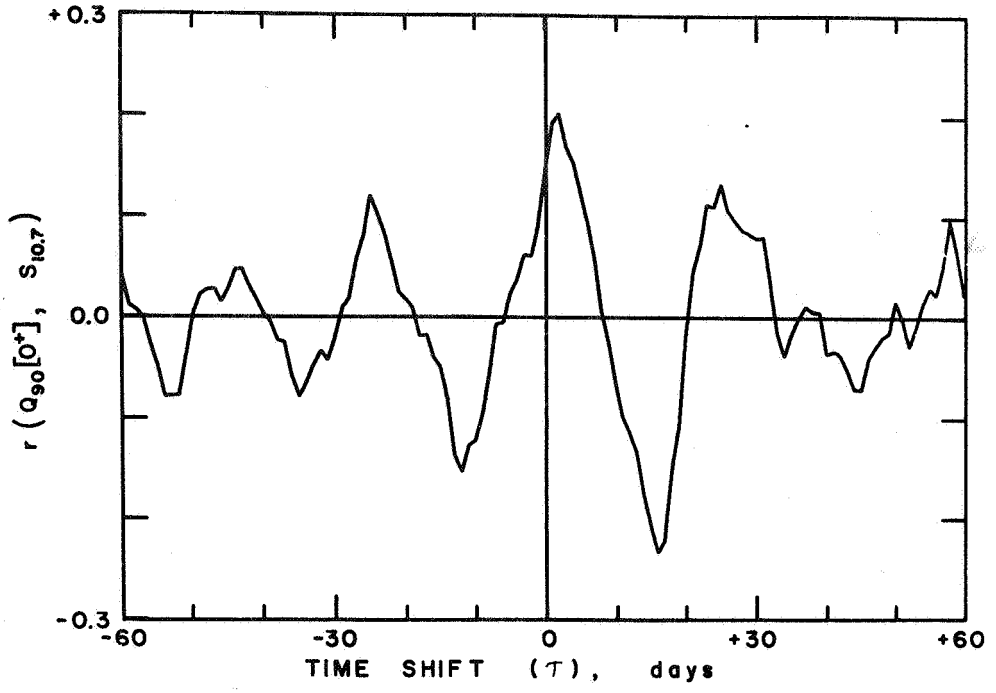

Fig. 41. COEFFICIENT OF CORRELATION BETWEEN $Q_{90}[O^+]$ AT TIME t AND $S_{10.7}$ AT TIME $(t - \tau)$. Points on the curve are computed at 1-day increments in τ.

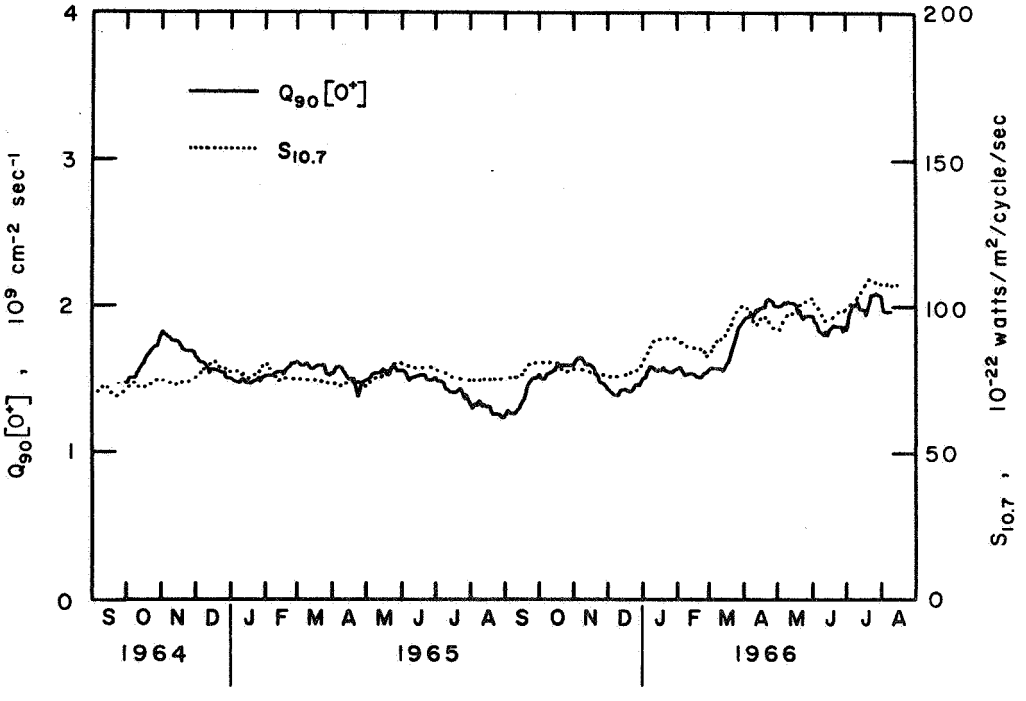

Fig. 42. THIRTY-DAY RUNNING MEANS OF $Q_{90}[O^+]$ AND THE SOLAR RADIO FLUX AT 10.7 cm VS DATE. The running mean of $Q_{90}[O^+]$ was obtained from Fig. 38.

observed a 2 day time shift when correlating $S_{10.7}$ with upper atmosphere temperatures derived from satellite drag data. He interpreted the lag as indicating that a particle flux from the sun was responsible for the fluctuations in temperature. But a particle flux should have no influence on $Q_{90}[O^+]$. The ion production being observed in the sunrise Faraday rotation data varies rapidly with the solar zenith angle near sunrise. Any production due to a particle flux would not behave in this manner and would not be reflected in the measurements of $Q_{90}[O^+]$.

As a check, a crosscorrelation between $Q_{90}[O^+]$ and the geomagnetic activity index was also computed. There is no reason to expect the production rates to be correlated with K_p, and apparently no significant correlation exists (Fig. 43).

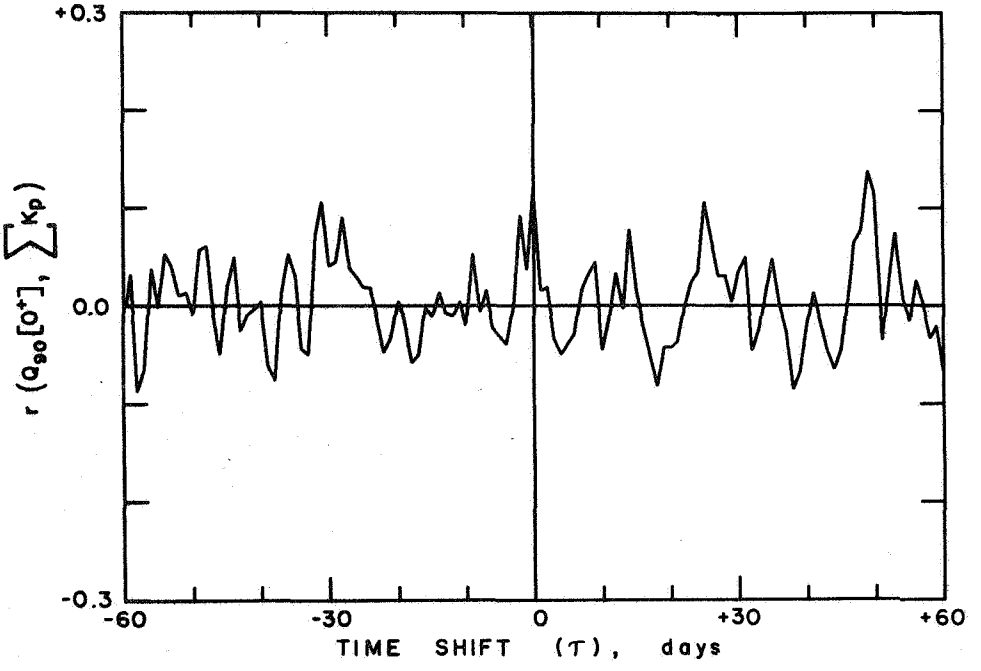

Fig. 43. COEFFICIENT OF CORRELATION BETWEEN $Q_{90}[O^+]$ AT TIME t AND ΣK_p AT TIME $(t - \tau)$. K_p is summed over a 12-hour interval ending at local sunrise. Points on the curve are computed at 1-day increments in τ.

D. Nighttime Ionosphere

As a byproduct of the curve-fitting process used to determine $Q_{90}[O^+]$, information regarding the presunrise ionosphere is also

obtained. The parameter μ in Eqs. (4-51) and (4-63) is proportional to the vertical ionospheric electron content at $\chi = 100°$. In Eq. (4-50), η gives the rate of change of the electron content during the 1 hour prior to $\chi = 100°$.

Figure 44 shows the electron content at $\chi = 100°$. The higher electron contents present at night in the summer are consistent with the

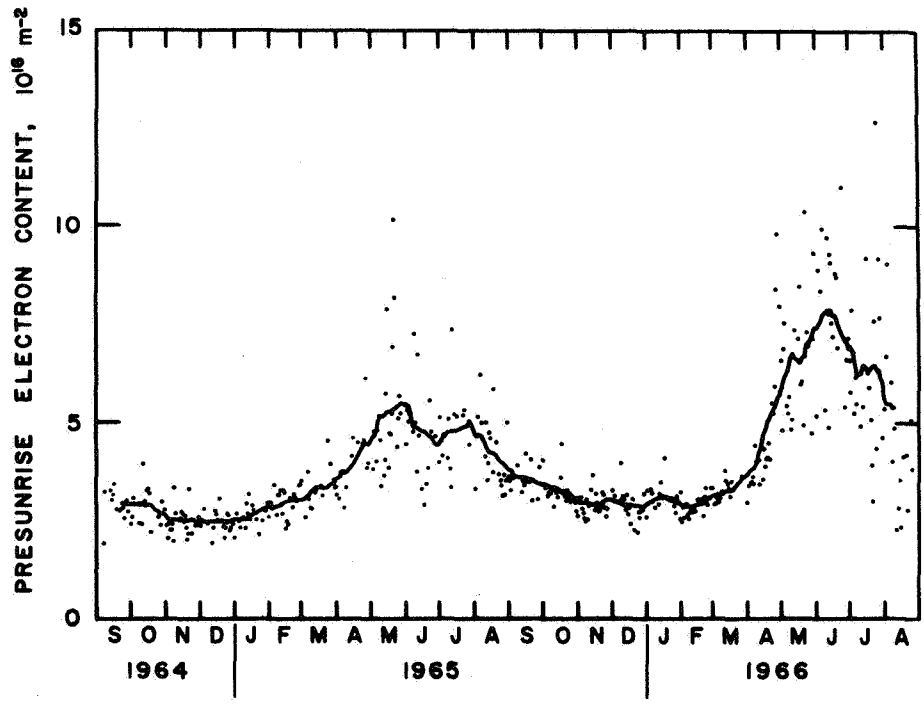

Fig. 44. ELECTRON CONTENT AT $\chi = 100°$ VS DATE.

fact that β_{300} was found to be less in the summer. Figure 45 shows the slope of the electron content curves prior to sunrise. In this case, the relatively large rates of decay of the electron content during the summer are not consistent with the smaller loss coefficients, but observations indicate that the nighttime ionization at sunspot minimum is not governed by a simple loss process alone [da Rosa and Smith, 1967].

E. Factors Affecting Accuracy

1. Assumptions Previously Considered

(a) The neutral atmosphere at F region altitudes is isothermal and composed of two constituents, atomic oxygen and molecular nitrogen, in diffusive equilibrium.

(b) Molecular nitrogen ions recombine instantly and thus do not contribute to the observable ionization.

(c) The recombination of atomic oxygen ions is governed by a linear loss law with a loss coefficient that decreases exponentially with altitude.

(d) The ambipolar diffusion coefficient is 3×10^{10} cm^2/s at 300 km and increases exponentially with altitude.

(e) All of the ions produced at sunrise are the result of solar EUV flux in the 911 to 165 Å range.

(f) The ionization efficiencies of the atmospheric constituents are on the average 100 percent, and the ionization cross sections are constant throughout the 911 to 165 Å range.

For the purposes of this study, these assumptions are all valid and have already been considered in Chapter IV.

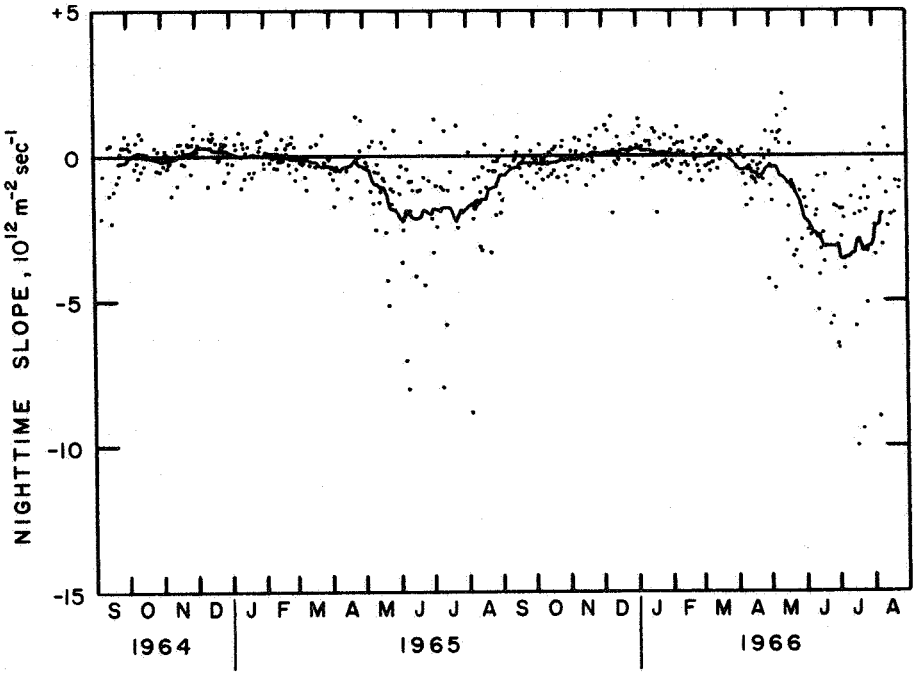

Fig. 45. THE RATE OF CHANGE OF THE ELECTRON CONTENT DURING THE 1 HOUR PRECEDING $\chi = 100°$ VS DATE.

2. Vertical Drift

An assumption that has not been covered previously is the neglect of all drifts of ionization due to electromagnetic forces.

A vertical movement of the ionization will not directly affect the columnar electron content of the ionosphere, though it may do so indirectly through its effect on the recombination rates. An upward drift, for example, will cause the ionization to begin moving, as soon as it is produced, to regions where the loss coefficient is smaller. The effective value of β_{300} observed under these conditions will be lower than the true value if the effects of the drift are not taken into account.

The production and loss rates are increasing rapidly enough throughout the sunrise period so that at any instant most of the O^+ ions recombining per second are ions produced within the previous ten minutes. Since β decreases exponentially with altitude with a scale height of 22.8 km ($H_2 = 40/1.75 = 22.8$), a vertical drift amounting to less than 22.8 km per 10 min, or about 38 m/s, will not result in errors in β_{300} of more than a factor of 2. The actual vertical drift velocity at sunrise is not known. Prasad [1967] observed a downward velocity of 17 m/s at 300 km at night during solar minimum conditions. Mitra et al [1964] observed downward nighttime velocities ranging from 7 to 15 m/s during solar maximum conditions. At sunrise when the ionosphere is by no means in equilibrium, it would be difficult to predict what vertical velocities might be present. If the vertical drifts are not significantly larger than those observed at night, the resulting errors in β_{300} will not be larger than about 40 percent.

The effect of a vertical drift on the determination of $Q_{90}[O^+]$ and $Q_o[O^+ + N_2^+]$ is negligible since its effect on the total electron content is only a second-order effect; that is, a vertical drift affects the sunrise increase in electron content only through its effect on the loss rates, but loss in turn has only a relatively small effect on the electron content before $\chi = 87°$ (Fig. 34).

3. Horizontal Drift

The effects of a horizontal drift can easily be investigated numerically by changing the manner in which the incremental electron

density profiles are added in computing $\underline{N}_i(z)$. If v_w is taken to be a constant westward drift velocity, Eq. (4-9) would become

$$\underline{N}_i(z) = \sum_{j=1}^{i} \underline{n}_j \left(z,\ t_i - t_j + j \frac{\Delta s}{v_w} \right) \qquad (5\text{-}2)$$

where Δs is defined by Eq. (4-12). Some interpolation is required when $\Delta s / v_w$ is not an integral multiple of Δt. Equation (5-2) takes into account the fact that the incremental electron density profiles begin moving to the west after being produced.

As a test of the effect of an east to west drift, Eq. (5-2) was substituted for Eq. (4-9) and the analysis was reapplied to the October and November 1965 data. A 50 m/s east to west drift caused the resulting values of $Q_{90}[O^+]$ to decrease by 12 percent over those based upon a $v_w = 0$ assumption. The same results are obtained by applying an analytical approach used by Rishbeth and Setty [1961] to estimate the effect of a horizontal drift on the effective production rates at sunrise.

Morriss [1967] found irregularities in the F region during 1964 and 1965 to be drifting westward with a velocity of about 50 m/s during the day and eastward with about the same velocity at night. It does not necessarily follow that the background ionization drifts with the same velocity as the small irregularities, but the background drift velocity itself is rather difficult to measure. If in fact the magnitude of the east-west drift velocity at sunrise is no greater than 50 m/s, the errors introduced in $Q_{90}[O^+]$ should be no more than 12 percent.

A constant horizontal drift has little effect on the determination of the loss coefficient, but the drift most likely does not remain constant during the sunrise period. Again referring to an approximate analytical treatment by Rishbeth and Setty, a linearly increasing v_w, at a latitutde of 20°N, will make β at all altitudes appear to be smaller by about 6×10^{-7} s^{-1} for each 1.0 m/s/hr in dv_w/dt. Though the loss coefficient was specified in terms of its magnitude at 300 km, primarily for comparison with other published data, most of the recombination takes place near the peak of the layer of ionization at sunrise, about 230 km. At this altitude, $\beta = 21(\beta_{300}) = 3 \times 10^{-4}$ s^{-1}. To affect

this value of β by 10 percent, dv_w/dt would need to be 50 m/s/hr, which is a possibility if the data of Morriss mentioned above are in fact representative of v_w.

4. Temperature of the Neutral Atmosphere

The temperature of the neutral atmosphere in the F region was assumed to be 700°K in accordance with both CIRA 1965 and Jacchia [1965b] models for periods of low solar activity. The assumed temperature of 700°K results in an atomic oxygen scale height, H_1, of 40 km. Through its influence upon the vertical distribution of the neutral constituents, and consequently upon $Ch(\chi,H)$, the assumed temperature does affect the theoretical Faraday rotation functions used in the curve-fitting process. An error in the assumed temperature will consequently lead to errors in the determination of both $Q_{90}[O^+]$ and β_{300}. The magnitude of the errors is most easily investigated by varying the neutral constituent scale heights, recomputing $\underline{F}$, and then noting the effects on the resulting production rates and loss coefficients.

In one case, while holding the concentrations of O and N_2 constant at 200 km, the assumed temperature was increased by 100°K (14 percent), which corresponds to an increase of 6 km in H_1. The loss coefficient at 300 km was held constant at 1.4×10^{-5} s^{-1} as before, and the daily data for October and November 1965 were reprocessed. The values obtained from the curve-fitting process for $Q_{90}[O^+]$ decreased by approximately 5 percent over those shown in Fig. 38. Varying β_{300} in order to find the best fitting loss coefficient for the October and November 1965 monthly average data yielded values 50 percent larger than were obtained with the $T = 700°K$ assumption.

In another case, where the assumed value of T was decreased from 700 to 600°K, resulting experimental values for $Q_{90}[O^+]$ increased by 6 percent while those for β_{300} decreased by 30 percent.

Data taken during the recent period of low solar activity indicate that the nighttime temperature of the neutral atmosphere was almost certainly within 100°K of the assumed temperature of 700°K [Jacchia, 1967]. Furthermore, CIRA 1965 shows that the temperature increase prior to $\chi = 87°$ should amount to less than 50°K. Possible errors in the assumed temperature should therefore not seriously affect the production

rates derived in this work, though the reported loss coefficients are subject to errors which could be as large as 50 percent.

5. Ion and Electron Temperature

In choosing the diffusion coefficient in Section IV-F, it was assumed that the ions and electrons both had temperatures of 700°K, the same as the temperature of the neutral atmosphere. The ion temperature at 300 km does remain near the temperature of the neutrals, but the electron temperature begins increasing rapidly at sunrise (or even before) to a daytime level of 1800 to 2200°K during solar minimum periods [Evans, 1967].

When the ions and electrons are not in thermal equilibrium, it is the average of the ion and electron temperatures that determines the ambipolar diffusion coefficient. Though the average is certainly greater than 700°K, it is not more than twice as great before $\chi = 87°$. In Section IV-F it was shown that a factor-of-2 error in the value of the diffusion coefficient produces negligible effects upon this analysis.

6. Conjugate Point Effects

Carlson [1966] has observed presunrise heating effects in the ionosphere that are apparently due to arrival of energetic electrons from the magnetic conjugate point along field lines. Such effects are observed only during seasons when the conjugate point is illuminated prior to the ionospheric point being studied. Though it apparently is possible for enough electrons to arrive from the conjugate point to cause an increase in the F region electron temperature, it is very unlikely that they could noticeably change the electron content. This effect, when it is present, should not therefore affect the determination of $Q_{90}[O^+]$ or β_{300}. Furthermore, for a station in Hawaii, the conjugate point is only illuminated prior to the ionospheric point during 3 months in the winter. No effects on the electron content were observed which can be attributed to conjugate point ionization.

F. Overall Estimate of Accuracy

It is believed that the running mean of $Q_{90}[O^+]$ shown in Fig. 38 is accurate to within ±15 percent. Daily values of $Q_{90}[O^+]$ vary about the mean with a standard deviation of ±15 percent. A correlation between $Q_{90}[O^+]$ and $S_{10.7}$ (see Section C), however, indicates that at least part of the day-to-day variation observed in $Q_{90}[O^+]$ is real.

Since the columnar electron content at sunrise is to a greater extent determined by production of ion-electron pairs than by loss, β_{300} is determined with less accuracy than $Q_{90}[O^+]$. It is difficult to place precise limits on the possible errors, but the value given in Eq. (5-1) should be accurate to within a factor of 2.

As a result of some uncertainties regarding the exact composition of the neutral atmosphere, the ionization efficiencies of O and N_2, and the temperature of the atmosphere, somewhat more error is involved in the determination of solar EUV photon flux values than in the determination of $Q_{90}[O^+]$. It should still, however, be possible to specify the solar EUV flux to within ±30 percent.

Chapter VI

CONCLUSION

The method of analysis presented allows for the determination of both the integrated rate of production of O^+ ions and the magnitude of the linear loss coefficient in the F region at sunrise. The only data required are measurements of the amount of Faraday rotation imposed upon transmissions from geostationary satellites. It has been shown that the integrated rate of production of O^+ ions and the magnitude of the loss coefficient at 300 km can be determined without an accurate knowledge of the composition of the neutral atmosphere. On the basis of recent data regarding the composition of the atmosphere, however, the total flux of solar radiation in the extreme ultraviolet portion of the spectrum may also be deduced.

The analysis has been applied to Faraday rotation measurements made by observing Syncom III in Hawaii between September 1964 and August 1966. Values of $Q_{90}[O^+]$, the integrated rate of production of O^+ ions at sunrise, were computed on a daily basis. On the average, $Q_{90}[O^+]$ was 1.7×10^9 cm^{-2} s^{-1}. Daily values fluctuated about the mean with a standard deviation of ±15 percent. No seasonal variation was observed. Rather, a gradual increase, presumably due to increasing solar activity, occurred during 1966. The daily values obtained for $Q_{90}[O^+]$ are tabulated in the appendix.

The magnitude of the linear loss coefficient at 300 km, β_{300}, was determined on a monthly average basis. It averaged 1.4×10^{-5} s^{-1}, with winter values tending to be about 50 percent higher than the average, and summer values about 50 percent lower.

With the use of a two-constituent model atmosphere with characteristics very similar to the COSPAR atmosphere [CIRA 1965], values of the integrated rate of production of both O^+ and N_2^+ ions for an overhead sun, $Q_o[O^+ + N_2^+]$, were derived from $Q_{90}[O^+]$. Taking $Q_o[O^+ + N_2^+]$ as a measure of the solar EUV flux between 165 and 911 Å, values of the flux were obtained that are in good agreement with data from rocket-borne spectrometers. But unlike rocket experiments, the method used here for measuring the solar flux can be applied easily on a day-to-day basis.

It would seem desirable for several reasons that this study be continued. In the first place, its continuation would permit a study of the effects of increasing solar activity on the rate of production of electrons. Knowledge of the variation of electron production rates with solar activity would provide a valuable input to numerous theoretical studies of the ionosphere.

An extension of this study would also provide daily values of the integrated electron production rate to overlap daily measurements of the solar EUV flux, which should soon be available from several of the OSO satellites. Since these two quantities are directly related, a knowledge of either the total EUV flux or the integrated production rate at sunrise implies a knowledge of the other, provided an accurate calibration between the two has been established. Overlapping measurements of the production rates and EUV flux would allow this calibration to be obtained. The relationship between the two could then be checked against the relationship used in this study, which was based upon assumptions regarding the atmospheric composition, ionization cross sections, and ionization efficiencies. Once the calibration has been established, measurements of the integrated production rates could be converted more reliably into values of the solar EUV flux during the September 1964 through August 1966 interval. These values would be especially useful because they would most likely be the only measurements of the EUV flux available on a day-to-day basis during the recent period of IQSY.

Finally, if this study were to be continued now that a large quantity of suitable electron content data is becoming available from ATS satellites, production rates could be obtained simultaneously for stations at widely separated latitudes. Since the EUV flux is the same at all latitudes (after accounting for a solar zenith angle dependence), the presence or absence of significant differences in the production rate among different stations would confirm or deny a latitudinal dependence in the composition of the neutral atmosphere.

Appendix A

TABULATION OF INTEGRATED PRODUCTION RATES AND NIGHTTIME RATE OF CHANGE OF ELECTRON CONTENT

The tables on the following pages contain listings of the data plotted in Figs. 38 and 45 of Chapter V. The quantities tabulated are:

SLOPE: The rate of change of the electron content during the 1-hour interval prior to $\chi = 100°$ in units of 10^{8} cm^{-2} s^{-1}

Q90: The integrated rate of production of O^{+} ions at sunrise, $Q_{90}[O^{+}]$, in units of 10^{9} cm^{-2} s^{-1}

Q0: The integrated rate of production of both O^{+} and N_2^{+} ions for an overhead sun, $Q_o[O^{+} + N_2^{+}]$, in units of 10^{10} cm^{-2} s^{-1}

The 2-year period covered by the data extends from September 1964 through August 1966.

DATE	SLOPE	Q90	Q0
9 8 64	-2.19	1.62	4.28
9 9 64	-0.69	1.65	4.38
9 14 64	0.33	1.37	3.64
9 15 64	-1.39	1.54	4.07
9 16 64	0.38	1.55	4.10
9 17 64	-2.31	1.58	4.19
9 19 64	-1.22	1.38	3.67
9 22 64	-0.92	1.65	4.38
9 24 64	-0.68	1.28	3.40
9 25 64	0.08	1.34	3.54
9 26 64	0.30	1.43	3.78
9 28 64	0.30	1.42	3.76
9 29 64	0.71	1.37	3.64
10 2 64	0.30	1.18	3.14
10 3 64	0.46	1.61	4.26
10 4 64	0.22	1.43	3.78
10 8 64	-0.43	1.83	4.84
10 9 64	0.46	1.43	3.80
10 10 64	-0.24	1.37	3.62
10 11 64	-0.76	1.63	4.31
10 12 64	0.79	1.70	4.51
10 14 64	-0.54	1.37	3.62
10 15 64	0.63	1.32	3.49
10 16 64	0.08	1.53	4.05
10 17 64	-0.33	1.51	3.99
10 18 64	-0.05	1.77	4.68
10 19 64	0.07	2.13	5.64
10 26 64	0.28	1.85	4.90
10 28 64	-0.49	1.94	5.15
10 29 64	0.16	1.46	3.87
10 31 64	-0.54	1.83	4.84
11 2 64	0.00	1.80	4.77
11 3 64	-0.33	1.87	4.96
11 4 64	0.18	1.90	5.03
11 5 64	0.07	1.62	4.29
11 6 64	-0.43	1.93	5.12
11 7 64	0.00	1.53	4.05
11 8 64	-0.28	1.77	4.69
11 9 64	-0.25	1.63	4.31
11 10 64	-1.37	2.02	5.35
11 14 64	0.18	1.61	4.26
11 15 64	-1.03	2.17	5.74
11 16 64	0.41	1.78	4.71
11 17 64	0.04	2.05	5.42
11 18 64	0.42	1.56	4.14
11 19 64	-0.26	1.91	5.07
11 20 64	0.23	1.75	4.63
11 21 64	0.11	1.68	4.44

DATE	SLOPE	Q90	Q0
11 22 64	-0.29	1.52	4.03
11 24 64	0.42	1.58	4.19
11 25 64	0.37	1.43	3.79
11 27 64	-0.61	2.04	5.40
11 28 64	0.41	1.67	4.42
11 29 64	0.64	1.40	3.71
11 30 64	1.09	1.67	4.42
12 1 64	0.18	1.66	4.39
12 2 64	0.15	1.63	4.33
12 3 64	0.38	1.31	3.46
12 5 64	0.32	1.39	3.68
12 8 64	0.61	1.58	4.18
12 12 64	-1.05	2.18	5.77
12 13 64	0.60	1.41	3.74
12 15 64	0.55	1.43	3.78
12 16 64	0.80	1.60	4.25
12 17 64	0.65	1.77	4.69
12 19 64	0.44	1.47	3.89
12 21 64	-0.16	1.77	4.68
12 22 64	-0.12	1.63	4.31
12 23 64	0.28	1.52	4.02
12 24 64	0.44	1.40	3.71
12 25 64	0.31	1.32	3.51
12 26 64	0.43	1.08	2.85
12 27 64	-0.90	1.52	4.04
12 28 64	0.41	1.35	3.59
12 29 64	0.66	2.09	5.53
12 30 64	-0.24	1.59	4.21
12 31 64	-0.56	1.76	4.66
1 1 65	0.05	1.54	4.09
1 3 65	-0.28	1.32	3.51
1 5 65	0.43	1.19	3.15
1 6 65	0.24	1.35	3.58
1 9 65	0.81	1.49	3.94
1 11 65	-1.12	1.81	4.80
1 12 65	0.45	1.16	3.07
1 13 65	0.29	1.32	3.49
1 14 65	-0.80	1.66	4.39
1 15 65	0.10	1.33	3.53
1 17 65	0.33	1.45	3.84
1 18 65	-0.57	1.41	3.74
1 21 65	-0.73	1.51	4.01
1 23 65	-0.55	1.57	4.15
1 26 65	0.52	1.49	3.96
1 27 65	0.18	1.45	3.85
1 28 65	0.33	1.42	3.76
1 29 65	0.56	1.52	4.02
1 30 65	-0.02	1.62	4.28

DATE	SLOPE	Q90	Q0
1 31 65	-0.23	1.40	3.72
2 1 65	-0.41	2.03	5.38
2 2 65	0.12	1.20	3.17
2 3 65	0.85	1.38	3.66
2 4 65	0.75	1.51	4.00
2 5 65	0.09	1.56	4.13
2 6 65	-0.24	1.38	3.66
2 8 65	-0.10	1.60	4.23
2 9 65	-0.07	1.80	4.77
2 10 65	-0.42	1.63	4.33
2 11 65	-0.03	1.11	2.95
2 12 65	0.25	1.45	3.85
2 13 65	-0.43	1.67	4.43
2 14 65	-0.17	1.82	4.81
2 15 65	-0.07	1.54	4.08
2 16 65	-0.18	1.60	4.23
2 17 65	0.59	1.34	3.54
2 18 65	-0.16	1.45	3.85
2 20 65	0.27	1.45	3.83
2 21 65	0.07	1.42	3.75
2 22 65	0.41	1.54	4.09
2 23 65	-0.30	1.94	5.14
2 24 65	-0.57	1.76	4.67
2 25 65	0.45	1.63	4.32
2 26 65	0.67	1.64	4.35
2 28 65	0.30	1.34	3.55
3 1 65	-0.84	1.57	4.17
3 2 65	-0.45	1.34	3.56
3 5 65	-0.23	1.72	4.56
3 7 65	-0.30	2.03	5.39
3 8 65	-0.25	1.63	4.31
3 10 65	-0.73	1.81	4.80
3 11 65	-1.17	1.97	5.21
3 14 65	-0.33	1.76	4.67
3 15 65	0.33	1.23	3.25
3 19 65	-0.37	1.07	2.84
3 20 65	0.41	1.40	3.71
3 25 65	0.72	1.51	3.99
3 27 65	-0.23	1.45	3.85
3 30 65	-0.10	1.60	4.25
3 31 65	-0.14	1.66	4.40
4 1 65	-0.60	1.63	4.31
4 2 65	-0.41	1.42	3.77
4 4 65	-0.82	1.55	4.10
4 5 65	-1.76	1.48	3.92
4 7 65	-0.40	2.23	5.90
4 8 65	-1.14	1.75	4.64
4 10 65	-0.52	1.23	3.25

DATE	SLOPE	Q90	Q0
4 15 65	0.01	1.59	4.21
4 16 65	-0.51	1.42	3.77
4 20 65	-1.46	1.60	4.23
4 24 65	1.35	1.26	3.34
4 25 65	-0.87	1.55	4.12
4 27 65	-0.03	1.14	3.02
4 28 65	0.18	1.43	3.79
4 29 65	1.22	1.13	3.00
5 3 65	-0.23	1.63	4.33
5 4 65	-0.36	1.60	4.24
5 6 65	0.32	0.92	2.45
5 7 65	-1.23	1.30	3.44
5 9 65	0.50	1.39	3.69
5 10 65	-1.65	1.98	5.26
5 11 65	-0.56	1.69	4.49
5 12 65	-2.56	1.70	4.51
5 13 65	-0.29	1.71	4.54
5 14 65	-0.60	1.67	4.42
5 15 65	-1.63	1.23	3.27
5 16 65	-1.23	1.63	4.33
5 17 65	0.47	1.74	4.62
5 18 65	-0.78	1.63	4.31
5 19 65	-0.88	1.62	4.30
5 20 65	0.26	1.66	4.40
5 21 65	-2.66	1.99	5.28
5 22 65	-4.31	1.80	4.76
5 23 65	-5.16	1.44	3.82
5 25 65	-1.14	1.40	3.72
5 26 65	-1.67	1.52	4.03
5 27 65	-1.25	1.50	3.97
5 28 65	0.88	1.18	3.14
6 1 65	-0.75	1.20	3.18
6 2 65	-1.31	1.33	3.53
6 3 65	-0.35	1.09	2.90
6 4 65	-3.67	1.78	4.72
6 5 65	-2.56	1.34	3.56
6 7 65	-7.06	2.18	5.78
6 8 65	-0.46	1.49	3.94
6 9 65	-8.05	1.68	4.46
6 10 65	-0.90	1.64	4.35
6 11 65	-1.92	1.72	4.55
6 12 65	-0.88	1.03	2.72
6 13 65	-1.20	1.45	3.84
6 16 65	-4.16	1.97	5.22
6 18 65	-1.22	1.54	4.07
6 20 65	-1.18	1.47	3.90
6 21 65	0.48	1.27	3.37
6 23 65	-0.76	1.34	3.56

DATE	SLOPE	Q90	Q0
6 24 65	-4.46	1.95	5.16
6 28 65	-0.85	1.38	3.66
7 1 65	-2.17	1.53	4.06
7 2 65	-3.33	1.86	4.92
7 3 65	1.26	0.92	2.44
7 4 65	-1.05	1.14	3.01
7 5 65	-2.46	1.48	3.93
7 9 65	-1.08	1.40	3.72
7 10 65	-7.99	2.12	5.63
7 11 65	-1.17	1.30	3.44
7 12 65	0.87	1.17	3.10
7 13 65	-5.82	1.54	4.07
7 15 65	-1.20	1.84	4.87
7 17 65	-0.56	1.44	3.81
7 23 65	1.04	1.09	2.89
7 24 65	-2.49	1.12	2.98
7 27 65	-1.90	1.39	3.68
7 28 65	-1.12	1.14	3.03
8 3 65	0.12	1.34	3.55
8 5 65	-8.84	2.12	5.63
8 7 65	-2.18	1.10	2.92
8 8 65	-0.80	1.17	3.11
8 9 65	-1.59	1.32	3.50
8 11 65	-1.53	1.22	3.24
8 12 65	-0.73	1.66	4.39
8 13 65	-3.15	1.61	4.26
8 14 65	-1.26	1.15	3.06
8 15 65	-3.26	1.25	3.32
8 16 65	-0.40	1.02	2.71
8 18 65	0.39	0.97	2.56
8 19 65	-1.11	1.94	5.14
8 21 65	-0.51	0.98	2.59
8 23 65	-3.33	1.57	4.15
8 25 65	-0.53	1.03	2.73
8 26 65	-0.19	0.96	2.54
8 27 65	-0.54	1.31	3.46
8 28 65	-2.06	1.48	3.92
8 29 65	-0.19	1.11	2.94
8 30 65	-0.08	1.13	2.99
8 31 65	-1.32	1.34	3.54
9 1 65	-1.98	1.33	3.53
9 2 65	-1.55	1.36	3.61
9 3 65	0.19	1.03	2.72
9 5 65	-0.31	1.06	2.82
9 9 65	-0.38	1.12	2.97
9 13 65	-0.17	1.48	3.92
9 14 65	-0.09	1.25	3.31
9 15 65	0.12	1.15	3.06

DATE	SLOPE	Q90	Q0
9 16 65	0.65	1.54	4.07
9 18 65	-0.43	1.56	4.13
9 20 65	-0.71	1.51	4.00
9 21 65	-0.22	1.15	3.04
9 22 65	-0.10	1.26	3.34
9 25 65	-0.93	1.58	4.19
9 27 65	-0.35	1.37	3.64
9 28 65	0.16	1.35	3.57
9 30 65	-0.10	1.51	3.99
10 1 65	-1.14	1.61	4.27
10 3 65	-0.15	1.74	4.60
10 4 65	-0.63	1.74	4.61
10 6 65	0.38	1.77	4.68
10 7 65	-0.48	1.82	4.81
10 8 65	-0.15	1.62	4.29
10 9 65	-0.84	1.58	4.19
10 10 65	-0.11	1.49	3.95
10 11 65	0.03	1.61	4.27
10 13 65	-0.30	1.50	3.97
10 14 65	-0.73	1.71	4.53
10 15 65	0.11	1.39	3.69
10 16 65	0.04	1.34	3.56
10 17 65	-0.64	1.22	3.22
10 18 65	0.21	1.12	2.98
10 19 65	-0.51	1.55	4.12
10 20 65	0.31	1.32	3.51
10 21 65	-0.25	1.49	3.94
10 22 65	-0.76	1.61	4.27
10 23 65	-0.74	1.85	4.90
10 25 65	-0.01	1.72	4.55
10 26 65	0.30	1.53	4.06
10 27 65	0.50	1.69	4.47
10 29 65	-0.18	1.47	3.89
10 30 65	-0.70	1.51	3.99
10 31 65	-0.91	1.92	5.10
11 1 65	-0.41	2.08	5.50
11 2 65	-0.02	1.61	4.27
11 3 65	0.17	1.52	4.03
11 4 65	-0.36	2.09	5.53
11 5 65	-0.03	1.51	3.99
11 6 65	-0.10	1.62	4.28
11 7 65	0.60	1.83	4.85
11 8 65	0.15	1.70	4.51
11 9 65	-0.11	1.59	4.21
11 10 65	-0.48	1.51	4.01
11 11 65	0.53	1.43	3.80
11 13 65	-0.16	1.49	3.95
11 14 65	0.05	1.57	4.16

DATE	SLOPE	Q90	Q0
11 16 65	-0.01	1.54	4.08
11 17 65	-1.04	1.67	4.43
11 18 65	-0.18	1.68	4.45
11 19 65	0.35	1.65	4.38
11 20 65	0.00	1.58	4.20
11 21 65	0.68	1.45	3.83
11 22 65	-0.06	1.72	4.55
11 23 65	-0.21	1.45	3.83
11 24 65	-0.71	1.55	4.12
11 25 65	0.24	1.17	3.11
11 26 65	0.92	1.15	3.05
11 27 65	0.09	1.57	4.16
12 2 65	-0.51	1.74	4.60
12 4 65	1.04	1.25	3.30
12 6 65	0.87	1.17	3.10
12 9 65	1.36	0.97	2.58
12 10 65	-2.00	1.60	4.23
12 11 65	0.18	1.36	3.60
12 12 65	-0.21	1.38	3.67
12 14 65	-0.32	1.20	3.17
12 15 65	0.65	1.27	3.37
12 16 65	-0.14	1.25	3.31
12 17 65	0.36	1.39	3.69
12 18 65	0.05	1.59	4.22
12 20 65	0.00	1.35	3.57
12 21 65	0.02	1.56	4.13
12 24 65	0.18	1.73	4.59
12 25 65	-0.18	1.51	4.00
12 26 65	-0.01	1.69	4.47
12 27 65	0.25	1.48	3.91
12 29 65	0.76	1.74	4.60
12 30 65	-0.27	1.36	3.61
1 1 66	0.34	1.45	3.85
1 2 66	1.25	1.26	3.35
1 3 66	1.00	1.36	3.60
1 5 66	0.30	1.40	3.72
1 6 66	-0.79	1.77	4.69
1 7 66	-0.02	1.51	3.99
1 9 66	0.49	1.51	3.99
1 12 66	0.50	1.11	2.93
1 13 66	0.34	1.39	3.69
1 14 66	0.01	1.82	4.81
1 15 66	0.93	1.43	3.78
1 16 66	-0.37	1.72	4.55
1 17 66	0.81	1.42	3.75
1 19 66	-2.01	1.92	5.09
1 20 66	-0.31	2.16	5.72
1 22 66	0.58	2.14	5.66

DATE	SLOPE	Q90	Q0
1 24 66	-0.23	1.63	4.32
1 26 66	0.70	1.15	3.04
1 27 66	-0.17	1.47	3.90
1 28 66	-0.33	1.53	4.06
1 29 66	-0.02	1.52	4.03
1 30 66	-0.40	1.73	4.59
1 31 66	0.18	1.42	3.75
2 1 66	0.58	1.45	3.85
2 2 66	-0.19	1.57	4.16
2 3 66	0.03	1.56	4.13
2 4 66	0.36	1.26	3.33
2 6 66	0.98	1.34	3.56
2 7 66	0.44	1.26	3.33
2 8 66	0.14	1.51	4.00
2 9 66	-0.63	1.36	3.60
2 10 66	-0.32	1.79	4.74
2 11 66	0.44	1.46	3.87
2 12 66	0.13	1.49	3.96
2 14 66	-0.23	1.80	4.78
2 16 66	-0.36	1.86	4.94
2 18 66	-0.86	1.50	3.97
2 20 66	0.58	1.76	4.67
2 21 66	0.04	1.39	3.68
2 22 66	-0.15	1.70	4.50
2 23 66	0.22	1.82	4.81
2 25 66	-0.36	1.66	4.40
2 26 66	-0.55	1.32	3.50
2 27 66	0.49	1.27	3.37
2 28 66	0.03	1.40	3.70
3 1 66	-0.90	1.76	4.67
3 3 66	0.62	1.20	3.19
3 4 66	-0.37	1.31	3.48
3 5 66	0.66	1.38	3.67
3 6 66	0.24	1.37	3.62
3 7 66	-0.29	1.46	3.88
3 8 66	-0.54	1.40	3.70
3 9 66	0.01	1.50	3.98
3 10 66	0.12	1.75	4.63
3 11 66	-0.25	1.49	3.95
3 12 66	0.23	1.73	4.59
3 13 66	0.20	1.72	4.55
3 15 66	-0.46	1.85	4.91
3 16 66	0.48	1.69	4.47
3 17 66	-0.13	1.72	4.57
3 18 66	0.43	2.05	5.44
3 26 66	0.16	1.89	5.01
3 27 66	0.09	1.27	3.36
4 1 66	-0.42	2.25	5.95

DATE	SLOPE	Q90	Q0
4 3 66	0.16	1.67	4.43
4 5 66	0.03	1.42	3.76
4 6 66	0.25	1.84	4.87
4 7 66	-0.65	1.97	5.22
4 8 66	-0.10	2.21	5.85
4 9 66	-1.03	1.92	5.09
4 10 66	-1.76	2.15	5.69
4 11 66	-0.43	2.05	5.43
4 12 66	-0.38	1.97	5.21
4 14 66	-1.56	2.09	5.53
4 15 66	-0.78	2.01	5.32
4 16 66	-0.24	1.88	4.99
4 17 66	-0.85	2.00	5.29
4 18 66	-0.86	2.08	5.51
4 19 66	-0.97	1.83	4.86
4 20 66	-0.36	1.97	5.21
4 21 66	-0.51	2.30	6.09
4 23 66	-0.29	1.80	4.78
4 24 66	0.19	1.62	4.29
4 25 66	-0.83	2.37	6.29
4 26 66	-0.13	2.12	5.62
4 30 66	-4.29	2.37	6.29
5 1 66	0.12	2.01	5.32
5 2 66	-1.05	2.41	6.39
5 3 66	-1.58	2.13	5.65
5 4 66	0.78	1.43	3.80
5 6 66	-4.58	2.79	7.40
5 7 66	0.52	2.11	5.58
5 8 66	1.34	2.01	5.33
5 9 66	0.76	1.78	4.72
5 10 66	0.41	1.89	5.00
5 11 66	0.82	2.07	5.48
5 13 66	2.10	1.27	3.36
5 16 66	1.56	1.74	4.62
5 17 66	-2.95	2.10	5.56
5 18 66	-1.77	2.21	5.85
5 19 66	0.38	1.95	5.18
5 21 66	-0.92	2.25	5.95
5 22 66	-1.06	2.43	6.44
5 23 66	-3.49	1.71	4.54
5 24 66	-1.27	1.92	5.08
5 25 66	-3.32	2.03	5.38
5 28 66	-1.24	2.14	5.67
5 29 66	-3.88	2.02	5.34
5 30 66	-2.92	1.72	4.57
6 1 66	-1.50	1.86	4.94
6 3 66	-1.81	1.31	3.48
6 5 66	-2.58	2.01	5.33

DATE	SLOPE	Q90	Q0
6 7 66	-2.77	1.69	4.48
6 9 66	-1.26	2.17	5.75
6 11 66	-2.13	1.65	4.38
6 12 66	-1.92	2.45	6.48
6 13 66	-0.75	1.31	3.47
6 14 66	-5.33	1.62	4.30
6 15 66	-4.12	1.97	5.22
6 16 66	-3.24	1.92	5.09
6 18 66	-2.67	1.41	3.73
6 19 66	-3.68	1.73	4.59
6 20 66	-0.68	1.78	4.71
6 24 66	-5.83	1.52	4.04
6 27 66	-5.57	2.37	6.27
6 28 66	-1.76	1.83	4.85
6 30 66	-1.82	1.82	4.83
7 1 66	-6.50	2.47	6.55
7 2 66	-6.64	2.56	6.78
7 3 66	-1.88	1.48	3.93
7 4 66	-2.82	1.59	4.22
7 5 66	-1.85	1.61	4.27
7 6 66	-2.18	1.76	4.66
7 7 66	-3.91	1.89	5.01
7 11 66	-0.51	1.88	4.97
7 13 66	-1.45	1.90	5.03
7 16 66	-2.07	1.46	3.87
7 17 66	-5.91	2.66	7.06
7 18 66	-10.02	2.88	7.64
7 20 66	-2.91	2.05	5.43
7 21 66	-2.01	2.37	6.29
7 22 66	-1.54	1.72	4.55
7 23 66	-9.44	1.72	4.57
7 25 66	-1.12	2.02	5.36
7 26 66	-1.91	2.46	6.52
7 27 66	-5.10	1.90	5.03
7 28 66	-1.52	1.22	3.23
7 30 66	0.33	1.86	4.92
8 1 66	-0.21	2.13	5.65
8 3 66	-2.43	2.50	6.63
8 4 66	-3.43	1.88	4.98
8 7 66	-9.03	2.71	7.19
8 8 66	-0.83	1.94	5.14
8 10 66	-3.10	2.30	6.09
8 12 66	0.90	1.82	4.82
8 14 66	-1.33	1.73	4.59
8 15 66	-2.46	1.73	4.59
8 16 66	0.25	1.58	4.20
8 18 66	-2.08	1.46	3.88
8 21 66	-1.99	1.86	4.94

DATE	SLOPE	Q90	Q0
8 22 66	-0.89	2.19	5.81
8 25 66	-1.15	1.98	5.26
8 26 66	-0.94	2.35	6.24

BIBLIOGRAPHY

Allen, C. W., "The Interpretation of the XUV Solar Spectrum," Space Science Rev., 4, p. 91, 1965.

Anderson, A. D., and W. E. Francis, "The Variation of the Neutral Atmospheric Properties with Local Time and Solar Activity from 100 km to 10,000 km," J. Atmospheric Sci., 23, p. 110, 1966.

Appleton, E. V., "Wireless Studies of the Ionosphere," J. Inst. Elec. Engrs., 71, p. 642, 1932. (referred to by Ratcliffe [1959])

Bhatnagar, V. P., and A. P. Mitra, "An Upper Atmospheric Model for Solar Minimum Conditions," J. Atmospheric Sci., 23, p. 233, 1966.

Browne, I. C., et al, "Radio Echoes from the Moon," Proc. Phys. Soc. London, 69B, p. 901, 1956.

Carlson, H. C., Jr., "Ionospheric Heating by Magnetic Conjugate-Point Photoelectrons," J. Geophys. Res., 71, p. 195, 1966.

Champion, K. S. W., "Atmospheric Structure in the Lower Thermosphere," in CIRA 1965: COSPAR International Reference Atmosphere 1965, North-Holland Publishing Company, Amsterdam, p. 293, 1965.

Chapman, S., "The Absorption and Dissociative or Ionizing Effect of Monochromatic Radiation in an Atmosphere on a Rotating Earth, Part II, Grazing Incidence," Proc. Roy. Soc. of London, 43, p. 483, 1931.

CIRA 1965: COSPAR International Reference Atmosphere 1965, North-Holland Publishing Company, Amsterdam, 313 pp., 1965.

Dalgarno, A., "Ambipolar Diffusion in the F-region," J. Atmospheric Terrest. Phys., 26, p. 939, 1964.

da Rosa, A. V., "Thermal Behavior of the Ionosphere and Observations of the Exosphere and the Ionosphere by Means of Distant Earth Satellites," Rept. SEL-65-109 (TR No. 2, NASA Contract NASR-136), Stanford Electronics Laboratories, Stanford, Calif., Dec 1965.

da Rosa, A. V., and F. L. Smith, III, "Behavior of the Nighttime Ionosphere," J. Geophys. Res., 72, p. 1829, 1967.

Duncan, R. A., "The Behavior of a Chapman Layer in the Night F2 Region of the Ionosphere, under the Influence of Gravity, Diffusion, and Attachment," Australian J. Phys., 9, p. 436, 1956.

Dungey, J. W., "The Effect of Ambipolar Diffusion in the Nighttime F Layer," J. Atmospheric Terrest. Phys., 9, p. 90, 1956.

Evans, J. V., "Midlatitude F-region Densities and Temperatures at Sunspot Minimum," Planetary Space Sci., 15, p. 1387, 1967.

Ferguson, Eldon E., "Ionospheric Ion-Molecule Reaction Rates," Rev. Geophys., 5, p. 305, 1967.

Garriott, O. K., and F. L. Smith, III, "The Rate of Production of Electrons in the Ionosphere," Planetary Space Sci., 13, p. 839, 1965.

Garriott, O. K., F. L. Smith, III, and P. C. Yuen, "Observations of Ionospheric Electron Content Using a Geostationary Satellite," Planetary Space Sci., 13, p. 829, 1965.

Hall, L. A., W. Schweizer, and H. E. Hinteregger, "Improved Extreme Ultraviolet Absorption Measurements in the Upper Atmosphere," J. Geophys. Res., 70, p. 105, 1965.

Hedin, A. E., and A. O. Nier, "Diffusive Separation in the Upper Atmosphere," J. Geophys. Res., 70, p. 1273, 1965.

Hinteregger, H. E., L. A. Hall, and G. Schmidtke, "Solar XUV Radiation and Neutral Particle Distribution in July 1963 Thermosphere," Space Res., 5, p. 1175, 1965.

Holmes, J. C., C. Y. Johnson, and J. M. Young, "Ionospheric Chemistry," Space Res., 5, p. 756, 1965.

Jacchia, Luigi G., "Atmospheric Structure and Its Variation at Heights above 200 km," in CIRA 1965: COSPAR International Reference Atmosphere 1965, North-Holland Publishing Company, Amsterdam, p.293, 1965a.

Jacchia, Luigi G., "Static Diffusion Models of the Upper Atmosphere with Empirical Temperature Profiles," Smithsonian Contrib. Astrophys., 8, p. 215, 1965b.

Jacchia, L. G., "Recent Results in the Atmospheric Region above 200 km and Comparisons with CIRA 1965," Smithsonian Astrophys. Observatory Special Report 245, 1967.

Jacchia, L. G., and J. Slowey, "Temperature Variations in the Upper Atmosphere during Geomagnetically Quiet Intervals," J. Geophys. Res., 67, p. 4145, 1964.

Jensen, D. C., and J. C. Cain, "An Interim Geomagnetic Field," J. Geophys. Res., 69, p. 3568, 1962.

Johnson, Charles Y., "Ion and Neutral Composition of the Ionosphere," presented at IQSY COSPAR Joint Symposium, London, Jul 1967.

Johnson, C. Y., E. B. Meadows, and J. C. Holmes, "Ion Composition of the Arctic Ionosphere," J. Geophys. Res., 63, p. 443, 1958.

Lorentz, H. A., "The Theory of Electrons." Course of lectures, Columbia University, 1906, published by Dover Publications, New York, 1952.

MacDonald, G. J. F., "The Escape of Helium from the Earth's Atmosphere," Rev. Geophys., 1, p. 305, 1963.

Maeda, K., and S. Kato, "Electrodynamics of the Ionosphere," Space Sci. Rev., 5, p. 57, 1966.

Martyn, D. F., "Processes Controlling Ionization Distribution in the F2 Region of the Ionosphere," Australian J. Phys., 9, p. 161, 1956.

Mitra, A. P., B. C. N. Rao, and K. K. Mahajan, "A New Method for Estimating Loss and Drift Terms in the Ionospheric F-region," J. Atmospheric Terrest. Phys., 26, p. 525, 1964.

Morriss, R. W., "Ionospheric Drift Measurements at Ibadan during the I.Q.S.Y.," J. Atmospheric Terrest. Phys., 29, p. 651, 1967.

Neupert, W. M., W. E. Behring, and J. C. Lindsay, "The Solar Spectrum from 50 Å to 400 Å," Space Res., 4, p. 719, 1964.

Nicolet, M., "Solar Radio Flux and Temperature of the Upper Atmosphere," J. Geophys. Res., 68, p. 6121, 1963.

Nier, Alfred O., et al, "Neutral Composition of the Atmosphere in the 100 to 200 Kilometer Range," J. Geophys. Res., 69, p. 979, 1964.

Norton, R. B., T. E. VanZandt, and J. S. Denison, "A Model of the Atmosphere and Ionosphere in the E and F1 Regions," Proc. Intern. Conf. Ionosphere 1962, London, p. 26, 1963.

Prasad, S. S., "Determination of Loss and Transport in the Nighttime F-region from Backscatter N-h Profiles," J. Atmospheric Terrest. Phys., 29, p. 987, 1967.

Quinn, T. P., and J. S. Nisbet, "Recombination and Transport in the Nighttime F Layer of the Ionosphere," J. Geophys. Res., 70, p. 113, 1965.

Ratcliffe, J. A., The Magneto-Ionic Theory and Its Applications to the Ionosphere, Cambridge University Press, 206 pp., 1959.

Ratcliffe, J. A., et al, "The Rates of Production and Loss of Electrons in the F Region of the Ionosphere," Phil. Trans. Roy. Soc. London, A248, p. 621, 1956.

Ratcliffe, J. A., and K. Weekes, "The Ionosphere," in Physics of the Upper Atmosphere, edited by J. A. Ratcliffe, Academic Press, New York and London, p. 377, 1960.

Rishbeth, H., "Diffusion of Ionization in the Sunrise F-layer," J. Atmospheric Terrest. Phys., 20, p. 277, 1961.

Rishbeth, H., "A Time Varying Model of the Ionspheric F_2 Layer," J. Atmospheric Terrest. Phys., 26, p. 657, 1964.

Rishbeth, H., "A Review of Ionospheric F Region Theory," Proc. IEEE, 55, p. 16, 1967.

Rishbeth, H., and D. W. Barron, "Equilibrium Electron Distributions in the Ionospheric F2-layer," J. Atmospheric Terrest. Phys., 18, p. 234, 1960.

Rishbeth, H., and C. S. G. K. Setty, "The F-layer at Sunrise," J. Atmospheric Terrest. Phys., 20, p. 263, 1961.

Watanabe, K., and H. E. Hinteregger, "Photoionization Rates in the E and F Regions," J. Geophys. Res., 67, p. 999, 1962.

Yeh, K. C., and V. H. Gonzales, "Note on the Geometry of the Earth Magnetic Field Useful to Faraday Effect Experiments," J. Geophys. Res., 65, p. 3209, 1960.

Yuen, P. C., and T. H. Roelofs, "Seasonal Variations in Ionospheric Total Electron Content," J. Atmospheric Terrest. Phys., 29, p. 321, 1967.